UNIVERSITY OF CAPE TOWN

Developing a Methodology for Characterising In-situ Viscosity Profiles in Tumbling Mills

By

MANGESANA, NOBATHEMBU
(BSc Chemical Engineering), University of Cape Town

Thesis submitted in fulfilment of the requirements for the degree of Master of Science in Engineering.

July 2012

Declaration

I know the meaning of plagiarism and declare that all work in the document , save for that which is properly acknowledged is my own .

Signature……

Date……

Acknowledgement

Above all, I would like to thank God for this opportunity to further my studies and complete this Masters degree and for all the blessings bestowed upon me by Him. I am truly grateful for the lessons learnt along this journey.

To my parents, I am continuously grateful to God for being selflessly and unconditionally loved and natured by you. Thank you for your eternal support and encouragement. For always believing in me especially at times when I was doubting myself. You are my pillar of strength. I love you dearly.

Dr. A.N Mainza and Dr. I. Govender, I am thankful to you for being such great teachers and mentors. Thank you for your time, patience, support and guidance throughout this thesis. It has been a character building and challenging experience.

I would like to thank Jason Waters, Monde Bekaphi and all members of the comminution group for assisting with the rheology experimental work.

Anglo American Research for making their pilot plant available and providing the ore material used in the experimental work. Mxolisi Ntombela for the assistance rendered with the rheology experiments.

Lawrence Bbosa, thank you for your guidance and assistance with the PEPT Matlab simulations and modelling.

Executive Summary

Milling is the most expensive operation in a mineral processing circuit and accounts for the highest amount of energy utilized. The efficiency of the milling process is affected by the rate of breakage of bigger rocks and the rate of transport of the slurry within and out of the mill. The transport of material in the mill is dependent on the rheological properties of the slurry such as viscosity.Viscosity is therefore one of the important parameters that influences the transport of the material in the mill. Slurries in tumbling mills are known to exhibit non- Newtonian behaviour. This means slurry viscosity is not constant but is a function of shear rate. To characterize slurry transport in the mill it is necessary to study the viscosity distributions in order to determine regions of high and low resistance to flow in the mill. To determine the influence of slurry viscosity on the transport of particles it is important to quantify the typical shear rate ranges that occur inside the tumbling mill.

The aim of this project was to develop a methodology for characterising viscosity distributions inside a tumbling mill using in-situ shear rate distributions obtained from PEPT at different solids concentrations and mill speeds. The PEPT technique was used to study the in-situ motion of slurry particles within tumbling mill charge using a single radioactive tracer. Rheology experiments were conducted using a U-tube rheometer. The rheometer experiments were performed to characterise the rheological behaviour of the El Soldado slurry at a wide range of shear rates. The PEPT results provided information about the typical shear rate ranges that occur inside the mill. The combination of these results enabled the quantification of viscosity distribution from the slope of the rheogram at typical shear rates found in the tumbling mill.

The rheology results indicated that the Bingham model is the rheological model which gives the best description of the rheology of El Soldado slurry. It had the highest R^2 adjusted values at all tested solids concentrations concentration ranges. The rheological behaviour of El Soldado slurry with a particle size fraction of -75+53 microns can be described as Newtonian. This means that the viscosity is constant and does not vary with shear rate. At low solids concentrations up to 30wt%, the viscosity values attained are equivalent to that of water at room temperature at 0.001 Pa.s. At higher solids concentrations up to 60wt%, the viscosity increases to 0.007 Pa.s for the shear rate range

tested. The Bingham viscosity and yield stress increases in an exponential form with increasing solids concentration.

PEPT experiments were conducted to quantify and characterise in-situ shear rates in a laboratory scale tumbling mill. The highest shear rates were obtained at the lowest solids concentration for both mill speeds. It was $30s^{-1}$ at 60% critical mill speed and $36s^{-1}$ at 75% critical mill speed. Mill shear rates decreased with increasing slurry solids concentration. This was attributed to increased particle-particle interactions and reduced voidage. There is less volume available for particle shearing. The magnitude of the maximum shear rate is higher for the 75% critical mill speed at all slurry solids concentrations compared to the shear rates at the lower mill speed. At a higher speed the mill charge is fairly dilated by the strong centrifugal effects that oppose the natural packing structure which results in an overall decrease in bulk density. The increased voidage allows more volume for relative motion, producing an overall increase in shear rate.

The narrow shear rate range and the Bingham rheological behaviour of the slurry resulted in a constant viscosity value that could be used in a viscosity model provided the solids concentration is uniform across all regions of the mill. Viscosity is more significantly impacted by solids concentration than shear rate distributions in the tumbling mill. Work should be done to study the solids concentration profiles in the tumbling mill to provide better insight on areas of active transport.

Table of Contents

Declaration ..... **i**

Acknowledgements ..... **ii**

Executive Summary ..... **iii**

Table of Contents ..... **iv**

List of Figures ..... **v**

List of Tables ..... **iv**

Nomenclature ..... **vii**

1. INTRODUCTION **1**

1.1. Background to the research project **1**

1.2. Problem statement **2**

1.3. Scope of study **2**

1.4. Hypotheses **3**

1.5. Aim and objectives of the project **4**

1.6. Layout of the thesis **4**

2. LITERATURE REVIEW **6**

2.1. Overview of the grinding process in comminution **6**

2.2. Charge motion in tumbling mills **7**
2.2.1. The effect of mill speed on charge motion. 9
2.2.2. The effect of the mill filling on charge motion 10

2.3. The mechanisms of transport of slurry in tumbling mills **11**

2.4. Basic concepts of slurry rheology **13**

2.5. The effect of slurry rheology in grinding mills **14**

2.6. The key variables that affect slurry rheology **16**
2.6.1. Solids concentration 16
2.6.2. Particle size distribution and particle size 18
2.6.3. Temperature 21

2.7. The rheological measurement of mineral slurries **22**

2.8. Key issues to be considered when selecting a type of viscometer 24
2.8.1. Shear rate range..... 24
2.8.2. Particle size distribution..... 25
2.8.3. Turbulence 25

2.9. Rheological models..... 25

2.10. The development of Positron Emission Particle Tracking (PEPT)..... 27

2.11. A description of the PEPT technique..... 28
2.11.1. A description of the Birmingham positron camera..... 28
2.11.2. The Labelling technique of the tracer particle 31
2.11.3. Estimation of velocity distributions from particle paths using PEPT..... 33
2.11.4. Methods for computing estimates of shear rate in a tumbling mill 35

3. SAMPLE PREPARATION AND EXPERIMENTAL PROCEDURES..... 38

3.1. Introduction..... 38

3.2. Test materials and particle characterization..... 39

3.3. Description of PEPT experimental apparatus 39
3.3.1. The PEPT Experimental Programme..... 40
3.3.2. PEPT slurry tests procedure..... 41

3.4. Description of the Rheology experimental apparatus 45
3.4.1. The water curve calibration on the Paterson and Cooke U-tube rheometer .. 47
3.4.2. The Rheology Experimental Programme..... 48
3.4.3. Rheology tests sampling procedure 48

4. RHEOLOGY RESULTS AND DISCUSSION..... 50

4.1. Presentation of rheology experimental data..... 50
4.1.1. Rheograms at different solids concentrations 50

4.2. Correction of systematic error in rheological measurements..... 51

4.3. Fitting rheology models to experimental data..... 54

4.4. The computation of viscosity at different solids concentrations..... 58

4.5. Discussion of results..... 60
4.5.1. Effect of solids concentration on viscosity 60

5. PEPT RESULTS AND DISCUSSION..... 63

5.1. Introduction to PEPT data analysis..... 63

5.2. Computing absolute velocity profiles from PEPT data..... 65
5.2.1. Absolute velocity profiles trends at different solids concentrations and mill speeds. 66

5.3. Computing the tangential velocity profiles in the tumbling mill from PEPT data 68
5.3.1. Tangential velocity profile trends at different solids concentrations and mill speeds 70

5.4. Computing shear rate profiles in a tumbling mill using PEPT data 72

5.5. Shear rate Discussion 74

6. COMPUTATION OF VISCOSITY PROFILES IN TUMBLING MILLS 76

6.1. Summary of results 76
6.1.1. Key findings from rheology experiments 77
6.1.2. Key findings from PEPT experiments 78
6.1.3. Viscosity profiles in the tumbling mill. 80

7. CONCLUSIONS AND RECOMMENDATION 83

7.1. Conclusions 83

7.2. Recommendations 85

8. REFERENCES 87

APPENDIX A: RHEOLOGY RESULTS 100

APPENDIX B: PEPT RESULTS 109

List of Figures

Figure 2-1 A picture showing different regions of the tumbling mill charge (Powell and Nurick, 1995). 8

Figure 2-2: A schematic diagram showing the trajectory of grinding media in a tumbling mill (Wills and Napier-Munn, 2006). 9

Figure 2-3: The variation of shoulder position with mill filling and mill speed (Morrell, 1993) 11

Figure 2-4: The variation of toe position with mill filling and mill speed (Morrell, 1993) 11

Figure 2-5: Schematic diagram showing the components of a typical grate discharge tumbling mill (Latchireddi and Morrell , 2003a). 12

Figure 2-6: Shear stress vs. shear rate curves (He, et al., 2004) 13

Figure 2-7: Net production and Brookfield viscosity as a function of percent solids in batch grinding tests run to a constant grind time under constant mill and feed conditions (Klimpel,1982). 15

Figure 2-8: Variation of apparent viscosity with solids concentration for limestone slurries (He et al., 2006) 18

Figure 2-9: Typical flow curves flow curves for a base metal are at different solids concentration and particle sizes (Shi, 1994) 19

Figure 2-10: Effect of particle size and distribution on the rheological behaviour of limestone slurry at 70wt% (He et al., 2006) 21

Figure 2-11: The Paterson and Cooke U-tube rheometer used to conduct all the rheology experiments. 23

Figure 2-12: A sequence of particle position tracking in PEPT. (Bbosa, 2010) 28

Figure 2-13: The configuration of the PEPT camera at the University of Birmingham (UK) 30

Figure 2-14: Different event pairing recorded by the Birmingham positron camera (Stellema et al., 1998) 30

Figure 2-15: Velocity profile across a perpendicular line to free surface in a rotating cylinder (Yamane et al., 1998) 36

Figure 3-1: The experimental rig setup used to conduct the slurry PEPT experiments 40

Figure 3-2: A picture of the 1mm bluestone particle used to represent the slurry particle. 41

Figure 3-3: Positron emitting glass bead used as location marker to trace out the mill shell 43

Figure 3-4: The rheometer experimental set-up used to conduct the rheology tests using mineral ore-water suspensions. 45

Figure 3-5: Rheogram of the water calibration curve obtained from the tube rheometer 47

Figure 4-1: Rheograms for the -75+53 microns size fraction at different solids concentrations 50

Figure 4-2 Water rheogram data fitted to a straight line and a quadratic polynomial .. 51

Figure 4-3: Corrections to rheogram data for the d=-75+53 size fraction at different solids concentration 53

Figure 4-4: Bingham Model fit to -75+53 microns El Soldado slurry rheograms at different solids concentrations 55

Figure 4-5: Casson Model fit to -75+53 microns El Soldado slurry rheograms at different solids concentrations. 56

Figure 4-6: Herschel-Bulkley Model fit to -75+53 microns El Soldado slurry rheograms at different solids concentration. 57

Figure 4-7: Apparent viscosity for d=-75+53 El Soldado slurry at different solids concentrations 59

Figure 4-8: Yield stress for d=-75+53 El Soldado slurry at different solids concentrations..... 60

Figure 5-1: An example of the raw data file generated from PEPT..... 64

Figure 5-2: Magnitude plot of absolute velocity profile for a1mm bluestone slurry particle at 30%wt solids concentration at 60% (left) and 75% (right) critical mill speeds. 66

Figure 5-3: Velocity vector profile for a1mm bluestone slurry particle at 30%wt solids concentration at 60% (left) and 75%(right) critical mill speeds. 67

Figure 5-4: Magnitude plot of the tangential velocity profile for a1mm bluestone slurry tracer particle in 30%wt slurry at 60% (left) and 75% (right) critical mill speed..... 69

Figure 5-5: Variation of tangential velocity along a diametrical line passing through the mean CoC for a1mm bluestone tracer particle in 30%wt slurry at 60%(left) and 75% (right) critical mill speed. 71

Figure 5-6: Magnitude plot of shear rate profile for a1mm bluestone slurry particle at 30%wt solids concentration at 60% (left) and 75%(right) critical mill speeds..... 73

Figure 5-7: Mill shear rates at different angular positions for a 1mm bluestone slurry particle at 30%wt solids concentration and 60%(left) and 75%(right) critical mill speeds. 74

Figure 5-8: Maximum shear rates at different solids concentrations and mill speeds. . 75

Figure 6-1 : El Soldado slurry rheograms for different solids concentrations at the measured in-situ shear rate ranges obtained at 60% critical mill speeds. 81

Figure 6-2: El Soldado slurry rheograms for different solids concentrations at the measured shear rate ranges obtained at 75%% critical mill speeds. 81

List of Tables

Table 2-1: The distribution modulus (m) and size modulus (k) obtained by fitting the experimental size distribution data to the Rosin-Rammler equation. 21

Table 2-2: Models describing slurry rheograms 26

Table 3-1: The PEPT mill specifications 39

Table 3-2: Experimental variables used during PEPT experiments..... 39

Table 3-3: The experimental programme used for PEPT tests 41

Table 3-4: The measured slurry tracer particle activity. 44

Table 3-5: Tube rheometer, pump and sump dimensions..... 46

Table 3-6: The experimental programme for rheology tests..... 48

Table 4-1: Bingham Model Parameters at different solids concentrations for the -75+53microns particle size fraction..... 56

Table 4-2: Casson Model Parameters at different solids concentrations for the..... 57

Table 4-3: Herschel-Bulkley Model Parameters at different solids concentrations for the -75+53microns particle size fraction..... 58

Table 6-1: Slurry viscosities obtained at 60% and 75% critical mill speeds 82

Nomenclature and Abbreviations

τ: shear stress (Pa)

τ_B: Bingham yield stress (Pa)

$\tau_{HB:}$ Herschel Buckley (HB) yield stress (Pa)

τ_c: yield stress correction factor (Pa)

C: consistency index

P: power index

γ: shear rate (s^{-1})

η: viscosity (Pa.s)

$\eta_{B:}$ Bingham viscosity (Pa.s)

$\eta_{\infty:}$ asymptotic shear viscosity(Pa.s)

wt%: weight percentage by mass (kg)

vol%: weight percentage by volume (m^3)

ϕ: solids concentration by volume (vol%)

V_c : minimum settling velocity ($m.s^{-1}$)

$F_{L:}$ dimensionless factor

Dpipe: pipe/tube diameter (m)

$\rho_{s:}$ density of transported solid particles ($kg.m^{-3}$)

$\rho_{L:}$ density of the fluid ($kg.m^{-3}$)

N_c : critical speed (rev/min)

Dmill: mill diameter (m)

d : rod/ball diameter (m)

d50: particle size at which 50% of the material passes (μm)

k-: size modulus

m: distribution modulus

g: gravitational constant =$9.81 m^2/s$.

PEPT: Positron Emission Particle Tracking

CoC: Centre of circulation

μCi : micro curie.

DC: Direct Current

1. INTRODUCTION

1.1. Background to the research project

Grinding is an important industrial operation which enables the liberation of valuable minerals for subsequent processing. Grinding is an expensive operation and forms a significantly large portion of both the capital and operating costs in mineral processing plants (Napier-Munn et al., 1996). It accounts for the highest amount of energy utilized on a concentrator. Industrial grinding efficiencies are quoted to be 1% to 30% of the theoretical energy required to break material. Wet grinding is more favourable than dry grinding because wet grinding is 1.2 to 1.5 times faster and most material can be ground finer when wet (Klimpel,1997).

The efficiency of wet grinding processes is affected by the rate of breakage of particles and the rate of transport of the slurry within and out of the mill. The focus of this research is on the transport of material in the mill. The grinding mill must allow the breakage products to flow out at a sufficiently high rate out of the mill to prevent the overloading of the mill or over grinding of the already liberated material. For grate discharge mills, the pan lifters must also have sufficient capacity to remove all the material that flows through the grate. The transport of material in the tumbling mill is influenced by the rheological properties of the solid-liquid mixture that forms the slurry. Viscosity is an important factor controlling mill hold up and discharge through the grate (Moys, 1989). The optimization of the rheological behaviour of slurries during grinding can increase throughput, product fineness and energy efficiency.

The existing transport and discharge models are empirical due to the difficulty associated with the measurement of fundamental drivers in their formulation. The complex environment in the tumbling mill and the non-linear flows through the interstices of the charge make the existing flow models such as the Ergun equation insufficient to fully describe the transport of both fluid and particles in these systems. There is a need to develop a mechanistic transport model that can be used for design and optimization studies of tumbling mills. Equations formulated by (Ergun, 1952) and (Shi, 1994) show that viscosity and porosity have a significant influence on the transport of slurries in packed bed systems. The work in this study aims to develop a

methodology for characterising in-situ viscosity profiles in tumbling mills that can possibly be incorporated in transport models.

Mineral slurries are known to exhibit non- Newtonian behaviour. For the suspensions encountered in grinding mills, slurry viscosity is not constant but is a function of shear rate (Shi and Napier-Munn, 1999). According to (Bazin and Chapleau, 2004) the identification of shear rates existing in a grinding mill is important as it determines the slurry viscosity values which will be used to assess the effect of viscosity on grinding performance. In this work the Positron Emission Particle Tracking (PEPT) technique was used to obtain the in-situ shear rate distributions in the different regions of the grinding mill. For the same slurry used in PEPT experiments, rheology experiments were conducted using a tube rheometer to obtain rheograms which describe the rheological properties of the slurry at different solids concentrations. The rheometer experiments enabled the quantification of viscosity from the slope of the rheogram curves at the shear rate ranges obtained from the PEPT experiments. Viscosity distributions in regions of interest in the mill were then determined.

1.2. Problem statement

Slurry viscosity distributions across the mill have a significant effect on the transport of material inside the mill. To determine the influence of slurry viscosity on the transport of particles it is important to first quantify the typical shear rate ranges that occur in the various regions of the tumbling mill when operated under different conditions. Shear rate characterization in the mill can be calculated from average velocity distributions and displacement data obtained by performing tumbling mill experiments using the PEPT technique. PEPT is a technique that is used to study the in-situ motion of particles in granular and fluid systems using a single radioactive tracer. Rheology experiments were performed using a tube rheometer to obtain rheograms of the slurry under consideration. The shear rate distributions from the PEPT data were then combined with the rheology data from the rheometer experiments to obtain viscosity distributions for regions of interest in the mill.

1.3. Scope of study

This research project made use of in-situ data obtained from the PEPT technique to determine shear rate distributions for the various regions in the mill. The PEPT

experiments were performed at the University of Birmingham. PEPT experiments were conducted using slurry at different solids concentrations and mill speeds. The solids concentration was varied from 10% to 60% by mass. The mill speed ranged between 60% and 75% of the critical mill speed. All other mill configuration parameters such as mill filling and the lifter profiles were kept constant. The PEPT results provided information about the in-situ shear rate distribution across the mill at different mill operation conditions.

Rheology experiments were conducted at the University of Cape Town using a rheometer supplied by Paterson and Cooke (Kahn, 2005). The solids concentrations for these experiments were varied from 10% to 60% by mass. Although most mills operate at solids content from 68% - 78%, lower values were chosen due to the limitations imposed by the equipment which will be discussed in Chapter 3. The rheograms obtained provided information to characterize the slurry for a wide range of shear rates.

A methodology for combining in-situ shear rates from PEPT and rheology data from rheometer experiments to obtain viscosity distributions profiles in the tumbling mill has been developed and demonstrated using the data from the two sets of experiments.

1.4. Hypotheses

The hypotheses that were tested in this work are as follows:

- ***Shear rates of slurry decrease with increasing solids concentration due to increased particle-particle interactions.***

- ***Shear stress is maximum at the rising charge region of the mill towards the mill shell due to an increase in particle number density and particle slippage.***

- ***Insitu viscosity distributions can be computed from combining the shear rate information from particle tracking using PEPT and rheograms data from Rheology experiments.***

1.5. Aim and objectives of the project

The aim of this project was to develop a quantitative methodology for computing and characterising viscosity distributions across the tumbling mill. The objectives formulated for this thesis were:

- To obtain the rheological characteristics of the slurry for a wide shear rate range at different solids concentrations using a U-TUBE rheometer.

- To investigate the variation of shear rate distributions with solids concentration in a tumbling mill by tracking a single particle using PEPT at different solids concentrations.

- To investigate the variation of shear rate distributions with mill speeds by tracking a single particle using PEPT in a tumbling mill operated at different mill speeds.

- To develop a methodology for computing viscosity distributions at regions of interest in a tumbling mill from combining in-situ shear rate information from PEPT experiments and rheology data obtained from rheometer experiments.

1.6. Layout of the thesis

Chapter 1: This chapter introduces, contextualises and provides a motivation for the research that was carried out in this thesis. It also provides a background to the thesis which led to the formulation of the thesis objectives and hypotheses.

Chapter 2: This chapter presents a review of literature related to the subject of this thesis. An overview of the comminution process and a discussion and review of slurry rheology and PEPT literature is also presented.

Chapter 3: A description of the experimental methodology used to conduct rheology and PEPT experiments is provided. The sample preparation and sampling methods are discussed and other materials used in the experimental work are also presented.

Chapter 4: This chapter presents the results and discussion of the Rheology experiments.

Chapter 5: This chapter presents the results and discussion of the PEPT experiments performed using a laboratory scale tumbling mill.

Chapter 6: The methodology developed for combining PEPT and Rheology information to obtain the viscosity distributions for regions of interest in the tumbling mill is presented in this chapter.

Chapter 7: Conclusions focussing the significant findings from the work performed in this thesis are presented and recommendations for further work are given in this chapter.

2. LITERATURE REVIEW

Overview

This chapter presents a review of existing literature related to the subject of this thesis. The mechanisms of slurry transport and charge motion in tumbling mills are described. A review of slurry rheology literature is also presented. A description of the PEPT technique and how it can be used to estimate in-situ tumbling mill shear rates is also given.

2.1. Overview of the grinding process in comminution

Grinding is an important industrial process which enables the liberation of valuable minerals for the subsequent concentration process. It is the last stage in the comminution process (Napier-Munn et al., 1996) .The degree of grinding of an ore particle depends on the probability of it entering a zone between the medium shapes and the probability of some breakage occurrence taking place after entry. Since grinding is the single highest operating cost, the ore should not be ground any finer than is justified economically. Overgrinding reduces the particle sizes of both the valuable mineral and gangue below the size required for the most efficient separation (Wills and Napier-Munn, 2006). Finer grinding should not be carried out beyond the point where the net smelter return for increased recovery becomes less than the added operating costs (Steane, 1976; Fuerstenau and Abouzeid, 2002). Undergrinding results in a mill product that is too coarse with a low degree of liberation for economic separation. This also results in poor recovery and low enrichment ratio being achieved in the concentration stage (Wills and Napier-Munn, 2006; Klimpel, 1997).

Grinding is the most energy intensive operation in a minerals operation circuit. According to Wills and Atkinson (1993) most of the kinetic energy of the tumbling load is dissipated as heat, noise and only a small fraction being expended is actually utilized for breaking the particles. Grinding mills are classified into two types which are namely tumbling and stirred mills. In this research work a laboratory scale tumbling mill was used to conduct all the PEPT experimental investigations. Tumbling mills are typically used in the minerals industry for coarse grinding in which particle sizes are reduced to between 40 and 300 microns. In tumbling mills, the mill shell is rotated and motion is imparted to the charge via the mill shell. The

grinding media used may be steel balls, rods or the rock particles themselves (Wills and Napier-Munn, 2006). Tumbling mills are extremely energy inefficient but they have a high degree of mechanical efficiency (Fuerstenau and Abouzeid, 2002). The ore is broken as a result of repeated, random impacts which break both the liberated and unliberated particles. Optimum liberation could be obtained if these impacts could be directed at the interfaces between the mineral grains. The product size is controlled by the type of medium used, charge level, speed of rotation, nature of ore feed and the type of circuit used (Fuerstenau et al., 1999; Napier-Munn et al., 1996; Austin, 2002; Wills and Napier-Munn, 2006). For the purposes of this work, mono-sized 5mm glass beads were used as grinding media and no breakage was intended to take place since the focus of this work was on slurry transport in tumbling mills.

2.2. Charge motion in tumbling mills

The mill charge is composed of the ore particles, water and the grinding media. The mill filling is the volume fraction of the charge in a tumbling mill which occupies the volume of the mill. As the mill rotates, the charge is lifted up the rising face of the mill until a position of dynamic equilibrium also referred to as the shoulder position is reached. At the shoulder position, the bulk of the charge falls down towards the toe region (Davis, 1919; Liddell, 1986; Morrell, 1992, 1993). The two types of charge motions that are dominant in grinding mills are cascading and cataracting motions. Cascading motion is when the grinding media rolls down to the toe of the charge. Cataracting motion is when the grinding media is projected clear of the charge before landing on the toe of the charge. The charge bodies cascade and cataract down the free surface of the other bodies, about a dead zone where little movement occurs down to the toe of the mill charge (Napier-Munn et al., 1996).

According to Napier-Munn et al., (1996), there are also two main regions within the charge where breakage takes place. The first is the toe region where impact breakage occurs. The frequency with which the charge turns over and the energy generated on impact influences the amount of breakage which takes place. The second region of breakage is within the body of the charge as it is rotated within the mill. In this region the charge is composed of a series of layers which slip over one another. This results in an angular velocity gradient in the charge. This motion promotes abrasion and

attrition breakage within the mill. The frequency of this type of breakage depends on the number and relative velocity of the layers. This second region of breakage resulting from the angular velocity gradient in the charge layers is the area of interest in this thesis. The quantification of the velocity gradient between charge layers leads to the computation of shear rates.

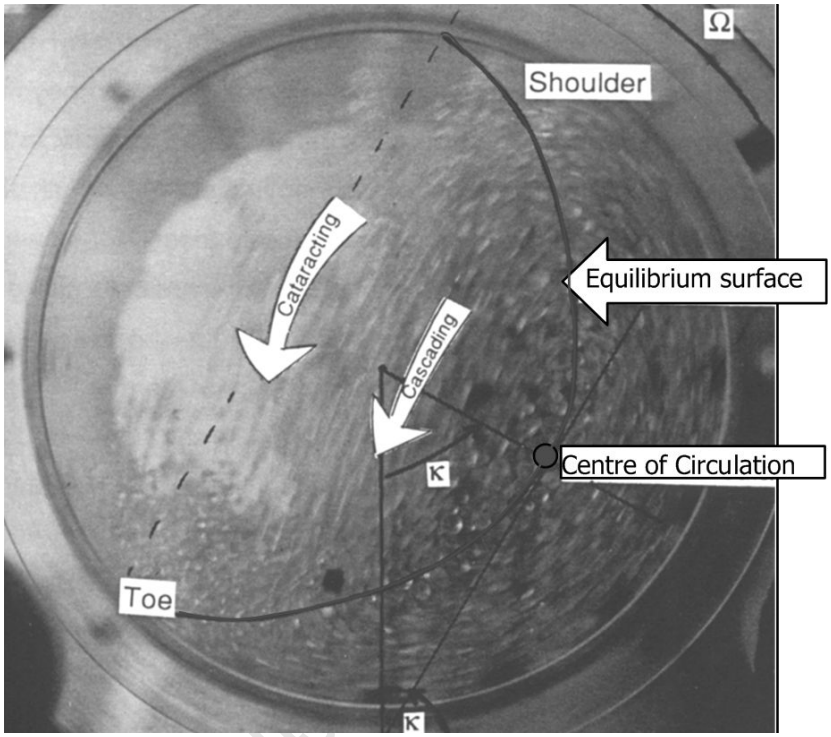

Figure 2-1 A picture showing different regions of the tumbling mill charge (Powell and Nurick, 1995).

Figure 2-1 shows the different regions found in a tumbling mill charge. The equilibrium surface is the surface that divides the ascending, en masse charge from the descending charge. It starts at the toe and ends at the shoulder of the charge. It passes through the centre of circulation (CoC) of the charge and is seen as a line in an end-view of the mill in Figure 2-1 (Powell and Nurick, 1995, 1996). The CoC is a region within the charge about which the entire charge circulates. It gives a good measure of the location of the charge. The COC is located at the point where a tangent line to the equilibrium surface intersects a radial line at exactly 90degrees (Govender, 2005). The angle of repose κ shows the angular location of the CoC (Vermeulen, 1988; Powell and Nurick, 1995).

2.2.1. The effect of mill speed on charge motion.

Liddell, (1986); Liddell and Moys, (1988); Wills and Napier-Munn, (2006); observed that the motion of the charge varies with mill speeds. The mill speed governs the nature of the mill product and the amount of wear on the shell liners. The driving force of the mill is transmitted via the liner to the charge. At low speeds, the medium rolls down to the toe of the mill and abrasive comminution mainly occurs. This cascading results in finer grinding with increased slimes production and liner wear.

During rotation the medium follows a path which has two parts. The lifting section near the shell liners is circular while drop back to the toe of the mill charge is parabolic.

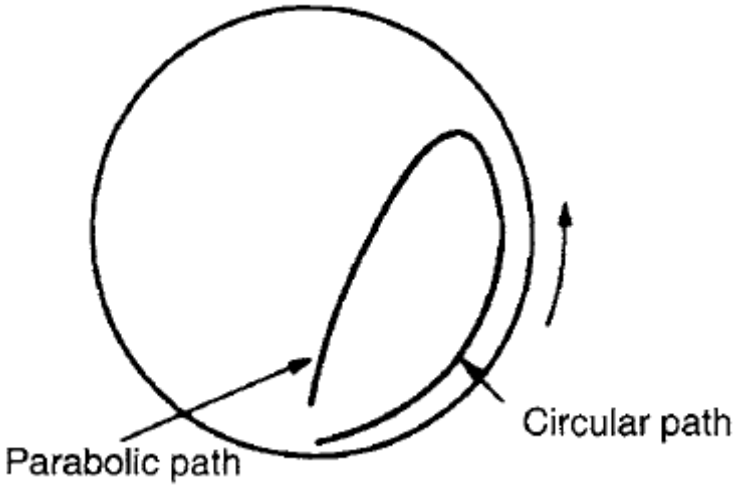

Figure 2-2: A schematic diagram showing the trajectory of grinding media in a tumbling mill (Wills and Napier-Munn, 2006).

At higher speeds, the medium is projected clear of the charge before landing on the toe of the charge. This projection can be described by a series of parabolas. This cataracting motion results in comminution by impact and a coarser end product with reduced liner wear (Wills and Napier-Munn, 2006). Powell and Nurick, (1995) also observed that as the mill speed increases, the angle of repose of the CoC also increases.

At the critical mill speed, centrifuging occurs and the medium rotates in a fixed position against the mill shell. The entire charge does not centrifuge at the same speed. Centrifuging starts in the outer layers of the charge. Further increases in mill speed causes more charge layers to centrifuge until the entire charge is centrifuging (Morrell, 1993).

The critical mill speed is calculated using the formula below:

$$N_c = \frac{42.3}{\sqrt{Dmill - d}} \quad \text{rev/min where:} \qquad (2.1)$$

N_c = critical speed (rev/min)

Dmill= mill diameter (m)

d = rod/ball diameter (m)

This formula assumes there is no slip between the medium and the shell liner (Napier-Munn et al., 1996; Wills and Napier-Munn, 2006).

In practice mills are operated at speeds between 50%- 90% of the critical speeds depending on economic considerations. Increasing the mill speed will increase the mill capacity. Very low speeds are sometimes used when full mill capacity cannot be attained and high speeds are used for high capacity coarse grinding (Wills and Napier-Munn, 2006; Liddell and Moys, 1988). In this work, the mill speed was varied between 60% and 75% of the critical mill speed which covers the most commonly applied industrial mill speeds.

2.2.2. The effect of the mill filling on charge motion

Mill filling mainly influences the position of the toe and shoulder regions in the charge. The charge behaves as a collective body. The material lower down the rising face of the mill pushes the higher material further up. At higher mill fillings, this pushing effect becomes more pronounced and results in higher shoulder angles. As demonstrated by Figure 2-3 and Figure 2-4, shoulder angles increase with mill speed at any given mill filling. At any given mill speed, the highest mill filling has the highest shoulder angle. Larger mill fillings result in higher shoulder angles but lower toe angles (Morrell, 1993).

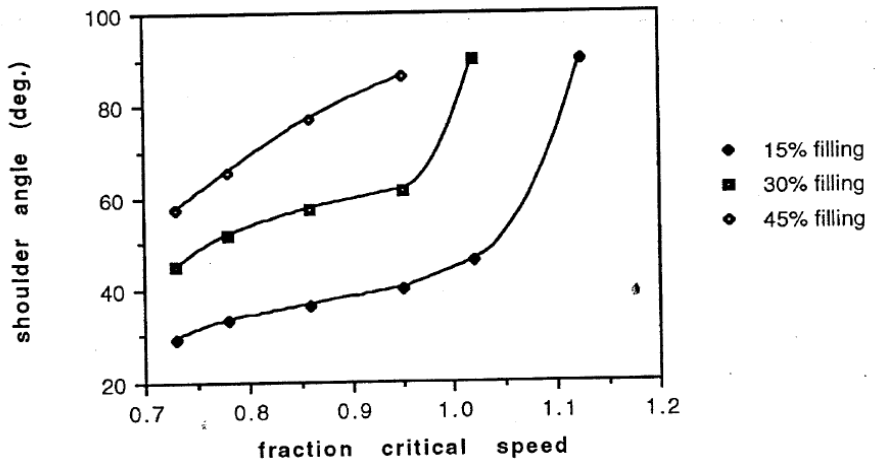

Figure 2-3: The variation of shoulder position with mill filling and mill speed (Morrell, 1993)

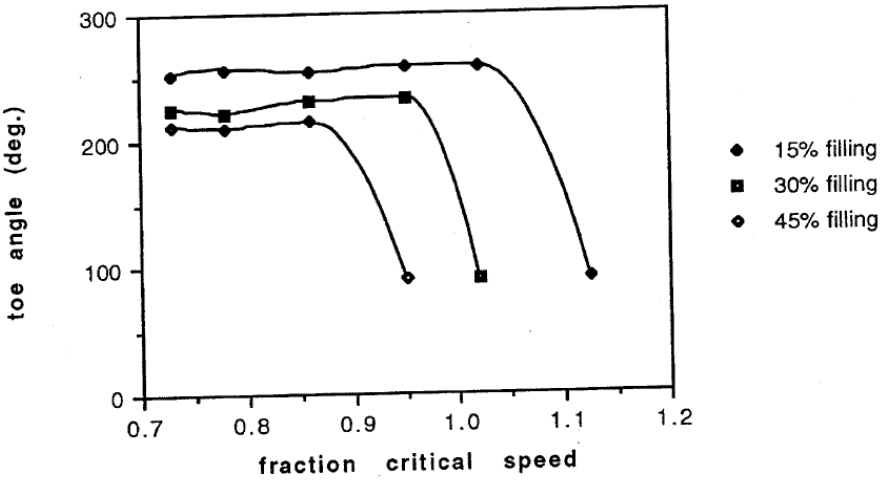

Figure 2-4: The variation of toe position with mill filling and mill speed (Morrell, 1993)

The mill speed at which centrifuging begins is also a strong function of the mill filling. Higher mill fillings centrifuge at much lower speeds (Morrell, 1993).

2.3. The mechanisms of transport of slurry in tumbling mills

Moys, (1986); Hogg and Rogovin, (1982); Klimpel et al.,(1989); Morrell and Stephenson, (1996); Latchireddi and Morrell, (2003); were in agreement that in grinding mills, the slurry and sub grate particles exits the mill by either going through

the grate for grate discharge mills or flowing over the discharge trunnion for overflow mills. The driving force of flow of slurry from the feed to the discharge end of the mill is the flow gradient between the feed trunnion and the discharge trunnion. The driving force for slurry transport from the mill shell to the grate holes is the pressure head difference across the grate. If the grate provides higher resistance to the flow of slurry, then the mill will fill up with an excessive amount of slurry to a level where inefficient grinding occurs. All autogenous and semi-autogenous grinding mills use steel or rubber grates to hold back the grinding media whilst allowing the product slurry to flow through and out of the mill. The different components of the mill which are relevant to the transport of material inside the mill are shown in Figure 2-5.

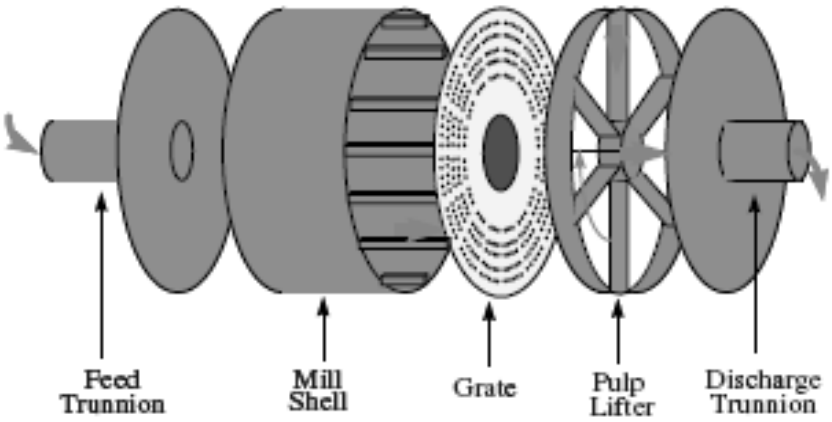

Figure 2-5: Schematic diagram showing the components of a typical grate discharge tumbling mill (Latchireddi and Morrell , 2003a).

1. Feed trunnion: assembly through which the solids and water enter the mill.

2. Mill Shell: the main chamber where ore particles are broken due to the tumbling action of the mill.

3. Grate: screen which allows the ground ore particles and water to pass through in the form of slurry.

4. Pulp lifter: transports the slurry that passes through the grate into the discharge trunnion.

5. Discharge trunnion: assembly through which the mill product discharges.

2.4. Basic concepts of slurry rheology

Rheology is the science of the flow and deformation of matter (Whorlow, 1992; Tanner, 2000). There are different types of laminar deformations which are expressed using shear stress and shear rate. Shear stress (τ) is a force applied per unit area tangentially to the surface of the body to produce flow. It is expressed in Pascals (Pa) Shear rate (γ) is the rate of deformation of flow expressed in seconds^{-1} (s^{-1}).

A plot of shear stress versus shear rate is called a rheogram or a flow curve (Van Wazer et al, 1963). There are two types of flow curves, namely Newtonian and non-Newtonian. Figure 2-6 illustrates the different types of flow curves. Most slurries exhibit non - Newtonian behaviour at solid concentrations above 15% by volume. For example a base metal slurry with a 20% fines content passing 38μm would exhibit non-Newtonian behaviour (Shi and Napier, 1996a). The types of non- Newtonian fluids include pseudoplastics, dilatant fluids with or without yield stress and Bingham plastics. Pseudoplastics exhibit shear thinning behaviour while dilatant fluids exhibit shear thickening behaviour. Mineral slurries found in tumbling mills are known to exhibit non-Newtonian behaviour (Shi, 1994; Wang and Forssberg, 1995; Kawatra et al., 1996; Klimpel, 1999).

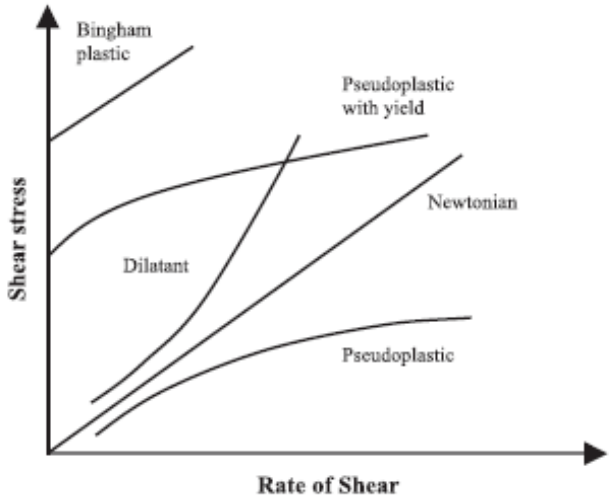

Figure 2-6: Shear stress vs. shear rate curves (He, et al., 2004)

Rheological behaviour of slurries can be classified as either time dependent or time independent behaviour. Time dependent behaviour is characterized by the viscosity of

the fluid changing with time under constant shear conditions. When a material becomes more fluid with increasing time of flow under steady state conditions, it is called thixotropy while rheopexy behaviour results in a fluid becoming more resistant to flow with increasing time under steady state. Most industrial grinding operations are continuous; the rheology involved is denoted as time –independent slurry behaviour (Kawatra et al., 1996; Klimpel, 1997).

Viscosity (η) is the resistance to deformation and is expressed in Pascal-seconds (Pa.s). It determines the fluidity of slurry. The apparent viscosity is defined as the ratio of shear stress to shear rate. It is the slope of the flow curve from the origin to a particular point on the flow curve (Van Wazer et al., 1963; Whorlow, 1992; Wang and Forssberg, 1995). For Newtonian fluids, the apparent viscosity is constant at different shear rates while for non- Newtonian fluids the apparent viscosity varies with shear rates. The apparent viscosity for dilatant materials increases with increasing shear rates whereas for pseudoplastic materials, it decreases with increasing shear rate. It is therefore critical to compare the apparent viscosities for non- Newtonian fluids at the same shear rate (Shi, 1994). This is because the apparent viscosities attained for non-Newtonian flow curves are dependent on the shear rates at which they were measured.

Another property that affects the rheology of slurries is yield stress. The intercept at the shear stress axis on a rheogram is the apparent yield stress. Most slurries at high solid concentrations will not flow if the shear stress does not exceed a certain value called yield stress. Plastic viscosity is another property used to characterize the rheological behaviour of non- Newtonian fluids. At high shear rates the, pseudoplastics behave like Bingham plastics in that there is a near linear relationship between shear rate and shear stress (Gao and Forssberg, 1993; Napier-Munn,1983; Govier et al, 1957).

2.5. The effect of slurry rheology in grinding mills.

Slurry rheology influences the breakage mechanism of ore and the transportation of materials inside the mill in grinding circuits. It affects the wet comminution of materials in grinding mills as a result of increased inter-particle interactions or aggregation in the slurry (Jinescu, 1974; Tucker, 1982; Klimpel, 1982; Klimpel, 1983;

Napier-Munn et al., 1996; Shi and Napier- Munn, 2002; He et al, 2004). A viscous slurry reduces grinding efficiency by acting as a cushion and retarding impact forces between the media and the ore (Fuersteanau et al., 1984). A dilute slurry will result in an inefficient use of impact energy because the slurry will not be viscous enough to hold slurry in the impact zone of the media. The grinding media will not be adequately covered with particles therefore not all the energy is utilised to grind particles during impact. Grinding mill performance is therefore strongly influenced by the flow resistance of the slurry. An optimum slurry viscosity is required to obtain an efficient mill performance (Kawatra et al., 1997). Klimpel, (1982) also showed how grinding performance can be affected by the rheological characteristics of the slurry. Klimpel's observations are summarised in Figure 2-7.

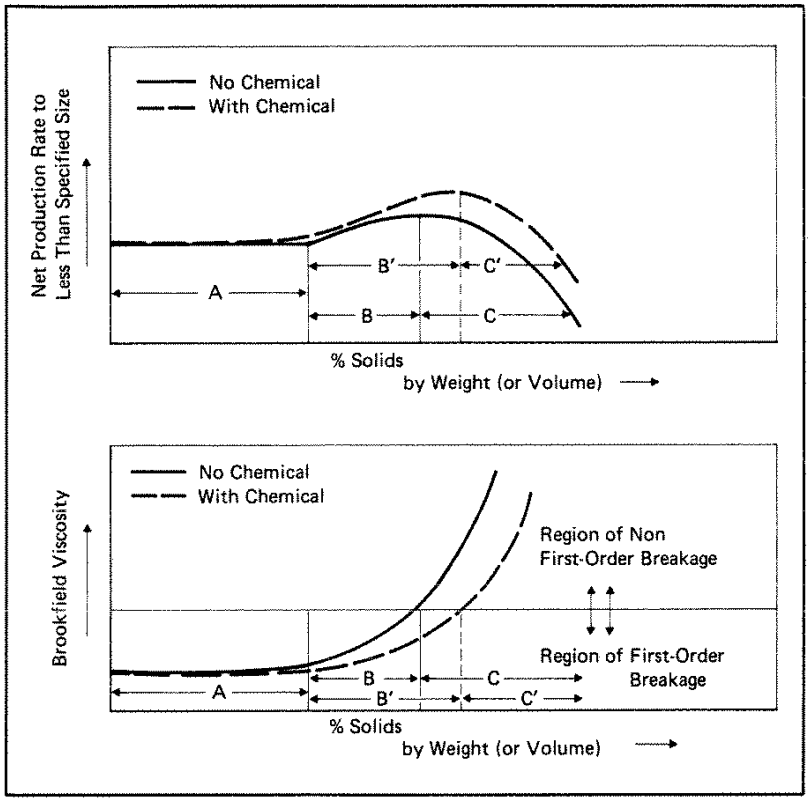

Figure 2-7: Net production and Brookfield viscosity as a function of percent solids in batch grinding tests run to a constant grind time under constant mill and feed conditions (Klimpel,1982).

Region A: At solids concentrations less than 40-45% by volume, slurry behaviour is dilatant. At these low slurry density and viscosity conditions, breakage is first order and there is no variation of mill production with viscosity.

Region B: At solid concentrations above 45% by volume, slurry behaviour becomes pseudoplastic. In the absence of yield stress the breakage rate increases and remains first order. This higher viscosity represents the most efficient grinding practice.

Region C: A further increase in solid concentration results in a yield stress which lead to undesirable non-first order breakage. This translates to a reduction in breakage rates. The excessive viscosity leads to decreased production.

Regions A', B' and C' represent the trends which will be observed if chemical additives where used as grinding aids to control the slurry rheology.

The breakage products must be transported out of the mill at a sufficiently high rate to prevent the mill from overfilling. The flow of material out of the mill is thus significantly influenced by slurry rheology.

2.6. The key variables that affect slurry rheology

The key factors that are considered to influence slurry rheology are solids concentration, temperature, and particle size and distribution (Klimpel, 1984; Kawatra and Eisele, 1988; He et al., 2004). The various ore types used in the mining industry have different densities and particle interactions which result in different rheological responses. There is a lot of literature which describes the effect these factors on slurry rheology but there are inconsistencies in the findings reported (Rutgers, 1962; Thomas, 1965; Clarke, 1967; Klimpel, 1997; Napier-Munn, 1983;1984; Kawatra et al,1988; De Bruijn,1951). Shi, (1994) deduced that the discrepancies imply that the rheology of suspensions is governed by the interaction of all the factors and not just a specific factor by itself. This is the view held by the author of this thesis.

2.6.1. Solids concentration

Solids concentration is one of the most important factors that affect the rheological behaviour of slurry of time independent suspensions. The effect of solids concentration is significant particularly at high percent solids as small changes in solids concentration result in large shifts in viscosity (Kawatra and Eisele, 1988). The influence of solids concentration on the slurry transport in the tumbling mill is thus significant.

At low solids concentration, viscosity increases linearly with increasing solids concentration (Rutgers, 1962). He et al., (2004) was in agreement with Rutgers, (1962) and also observed that at low solids concentrations, the rheological behaviour of slurries such as those found in the minerals industry may be Newtonian with viscosity being independent of shear rate. As the solids concentration increases, the rheological behaviour of slurry becomes more non-Newtonian (Tangsathitkulchai and Austin, 1988; Gao and Forssberg, 1993; Prestidge, 1997; Tangsathitkulchai, 2002). He et al., (2006); made similar observations when conducting rheological investigations using limestone, galena, dolomite slurries. It was observed that an increase in solids concentration transformed slurry rheological behaviour from a weakly dilatant (shear thickening) to a pseudoplastic (shear thinning) one with yield stress at solids concentration ranging from 60wt% (35.71vol%) to 78.5wt% (57.49vol%). At solids concentrations less than 65wt% (40.75%), the slurry showed a weakly dilatant behaviour. This was attributed to large inter-particle distances between particles which resulted in weak van der Waals forces. At low shear rates particles slip over each other and at higher shear rates the movement of particles is restricted. Investigations conducted using many coal and mineral slurries also showed dilatant characteristics at slurry concentrations in regions less than 40-45% solids by volume for a particular size distribution (Klimpel, 1982).

He et al., (2006) observed that at higher solids concentrations up to 67wt% (42.92vol%), the limestone slurry exhibits a pseudoplastic characteristic without yield stress at shear rates less than $663s^{-1}$ and a weakly dilatant behaviour at shear rates above $663s^{-1.}$ At lower shear rates, the attractive inter-particle forces are predominant over the hydrodynamic forces exerted by the flow field as opposed to shear rates higher than $663s^{1}$. Further solid concentration increases to above 70wt% (46.36vol %) lead to slurry behaviour changing to pseudoplastic with yield stress. Viscosity steeply increased at lower shear rates and showed shear thinning behaviour at increasing shear rates. At shear rates above $362s^{-1}$, there was a transition to a Bingham plastic flow behaviour. Similar rheological behaviour was observed for dolomite slurries (Gao and Forssberg, 1993; galena slurries (Prestidge, 1997); and quartz slurries (Tangsathitkulchai, 2002).

The limestone slurry viscosity increased exponentially with increasing solids concentration at certain shear rates as shown by Figure 2-8. This is in agreement with studies conducted on quartz slurries (Tangsathitkulchai and Austin, 1988) and on dolomite slurries (Velamakanni and Fuerstenau, 1993). The relationship between the apparent viscosity of limestone slurry and the solids concentration at a given shear rate can be described by the expression:

$$\eta p = a(\gamma)\exp b(\gamma)\phi \qquad (2.2)$$

where: ηp is the apparent viscosity; ϕ is the solids concentration by volume; $a(\gamma) and b(\gamma)$ are coefficients relating to a used shear rate. At higher shear rates, $a(\gamma)$ increases and $b(\gamma)$ decreases (He et al., 2006).

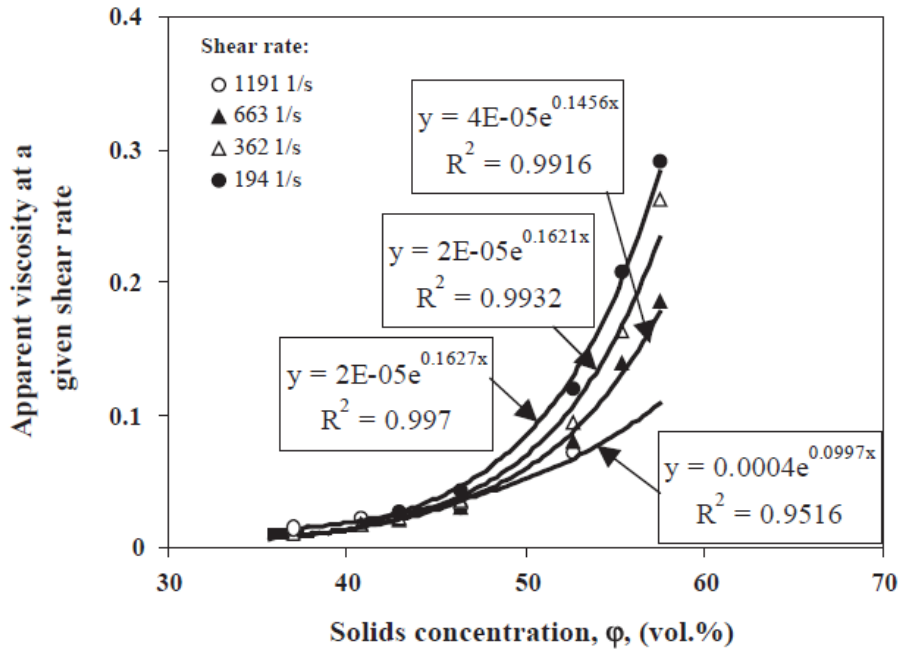

Figure 2-8: Variation of apparent viscosity with solids concentration for limestone slurries (He et al., 2006)

2.6.2. Particle size distribution and particle size

Particle size distribution and particle size have a significant influence on the rheological behaviour of slurry. Product fineness significantly increases with grinding time in wet comminution. Particle size is one of the dominant factors which give rise to the agglomeration and aggregation surface properties which result in rheological effects of slurries (He et al., 2004).

Figure 2-9 shows a wide range of rheological flow curves for a base metal ore as a function of solids concentration and particle size. This shows the interdependent relationship between solids concentration and particle size and their strong impact on the rheological behaviour of slurry (Shi, 1994). Tangsathitkulchai and Austin, (1988) also deduced that any rheological assessment of concentrated slurries which did not include a strong dependence of viscosity on particle size was incorrect. In this work, solids concentrations of up to 35% by volume and a particle size range of -75+53microns with a wide particle size distribution were investigated.

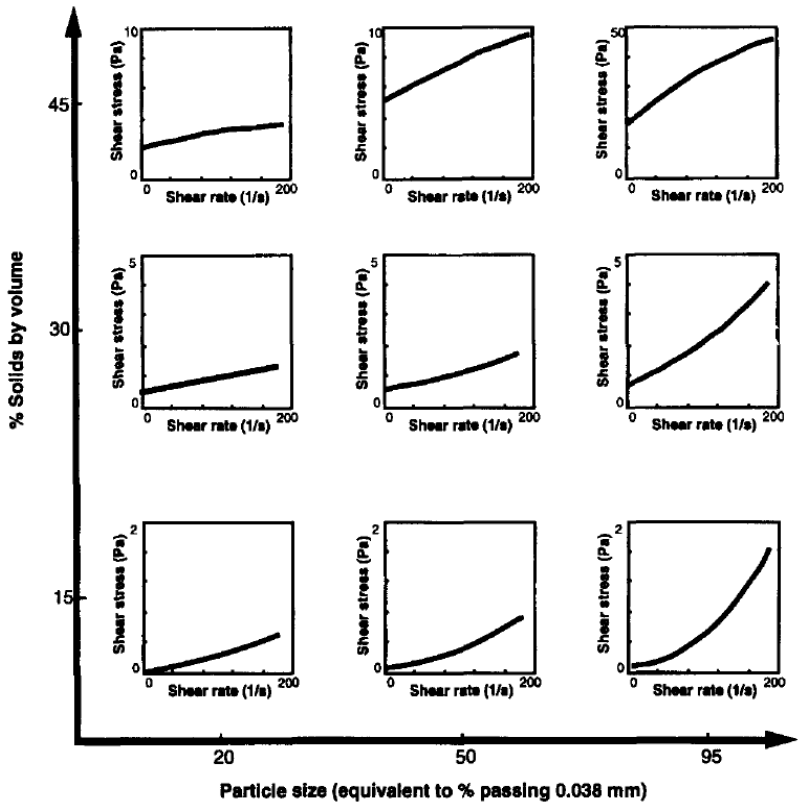

Figure 2-9: Typical flow curves flow curves for a base metal are at different solids concentration and particle sizes (Shi, 1994).

Kawatra and Eisele, (1988) observed that at a constant solids concentration, a reduction in particle size will result in an increase in slurry viscosity. This was attributed to an increased particle surface area. The amount of free fluid is reduced thus increasing the effective solids concentration. This was in contradiction with the work of Clarke, (1967) and De Bruijn, (1951) as reported by Thomas, (1965) which revealed that slurry viscosity increases with particle diameter. They attributed this to inertial effects which resulted in additional energy dissipation. Particle size

distribution is also an important parameter that affects the viscosity of the slurry. The viscosity of the slurry having a wide particle size distribution is smaller than that of slurry with particles of identical sizes (Jinescu, 1974). This conclusion is also in agreement with the work done by Logos and Nguyen, (1996) who added a narrow sized coarse coal fraction (208-279μm) to fine sub 45μm particles at a fixed solids concentration. They found that slurry viscosity was significantly reduced.

He et al., (2006) investigated the effect of three different particle size distributions on the rheological behaviour of limestone slurries at 70wt% (46.36 vol%) solids concentration as shown by Figure 2-10. Table 2.1 shows the extrapolated parameters of the particle size distributions from fitting the Rosin Rammler equation. K indicates the finess and m indicates the particle size distribution of the raw material. R^2 shows the goodness of fit. A decreasing k value means the material is finer while a reduction in m values means the particle size distribution is broader. Raw material 1 is coarse with a broad size distribution while Raw material 3 is the finest with a narrow size distribution. The slurries exhibited pseudoplastic behaviour with yield stress at lower shear rates followed by a transition to Bingham plastic behaviour at higher shear rates. At a finer particle size with a narrower size distribution, the degree of pseudoplasticity became more evident, the viscosity at a given shear rate and yield stress of slurries increased. The transition to pseudoplastic behaviour also shifted to higher shear rates. The Bingham yield stress exponentially increased with increasing distribution modulus (m) and decreases with higher k values. This was attributed to stronger inter-particle attractions in slurry with finer particle. Similar conclusions were observed for titanium dioxide (Yang et al., 2001) and for coal (Tangsathitkulchai and Austin, 1988; Lagos and Nguyen, 1996). The smaller the particle size and the narrower the size distribution, the more evident the pseudoplastic behaviour with a larger yield stress and apparent viscosity at any given range of shear rate.

Table 2-1: The distribution modulus (m) and size modulus (k) obtained by fitting the experimental size distribution data to the Rosin-Rammler equation.

Test samples	*m*	*k*	R^2 (correlation factor)
Raw 1	0.9658	37.2	0.9955
Raw 2	1.0967	22.14	0.9981
Raw 3	1.3137	13.01	0.9951

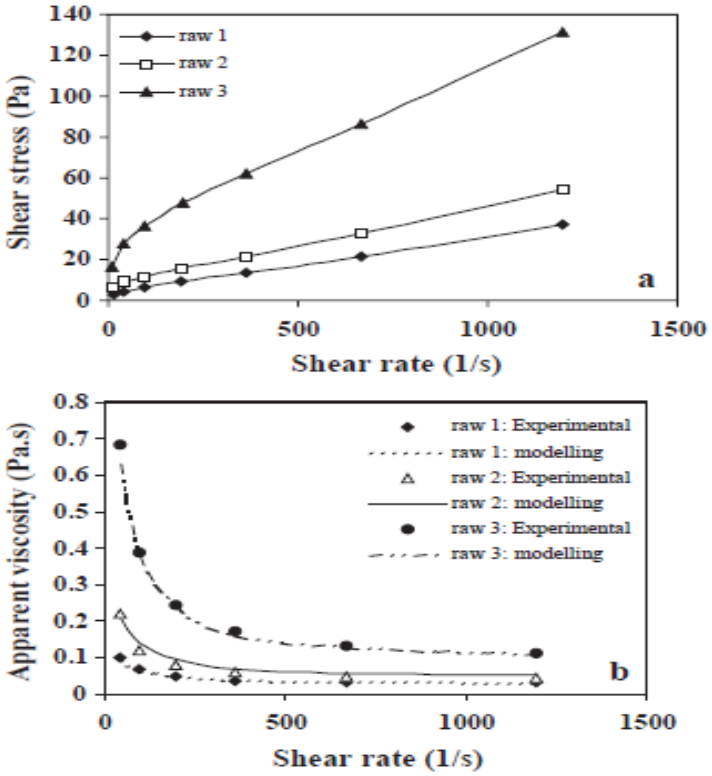

Figure 2-10: Effect of particle size and distribution on the rheological behaviour of limestone slurry at 70wt% (He et al., 2006)

2.6.3. Temperature

Slurry viscosity is a strong function of temperature. Various authors have reported that the viscosity of slurry increases with a decrease in temperature (Baguley, 1988; and Kawatra and Eisele, 1988). The effect of temperature on slurry viscosity is assumed to reflect corresponding changes in the viscosity of the carrier fluid which is usually water. On the basis of this assumption, the slurry viscosity measured at various temperatures is usually corrected to a standard temperature of 20.2^{o}C at which the viscosity of water is 1mPa.s (Napier-Munn, 1983).

2.7. The rheological measurement of mineral slurries

To achieve control of mill rheology, it is important to be able to directly measure and monitor slurry rheology. On-line measurement of mineral slurries has been difficult because a majority of viscometers are designed to measure the rheological characteristics of fluids and mineral slurries with low solids content. There are practical difficulties which are associated with measuring dense slurries. These are rapidly settling particles, particle packing variations and wall slippage. The inhomogeneous solution results in significant measurement errors (Kawatra et al., 1996 and Kawatra et al., 1999).

The rheological characterisation of slurry entails measurement of the relationship between shear stress and shear rate. This is an indication of the inter-particle forces in the mineral slurry. Direct characterisation of slurry is achieved from using rheometers and viscometers. He et al., (2004) noted that the three basic types of viscometers and rheometers which have been commercially used to characterise the rheology of mineral slurries are coaxial cylinder, capillary tube and vibrating spheres. Coaxial cylinder viscometers or rheometers are used to measure the variation of viscosity or shear stress at a specified shear rate over a specified period of time. The shear rate is varied by changing the rotational speed of the spindle. The viscosity is determined by measuring the torque required to rotate the spindle at a constant rotational speed. Common examples of this type of rheometer or viscometer are the Brookfield, Haake, and Debex viscometers or rheometers (Gao and Forssberg, 1993; Prestidge, 1997; Shi and Napier-Munn, 1996, 2002). Vibrating sphere viscometers or rheometers are operated at high shear rates which range from zero to a maximum value. The maximum shear rate attained is a function of the velocity propagation of the shear wave in the fluid which is dependent on the fluid viscosity. An example of this type of viscometer is a Nametre viscometer which has been used by Kawatra et al., (1996, 1999) to measure the apparent viscosity of rapidly settling slurries of coal and silica slurries at high shear rates and viscosities as low as 0.001Pa.s. Capillary tube rheometers or viscometers measure the variation of shear stress and shear rate along the cross section of the tube as the slurry flows through the tube. The shear rate and stress are calculated at the tube wall. Examples of this type of rheometers or viscometers are the pressure vessel and balanced beam tube viscometer (Kawatra et

al., 1999; Turian et al., 1997; Slatter, 1997). A pressure vessel type rheometer called a U-tube rheometer manufactured by Paterson and Cooke shown in Figure 2-11 was used to conduct all the rheological measurements in this study (Kahn, 2005). The inlet of this rheometer is attached to a recirculating fluid line and the other end is connected to a conical sealed chamber. A ball valve is attached to the base of the vessel to drain fluids or slurries after each test. An absolute pressure transducer measures the pressure of the air inside the vessel and a differential pressure transducer measures the pressure difference across the inlet tube. Data from both pressure transducers are collected by a digital computer. The tube rheometer works on a principle of measuring the pressure drop across a measured length of tube**.** The slurry flowrate in the tube determines the shear rates. These results are used to plot a pseudo rheogram of shear stress of tube wall versus the bulk shear rate (Kahn, 2005; He et al., 2004).

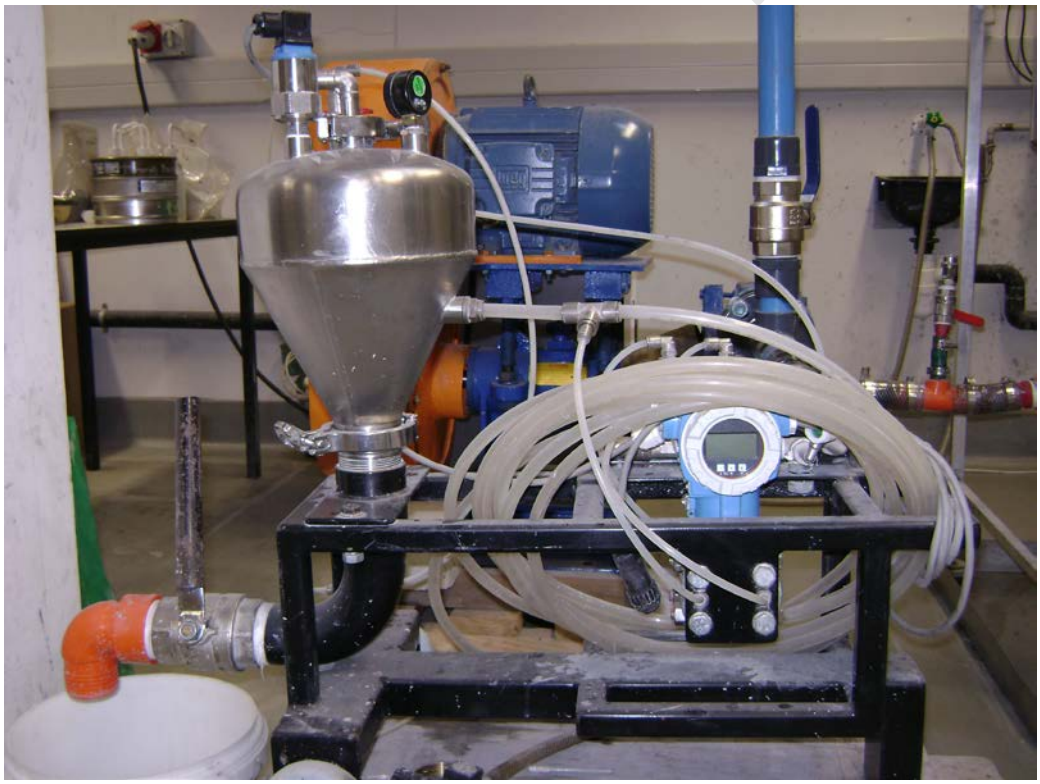

Figure 2-11: The Paterson and Cooke U-tube rheometer used to conduct all the rheology experiments.

Kawatra et al., (1996) conducted rheology experiments on silica slurry using a combination of rotating (Brookfield) and vibrating (Nametre) type viscometers to measure the apparent viscosities at low and high shear rates respectively. The

investigated solids concentration range was between 10 wt% to 70 wt%. One of the main objectives was to prevent the settling of solid particles during rheological measurements. Settling particles varied the percent solids in the sample holder before the instrument could display a steady reading thus resulting in erroneous results and incorrect flow curve characterisation. When using the rotational viscometer the flow of the sample was kept vertical because forces in any other direction interfered with the rotation of the spindle. Any turbulence also results in erroneous viscosity readings.

2.8. Key issues to be considered when selecting a type of viscometer

2.8.1. Shear rate range

The mean slurry velocity at which some of the solids start to settle out of the slurry and form a stationery bed is an important transport parameter. The transport of slurry at velocities equal or less than the minimum settling velocity is considered to be problematic because the flow regime is unsteady (Skudarnov et al., 2001). As a result plugging may take place due the gradual accumulation of solids in the system. It is therefore very important to identify the minimum settling velocity of the slurry and ensure that the slurry is transported at higher velocities than the minimum settling velocity. The Durand equation below can be used to calculate the minimum settling velocity of the slurry.

$$V_c = F_L\left[\frac{2gDpipe(\rho_s - \rho_L)}{\rho_L}\right]^{0.5} \qquad (2.3)$$

where: F_L: dimensionless factor, Dpipe: pipe/tube diameter, ρ_s=density of transported solid particles, and ρ_L=density of the fluid.

In the case of the tube viscometer used in this work, the shear rate range was adjusted by changing the pump flow rate. If the shear rate was too low the solids settled and caused plugging in the viscometer. Bazin and Chapleau, (2004) concluded that some viscometers are not designed to be operated at low shear rates and may give the result that suggests that the fluid exhibits a yield stress. This is likely to be the case if only the upper portion of the pseudoplastic curve is shown by the results. When the

viscometer operates only at low shear rates it may also give erroneous results that suggest that the fluid is Newtonian with a high viscosity. These conclusions were obtained when a Brookfield viscometer was used to measure the viscosity of mineral slurries (Bakshi et al., 1999).

2.8.2. Particle size distribution

The size of the tube of the viscometer should be at least three times the size of the particle diameter in order to eliminate particle size effects on the measurements (Kahn, 2005). The tube diameter on the viscometer used was 9mm so the largest particle size that could be allowed in the experiments was 3mm. The particle size range that was investigated in this study is -75+53 microns. This size range was chosen because rheological effects are evident on slurry behaviour at finer size classes below 75 microns (Somasundaran and Moudgil, 1988; He et al., 2004).

2.8.3. Turbulence

Turbulence is one of the main problems associated with most online viscosity measurements. It is associated with the design of the viscometer. Turbulence is created in viscometers with agitators such as the wide gap rotational viscometer. In turbulence the flow of fluids is not smooth and this results in a greater dissipation of energy than that occurring in laminar flow. It reduces the apparent shear rate and results in higher apparent viscosity readings being obtained (Shi, 1994). The effect of turbulence was not considered in the rheology results obtained since the U-tube rheometer is not a rotational rheometer.

2.9. Rheological models

There are different types of rheological models which describe the flow curves of a slurry. These models describe the mathematical relationship between shear stress τ and shear rate which is denoted by γ. The models commonly used to describe Newtonian slurry behaviour are the Newton and Bingham models. Non-Newtonian slurry behaviour is commonly described using the two- parameter Ostwald/de Waele power law (Somasundaran and Moudgil, 1988; Klimpel, 1982) , Bingham plastic (Muster and Prestidge, 1995; Tangsathitkulchai, 2002; Prestidge, 1997), Casson (Yang et al., 2001) and three-parameter Herschel-Bulkley (Muster and

Prestidge,1995; Prestidge,1997) and Sisko models (Turian et al.,1997; Bailey and Weir,1998) Table 2-2 summarises these models.

Table 2-2: Models describing slurry rheograms

Model name	**Equation**	**Interpretation of equation**
Newton (Bartos, 1992)	$\tau = \eta\gamma$	Shear stress proportional to shear rate, apparent viscosity constant at different shear rates
Ostwald/de Waele model (Atzeni *et al*, 1985)	$\tau = C\gamma^{P}$ C: consistency index P: power index	Applied to shear thinning or thickening fluids with no yield stress P>1: Shear Thickening P<1: Shear Thinning P=1: Newtonian Fluid
Bingham model (Tattersall, 1976)	$\tau = \tau_B + \eta_B\gamma$ τ_B: Bingham yield stress η_B: Bingham viscosity	Approximates yield point, does not take into account shear thinning or shear thickening behaviour
Herschel/Buckley (Atzeni *et al*, 1985)	$\tau = \tau_{HB} + C\gamma^{P}$ τ_{HB}: HB yield stress C: flow coefficient P: HB index	Similar to the Bingham model but it gives an indication of shear thinning or shear thickening. P>1: Shear Thickening P<1: Shear Thinning P=1: Newtonian Fluid
Sisko model (He et al.,2004)	$\tau = \eta_\infty\gamma + m\gamma^{n}$ m & n : constants η_∞: asymptotic shear viscosity at infinite shear rate	Combines low and intermediate shear power law with high shear Newtonian limiting behaviour

2.10. The development of Positron Emission Particle Tracking (PEPT)

Quantifying the range of shear rates in a grinding mill is important as it determines the slurry viscosity values which will be used to assess the effect of viscosity on grinding performance (Bazin and Chapleau, 2004). The aggressive internal environment in a grinding mill makes the measurement of particle properties difficult (Yamane et al., 1998). The understanding of particle motion in rotating drums is essential in order to optimize designs of process equipment used in milling and mixing. In this work; PEPT is the non-invasive measurement technique used to develop a methodology for estimating the shear rates in the mill. It gives insitu measurements of particle motion and allows for time averaged calculations of particle kinematic properties which cannot be obtained from other techniques.

Positron Emission Particle Tracking (PEPT) is a technique for studying the motion of a positron emitting labelled particle within a closed, circulating system. It has been used for studying the motion of particles in granular and fluid systems (Parker et al, 1997). Many of the first applications of PEPT have been in studies of granular mixing for batch ploughshare mixers (Bridgwater et al., 1993; Broadbent et al., 1993, 1995). It was developed at the University of Birmingham (United Kingdom) as a refinement of the Positron Emission Tomography (PET) technique. PET is a radioactive tracer imaging technique used to see the distribution of a radioactive fluid when it mixes inside a system. PEPT uses a single positron emitting labeled particle to study particle motion in a closed system provided that it is tracked for a long enough period of time. PET is a slow process requiring 10^6 to 10^7 events to produce an image. This makes it difficult to study rapidly changing systems. PEPT is a faster process only requiring 10^2 events to determine the tracer location. PEPT is a more powerful tool of observing bulk distribution in 3-D than PET because in PET some scatter and random events distort the image in a way that they can only be partially corrected after back-projection while in PEPT random and scatter events are almost entirely discarded by iteration and they do not contribute to tracer location (Sadrmomtaz, 2008). PET is also restricted in terms of the geometry, size and the position of the field of view of its cameras. PEPT provides greater flexibility in that it

can be applied to industrial equipment and can be arranged in any configuration to enable particle tracking (Ingram et al., 2007).

2.11. A description of the PEPT technique

PEPT is a technique used for tracking the trajectory of a radioactively labelled tracer particle. The radioactive tracer which is representative of the charge material being studied is prepared and placed within the field of view of the positron camera which consists of a pair of positron sensitive detectors. The tracer is tracked with respect to time and its position (Parker et al., 1994). PEPT works on the premise of using an unstable radionuclide which decays by β^+ emission. When the emitted positron annihilates with an electron, it produces two antiparallel back-to-back 511 keV γ-rays. The coincidence detection of these γ-rays defines a Line of Response (LOR) passing close to the location of the tracer. An event is recorded when the gamma rays are simultaneously detected by both detectors within a resolving time of 12ns. The speed and accuracy of tracking depend on the activity of the tracer and the amount of material which the gamma-rays have to traverse to reach the detectors (Parker et al., 1996). The location of the tracer is obtained by the triangulation of numerous LOR's within discrete periods of time passing in the field of view of the positron camera detectors using a location algorithm (Hawkesworth et al., 1989; Parker et al., 1993; Yang et al., 2006).

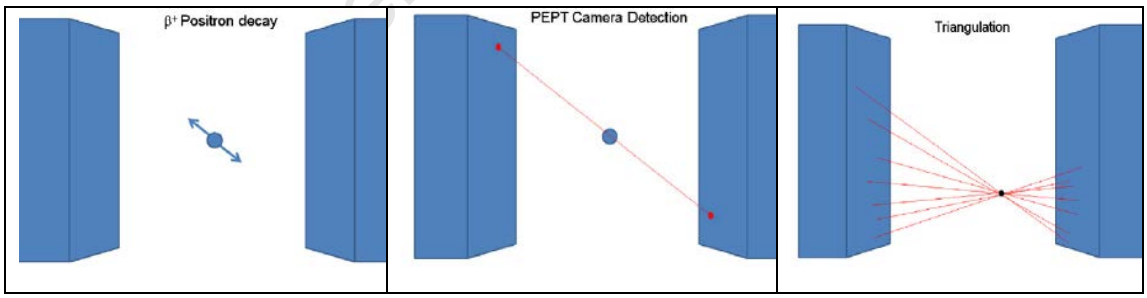

Figure 2-12: A sequence of particle position tracking in PEPT. (Bbosa, 2010)

2.11.1. A description of the Birmingham positron camera

The Birmingham positron camera was constructed in 1984 at the Rutherford Appleton Laboratory and was intended to be used for PET to study engineering systems. It was first applied in the study of lubricant distribution in operating engines and gearboxes (Parker et al., 1997). The Birmingham positron camera setup consisted of a pair of

detectors which are multi-wire chambers each with an active area of 600 x 300 mm^2, with a maximum separation distance of 750mm. These dimensions define the maximum field of view for tracking. Each chamber is filled with a mixture of isobutene and Freon at atmospheric pressure. The chamber is constituted of a stack of 21 cathode planes which are separated by anode wires held at a potential of 3.5kV. The cathode planes are made of a 50μm lead strips which serve as photon converters that are arranged in parallel strips and are 2.2mm wide with 0.8mm gaps. A γ ray interacting in the lead by photoelectric absorption or Compton scattering releases a fast electron into the gas and initiates a Townsend avalanche adjacent to the neighbouring anode wire. This is detected as a voltage pulse on this anode and its two neighbouring cathodes. The cathode strips on either side of the anode run in orthogonal directions to enable the location of the gamma ray interaction in both the x and y directions. Cartesian coordinates are used to describe locations (Parker et al., 1993).

According to (Parker et al., 1994) all cathode plane strips which run in the same direction in each detector are read out via a single delay line. Four delay lines serve the two detectors with each delay line being 300ns long. The coincidence detection efficiency for incident 511keV gamma rays is approximately 7% of the singles rate. Many detected photons do not a have partner incident on the other detector. High singles rates result in a significant rate of random and scattered coincidences taking place within the 25 ns resolving time of the coincidence. This limits the useful coincidence logging rate to a maximum of approximately 3000 per second.

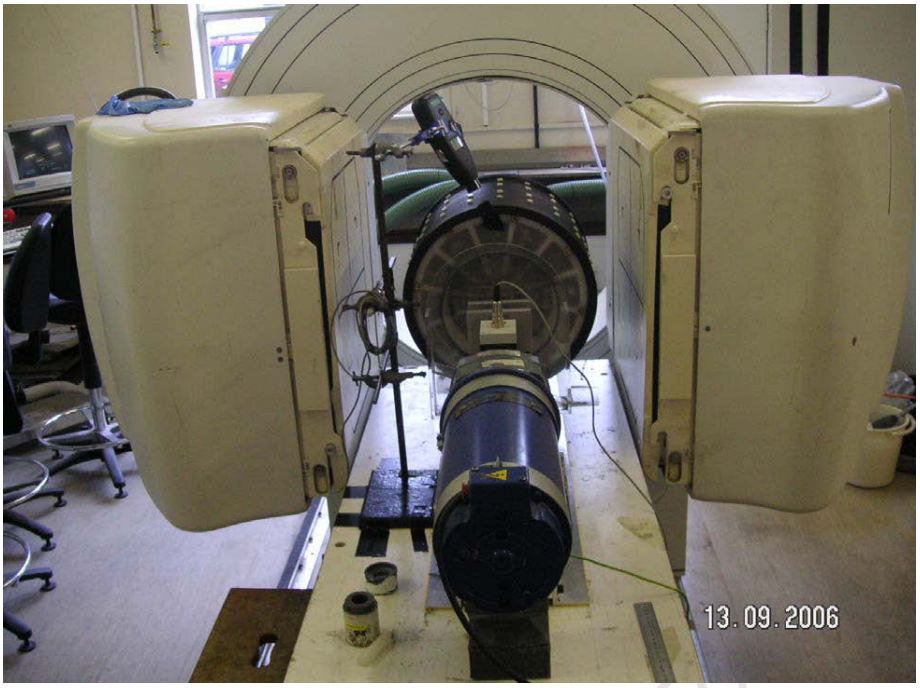

Figure 2-13: The configuration of the PEPT camera at the University of Birmingham (UK)

In principle only two pairs of detected coincident gamma rays are required for a tracer location reconstruction. In principle each pair should define a line passing close to the tracer particle. However, in practice reconstruction lines hardly intersect and corrupt lines occur due to scattering of one or both photons before detection. Several pairs of lines are therefore required to distinguish useful events from corrupt ones and enable reconstruction of the tracer particle location (Stellema et al., 1998). Figure 2-14 shows the different types of event pairings that can occur during detection.

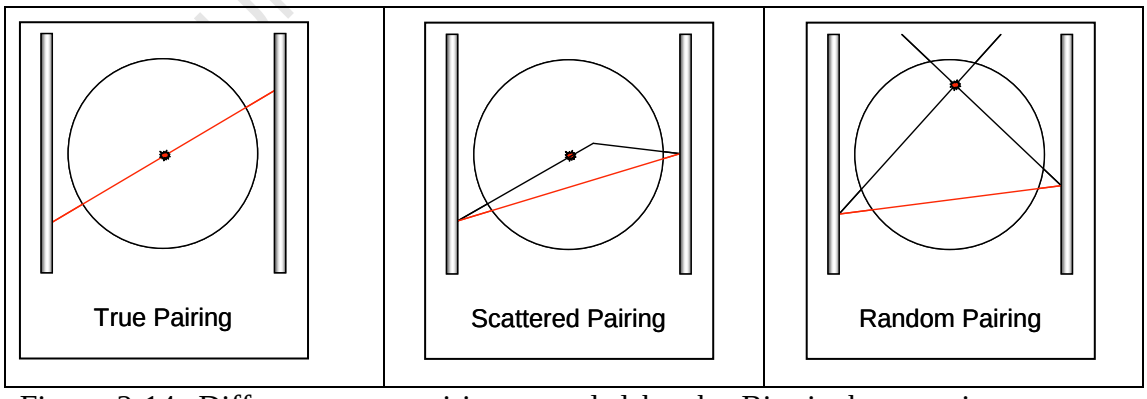

Figure 2-14: Different event pairing recorded by the Birmingham positron camera (Stellema et al., 1998)

An iterative reconstruction algorithm which selects useful events and is used to reconstruct the particle trajectory has been developed. (Parker et al.,1997). It calculates a point in space closest to which the initial set of events all pass and discards the events lying furthest from this point. The calculation is repeated using the remaining events until only a predefined fraction of *f* events remains. *f* is a fraction of useful events that lie closest to the point of emission. The chosen faction *f* depends on the amount of scatter in the material and the tracer position in the field of view of the camera. The scatter is a result of the attenuating environment. For a moving tracer there is an optimum useful events sample size that should be large enough to provide good statistics but not too large that the particle moves too far during the location process. This optimum is found to correspond to the tracer moving approximately 20mm during location. Tracer speed also decreases the precision of location. A particle moving at 1m/s can be located within 5mm at 250 times per second. Whereas one moving at 0.1m/s would be located to better than 2mm at 25 times per second (Parker et al.,1997). The expected particle speeds in the system being studied is between 0.73m/s and 0.91m/s at 60% and 75% of the critical mill speed respectively.

The PEPT technique can be used to obtain particle trajectories showing how the tracer moved through the equipment. PEPT data consists of a list of tracer position co-ordinates (x_i,y_i,z_i) each with its associated time t_i, camera angle and other important parameters relating to the system under study . All measurements are made in 3-dimensions. The coordinates of the detected accepted events are recorded and stored in a list form on a computer and can be accessed and transferred to other computers for subsequent data processing. From these events the tracer position is determined by triangulation (Parker et al, 1996).

2.11.2. The Labelling technique of the tracer particle

The PEPT technique tracks and uses a single radioactively labelled particle tracer to obtain detailed information on particulate motion in granular materials and flow fields in multiphase systems. The tracers used in PEPT are positron-emitting particles which are labelled using the ^{18}F radionuclide. There are other types of radionuclides such as ^{64}Cu and ^{66}Ga. The ^{18}F is the commonly used radionuclide because it has a convenient half-life of a 110min and it decays only by emitting 511keV positron

emission with no interfering gamma rays. This results in significant improvement in tracer location accuracy being achieved (Parker et al., 1993; 1997). Optimum tracking is achieved with a tracer activity in the range 300 -1000μCi using the Birmingham positron camera. The radioactivity with which a single particle can be labelled strongly depends on the particle size; composition and the labelling technique used (Fan et al., 2006).

The two methods used for tracer production by Fan et al., (2006) are direct irradiation and ion exchange. The particle to be labeled must contain oxygen. Direct irradiation entails bombardment of the particle to be studied (a typical rock or slurry particle) with the 35MeV ^{3}He beam using a cyclotron. The beam interacts with a few oxygen atoms in the particle which are converted; producing the radioisotope ^{18}F within the mineral particle. The chemical reactions that take place are shown in Equation (2.4) and Equation (2.5): where p=positron; n=neutron.

$$^{16}O\ (^{3}He,\ p)^{18}F \rightarrow {}^{18}F \quad (2.4)$$

$$^{16}O\ (^{3}He,\ n)^{18}Ne \rightarrow {}^{18}F \quad (2.5)$$

The level of radioactivity achieved in a single tracer is proportional to the cross-sectional area of the particle. It is thus required that the particle size be greater than 1000μm. If the particle size is less than 1000μm, the practical difficulty is that the radioactivity achieved is too low for accurate particle tracking using the ADAC Forte camera. Another practical constraint of this method is that the labelled particle must resist the high temperature during bombardment (Fan et al., 2006).

The ion exchange technique was developed to produce smaller tracers with a size range of 200-600μm. Ion exchange entails producing the radioactive material in solution and attaching it, via adsorption, to the particle of interest. In this technique the ^{18}F radioisotope is produced as a very dilute solution of fluoride ions in deionised water. The ^{18}F then exchanges with the counter-ions in the particle being labelled so the particle is labelled with a high radioactive level of 350-1000 μCi. The tracer particle is made representative for the material in the experimental setup in terms of size and density (Fan et al., 2006).

Common types of tracers used are glass beads, resin, alumina, rock fragments and copper. Resin beads are commonly used as PEPT tracers but they cannot be used to represent the bulk properties of many materials because they are perfectly spherical, are made of organic polymers and their densities are about 1g/cm^3. However; with the advancement of PEPT research experimental tracer material has extended to a wide range of organic and inorganic particles such as fine sand, fine glass beads, coal, crystallised cellulose and oil seeds. Surface modification is used to enhance the adsorption ^{18}F on various types of solid particles (Fan et al., 2006).

In this work the direct irradiation tracer production technique was used. The radioactive tracer was placed in the laboratory tumbling mill within the field of view of the positron camera. The information about the trajectory of the tracer over time enabled the computation of other physical properties of the system such as tracer particle velocity and shear rates.

2.11.3. Estimation of velocity distributions from particle paths using PEPT

The PEPT technique can be used to obtain particle trajectories and to determine particle velocities at each location within the system under study to show how the tracer moved through the equipment. Parker et al., (1993) tracked a 2mm silica tracer particle in a bed of 2mm salt particles in a horizontal cylinder rotating at 0.82 revolutions per second with 30% volume filling. For this closed system, the particle was tracked for a prolonged period to build up a statistical representation of typical particle behaviour at each point in space. The simplest estimate of the particle velocity *v* shown by Equation (2.6) using the time interval between locations was used. The difference between successive locations is used to estimate the vector velocity of the tracer.

$$v = (v_x^2 + v_y^2 + v_z^2)^{0.5} \quad (2.6)$$

$$v_{xi} = (x_{i+1} - x_i)/ (t_{i+1} - t_i)$$

$$v_{yi} = (y_{i+1} - y_i)/ (t_{i+1} - t_i)$$

$$v_{zi} = (z_{i+1} - z_i)/ (t_{i+1} - t_i)$$

Parker et al., (1997) applied the PEPT technique to study granular motion in a partially filled rotating cylinder. Experiments were conducted using different sizes of glass spheres at rotational speeds between 10 and 65rpm. Experiments were run between 3000 and 15000 seconds. The fraction of time spent by the tracer particle at each position in the radial plane was determined. This provided a method of plotting a map of the density of particles at each point in the bed. PEPT was also used to determine the average velocity field. The radial plane was arbitrarily divided into 5 X 5 pixels. An arrow was drawn from the centre of each pixel whose length and direction represented the tracer velocity. All the tracer velocities falling within the same pixel over the entire run were averaged.

The key findings were that using the position data about the single tracer from PEPT, most information on bulk properties of the system could be extracted if tracked for approximately 3 hours which is a sufficiently long period of time such that the trajectory of the tracer particle is able to be simulated. A distinction between the bulk bed and the active surface layers was identified. The position of the layer boundary was found to be independent of drum speed. At higher rotation speeds a significant slipping of the bed relative to the wall was observed. As a result of this the circulation frequency decreases relative to the drum rotation frequency as drum speed increases (Parker et al., (1997).

Bakalis and Fryer, (2001) and Bakalis et al., (2004) developed a method to estimate the velocity distributions of viscous fluids using PEPT. This method enables the quantification of velocity distributions under realistic conditions which had been a challenge due to the complex rheological properties of viscous fluids which are often time dependent and the opaque nature of the material (Bakalis et al., 2006). Experiments were conducted using a Newtonian fluid, shear thinning fluid and Herschel Bulkley fluid. The rheological properties of these fluids were measured using a cone and plate rheometer at shear rates up to $60s^{-1}$. PEPT experiments were conducted using an aluminium horizontal pipe under both isothermal and non-isothermal conditions. In the geometry chosen only the axial velocity component was considered. Scattered location data points were removed and a moving average was applied to smooth the particle path to enable the computation of the particle velocity from the first derivative of the position data. About 15 consecutive particle positions

were used. Using regression analysis a line was fitted to a number of z locations of the tracer particle versus time. The slope of the line was computed as the axial velocity of the particle. The axial distance travelled by the tracer particle was less than 1mm. It was assumed that in this distance there was no significant change in the radial location of the tracer. If the standard deviation in the radial location was greater than 0.5mm, the velocity values were discarded.

The key findings from this work were that the accuracy of the method decreased as the measured velocities increased. The faster the particle travelled, the less accurate was its detection. The accuracy of the method was acceptable for velocities up to 0.5m/s. More scatter in the velocity distributions was evident at higher flow rates as expected given that tracers are located more accurately when travelling at lower speeds. Smaller particles less than 600 microns were able to give better velocity measurements closer to the pipe wall. Smaller tracers give a better representation of the fluid system being studied. However; there are practical limitations to using smaller tracers. They dissipate easily during radioactive activation and it is difficult to maintain the activity of smaller particles for the duration of the experimental run which is approximately 3 hours (Bakalis and Fryer, 2001).

In this work a second order Lagrange interpolation polynomial function was fitted to the positional coordinates to generate a continuous and smooth trajectory from which the velocity was computed from the first derivative of the position data.

2.11.4. Methods for computing estimates of shear rate in a tumbling mill

Computing mean shear rates inside a ball mill is very difficult due to the complexity of charge motion. Identifying shear rates inside a grinding mill is important as it determines the slurry viscosity values which will be used to assess the rheological effects on grinding performance (Bazin and Chapleau, 2004). Zik et al., (1994) also noted that the pressure below the free surface of the charge is a complicated function of position and as a result the shear rate may vary non-linearly within the mill charge.

Most kinetic theory based continuum models of particulate flow in axially rotating cylinders have focused on the linear free surface of the charge which is formed at relatively low rotation speeds. The flow in a rotating cylinder is assumed to be comprised of a thin surface flowing layer which is also assumed to have no relative motion occurring inside the charge bed. This thin layer of particles exhibits Newtonian behaviour (Ottino and Khakhar, 2000). Yamane et al., (1998) observed surface flow in a horizontally rotating cylinder at 53% of critical speed. Magnetic Resonance Imaging (MRI) was used to measure the granular flow parameters using mustard seeds. The average diameter of the seeds was 1.5mm with a density of 1.3g.cm^{-3}.A acrylic cylinder of length 49cm with an inner diameter of 6.9cm was half filled with mustard seeds and rotated in the magnet. The range of rotation speeds investigated was 4rpm-31rpm. A departure from a flat free surface became significant at the upper end of this speed range. Mass conservation was applied and velocity profiles were analyzed across a perpendicular bisector to the free surface.

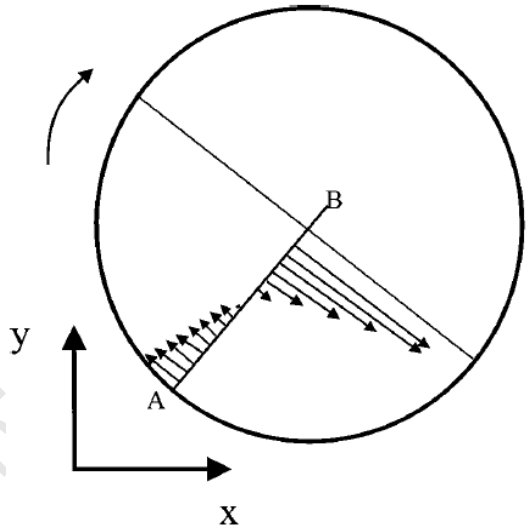

Figure 2-15: Velocity profile across a perpendicular line to free surface in a rotating cylinder (Yamane et al., 1998)

As shown by Figure 2-15, near the cylinder wall velocity varies linearly with distance from the centre of the cylinder. At the lower boundary of the sliding layer, the velocity deviates from linearity were the particles started to slip. As you move up the sliding layer towards the free surface, the velocity decreases to zero. At this point the sliding layer velocity is equivalent to the cylinder rotation. The velocity then rapidly increases until close to the free surface. At the free surface, the velocity is almost

constant and thus the shear is almost zero. A similar tangential velocity trend was observed for the investigated critical mill speeds at 46.3rpm and 57.9rpm.

Shi and Napier-Munn, (1999) conducted studies in which they estimated shear rates for cascading and cataracting charge motions inside a ball mill with a diameter of 4.57m. They used Morrell's power model to estimate shear rates for the cascading motion of the grinding media. For the cataracting motion the velocity of a free-flight ball striking the mill shell was resolved into two components and the shear rate was estimated from the tangential velocity of the ball mill. The results showed that shear rate ranges were between $13s^{-1}$ - $730s^{-1}$ inside a ball mill. Klimpel, (1984) also estimated mill shear rate to range from $0s^{-1}$ to $60s^{-1}$ but provided no evidence of how this figure was computed.

3. SAMPLE PREPARATION AND EXPERIMENTAL PROCEDURES

Overview

This chapter describes the experimental approach taken to meet the objectives of this thesis which are stated in the introduction. It begins with an overview of the tests objectives and proceeds with a detailed explanation of the experiments which were conducted using the Rheometer for rheology experiments and the Positron Camera for PEPT experiments.

3.1. Introduction

The main objective of this research project was to develop a methodology for characterising in-situ slurry viscosity profiles in tumbling mills at different solids concentrations and mill speeds. The Positron Emission Particle Tracking (PEPT) technique was used to quantify the in-situ shear rate distributions in the mill. Mill shear rates are closely related to mill rotational speeds. The effect of rotational speeds on slurry rheology is important to characterize correctly the flow behaviour of slurry (He, 2004). The slurry solids concentration for PEPT experiments was varied between 20%-40% by mass. The mill speed was operated at 60% and 75% of the critical speed. These mill speeds were chosen because they are the most commonly applied industrial speeds in the operation of a tumbling mill (Radziszewski et al., 2011).

Rheology experiments were performed to determine the rheological characteristics of the slurry similar to that used in the PEPT experiments. The slurry solids concentration for Rheology experiments was varied between 10%-60% by mass. Tumbling mils are usually operated at higher solids concentration ranges between 68% and 80% by mass. The trend from low to high solids concentrations was of significant interest in this work. The PEPT and rheological measurements could only be performed up to maximum solids concentrations of 40% and 60% by mass respectively. This was due to the measurement limitations imposed by the equipment. A wider range of solids concentrations could be obtained using the rheometer.

3.2. Test materials and particle characterization

El Soldado copper sulphate ore which has a density of 2.8 was used in both types of tests performed in this work. El Soldado ore in different size fractions was obtained from Anglo American Research. The different size fractions were -425+212, and - 75+53 microns. The slurry for PEPT and rheology experiments was prepared using the -75+53μm size fraction.

3.3. Description of PEPT experimental apparatus

Table 3-1 and Table 3-2 show the specifications of the tumbling mill and the experimental variables used in the PEPT experiments.

Table 3-1: The PEPT mill specifications

Internal mill diameter (m)	0.3
Internal mill length (m)	0.285
Mill speed at 60% crit (rpm)	46.3
Mill speed at 75% crit (rpm)	57.9
Volume filling (%)	31.25
No. of Pulp lifters	20
Grate open area (%)	~30

Table 3-2: Experimental variables used during PEPT experiments

El Soldado ore density(kg/m^3)	2800
Slurry particle size fraction (μm)	75+53
Mass of 5mm glass beads (kg)	10.2
Uncertainty in bead diameter (m)	0.3
Glass bead density(kg/m^3)	2700

Figure 3-1 shows a picture of the experimental rig set up used to conduct PEPT experiments. The Birmingham positron camera consisted of a pair of rectangular

detectors, each with an active area of 40x50 cm^2 with a maximum separation distance of 75 cm. These dimensions define the maximum field of view for tracking. A 300mm diameter mill was constructed from High Density Polyethylene (HDPE) with a specific density of 0.95 with aluminium lifters and a torque sensor. HDPE material was chosen because of its low gamma ray attenuation.

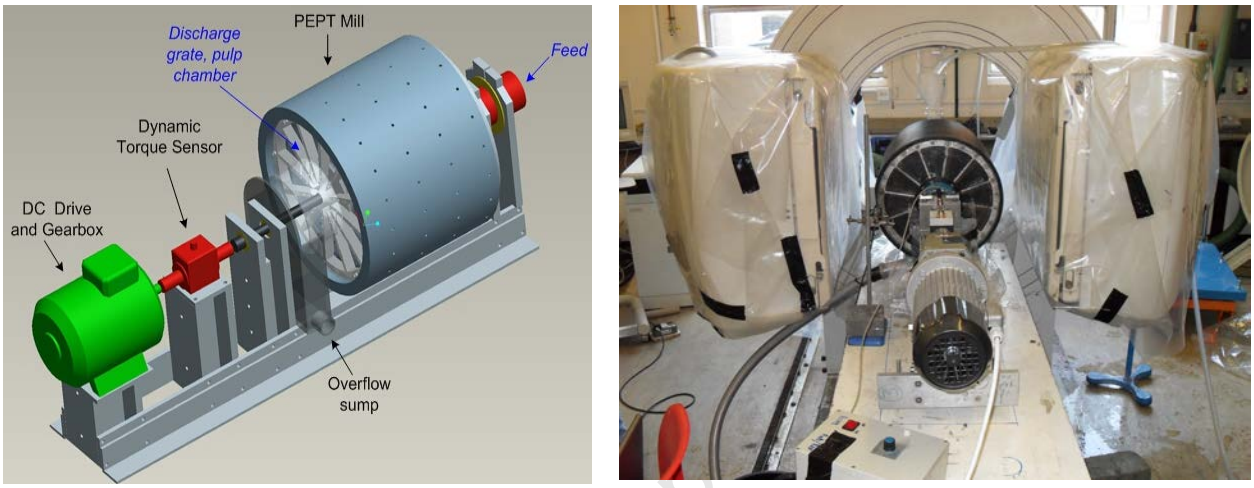

Figure 3-1: The experimental rig setup used to conduct the slurry PEPT experiments

3.3.1. The PEPT Experimental Programme

The tumbling mill PEPT experiments were conducted at the Positron Image Centre at Birmingham University, UK. Table 3-3 shows the experimental programme for the PEPT experimental work. The two parameters which were varied are solids concentration and mill speed. During the test, solids concentration was varied from 20% to 40% by mass and the mill speed was operated at 60% and 75% of the critical speed. El Soldado slurry was prepared using the -75+53 microns particle size fraction. 5mm glass beads were used to represent the bulk of the mill charge. It was assumed that the mill charge is mono-sized and that no breakage took place. A 1mm bluestone rock particle with the same density as that of the ore was used to represent a slurry particle in the mill. This is shown in Figure 3-2 . For all the tests performed, the mill charge was comprised of 5mm glass beads, slurry at a specified solids concentration and mill speed as shown in Table 3-3 and a radioactive 1mm blue stone particle. The blue stone particle was tracked and used to simulate the motion of slurry particles in the tumbling mill. Tests were performed for a period of over one hour. One hour

was the minimum time required to record statistically representative data such that tracking one particle would represent the behavior of the ensemble average using the PEPT data capturing system.

Table 3-3: The experimental programme used for PEPT tests

Solids concentration (%wt)	Mill speed (%critical speed)	Mill charge
20	60/75	5mm glass beads and slurry particle
30	60/75	5mm glass beads and slurry particle
40	60/75	5mm glass beads and slurry particle

Figure 3-2: A picture of the 1mm bluestone particle used to represent the slurry particle.

3.3.2. PEPT slurry tests procedure

PEPT experiments were performed by re-circulating slurry through a laboratory tumbling mill filled with a dynamic, porous network of 5mm glass bead charge at steady state. A fixed amount of 10.2 kg of 5mm glass beads which corresponded to 31.25% volumetric filling for the 300mm diameter X 300mm long laboratory tumbling mill was used. Slurry was prepared in a bucket to a specified solids concentration using El Soldado ore with a particle size range of -75+53microns. A fixed amount of water was weighed into the bucket. Pre weighed amounts of ore were

added to the water to attain the targeted slurry solids concentration. The slurry was kept well mixed in a bucket using a stirrer. The slurry temperature was measured using a thermometer.

The laboratory scale tumbling mill was placed between the two detectors of the PEPT camera. The mill was driven axially by a DC drive with a power delivery capacity of 0.55kW. A torque sensor supplied by HBM Instrumentation was placed between the DC drive and mill to measure the dynamic fluctuation of the mill load. The torque sensor was calibrated using static loading and torque readings were captured using an analogue-to-digital converter.

A 1mm conditioned bluestone ore particle and glass beads were used as tracer particles. The tracer particles were prepared by direct activation using the Birmingham MC40 cyclotron. The ore tracer particle was activated by being placed under a direct 36MeV ^{3}He beam which converted a small fraction of the oxygen atoms into a ^{18}F positron emitter. The ^{18}F positron emitter had a half-life of 110 minutes.

The trajectory field recorded by the detectors of the positron camera uses the Lagrangian coordinate system. The conversion of Lagrangian to the Eulerian coordinate system was achieved by placing location markers on the front, back and on the cylindrical part of the mill. Activated glass beads were used as location markers. These were used to locate the boundaries of the mill and supply the reference coordinates for tracking. The mill was slowly rotated to yield there circular traces of the mill shell. The mill shell was then reconstructed using the relative positions of the mill shell and the location markers. Figure 3-3 shows how the location markers were placed on the mill shell.

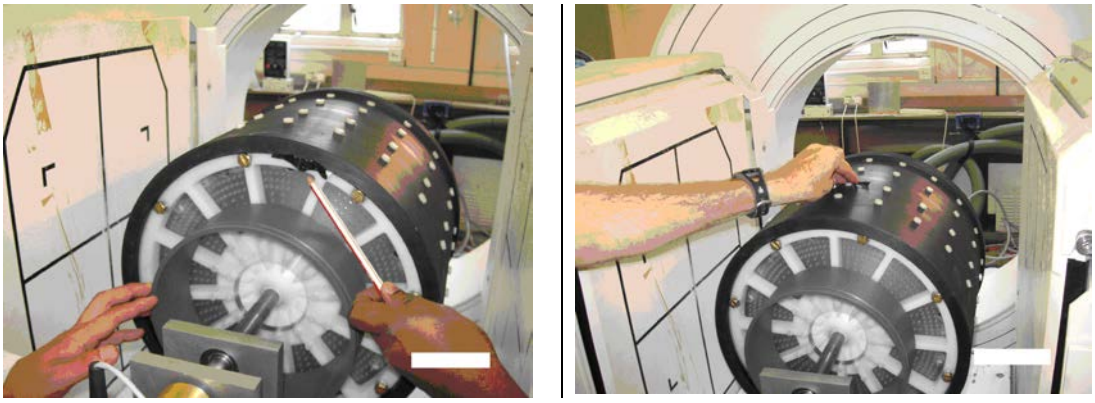

Figure 3-3: Positron emitting glass bead used as location marker to trace out the mill shell

The slurry was pumped at a set mill speed from the bucket, through the main chamber of the mill and discharge grate, into the pulp chamber and back into the bucket. An iterative procedure was applied to ensure standard operating conditions: The pump speed was adjusted and the mill “crash stopped” until visual inspection of the slurry level matched that of the stationary charge, i.e. the interstices of the stationary bed were completely filled by the slurry. Using this observation and the measured volumetric flow rates at the inlet and outlet, the fluid in the mill at steady state could be estimated. The glass beads remained in the mill between the feed end and the discharge grate as they are too large to pass through the 3mm diameter grate holes.

The 1 mm bluestone particle was used as the slurry tracer particle. The limitations of fine particle activation using the Birmingham cyclotron prevented the use of the typical slurry particle (-75 µm +53 µm) as it was too small to handle and it dissipated during the direct radiation process. The activity of the slurry tracer particle was measured before it was introduced into the mill. The slurry tracer particle was introduced into the system via the mill inlet pipe. The slurry test were conducted at 75% critical mill speed first and then reduced to 60% critical mill speed at each solids concentration.

Table 3-4: The measured slurry tracer particle activity.

Solids Concentration (wt%)	Measured slurry tracer particle activity(mCi)
20	1.35
30	1.38
40	1.15

The trajectory of the radioactive 1mm bluestone slurry tracer particle was monitored and tracked using the positron camera detectors. The tracer decays by emitting a pair of anti-parallel gamma rays which are called lines of response (Parker et al., 1996). The accurate location of the tracer position in the mill is determined from the detection and subsequent triangulation of these gamma rays. The details of this triangulation technique are discussed in section 2.11.

A Geiger was placed next to the discharge grate outlet pipe to detect the movement of the slurry tracer particle near the discharge. In some instances when tracer particle exited the mill, it was detected using the Geiger and collected into a beaker and immediately reintroduced back into the mill.

The Birmingham positron camera which consisted of a pair of rectangular detectors each with 40x50 cm^2 dimensions and separated by up to 75 cm were placed on either side of the laboratory tumbling mill. The detectors tracked the particle trajectories of the slurry tracer particle in the tumbling mill by detecting the gamma rays emitted by the slurry tracer particle. The measured PEPT data consists of a list of tracer position coordinates (x_i,y_i,z_i) each with its associated time t_i, camera angle and other important parameters relating to the system under study. The coordinates of the detected accepted events are recorded and stored in a list form on a computer which allows for subsequent data processing (Parker et al, 1996).The data processing techniques applied to the measured PEPT data are discussed in Chapter 5.

3.4. Description of the Rheology experimental apparatus

Figure 3-4 shows the experimental rig setup used to conduct the rheology measurements for this study. It consisted of a sump, variable speed pump and a U-tube rheometer connected to a computer. The computerised rheometer was designed by Paterson and Cooke (Kahn, 2005). The pump was manufactured by Weir Enviro Tech. The sump had an agitator which was used to mix the slurry. The well mixed slurry was pumped from the sump to the rheometer at pumping flow rates recommended by the supplier of the rheometer. These flow rates were chosen such that they allowed the mixed slurry to flow through the rheometer without settling out in the piping system.

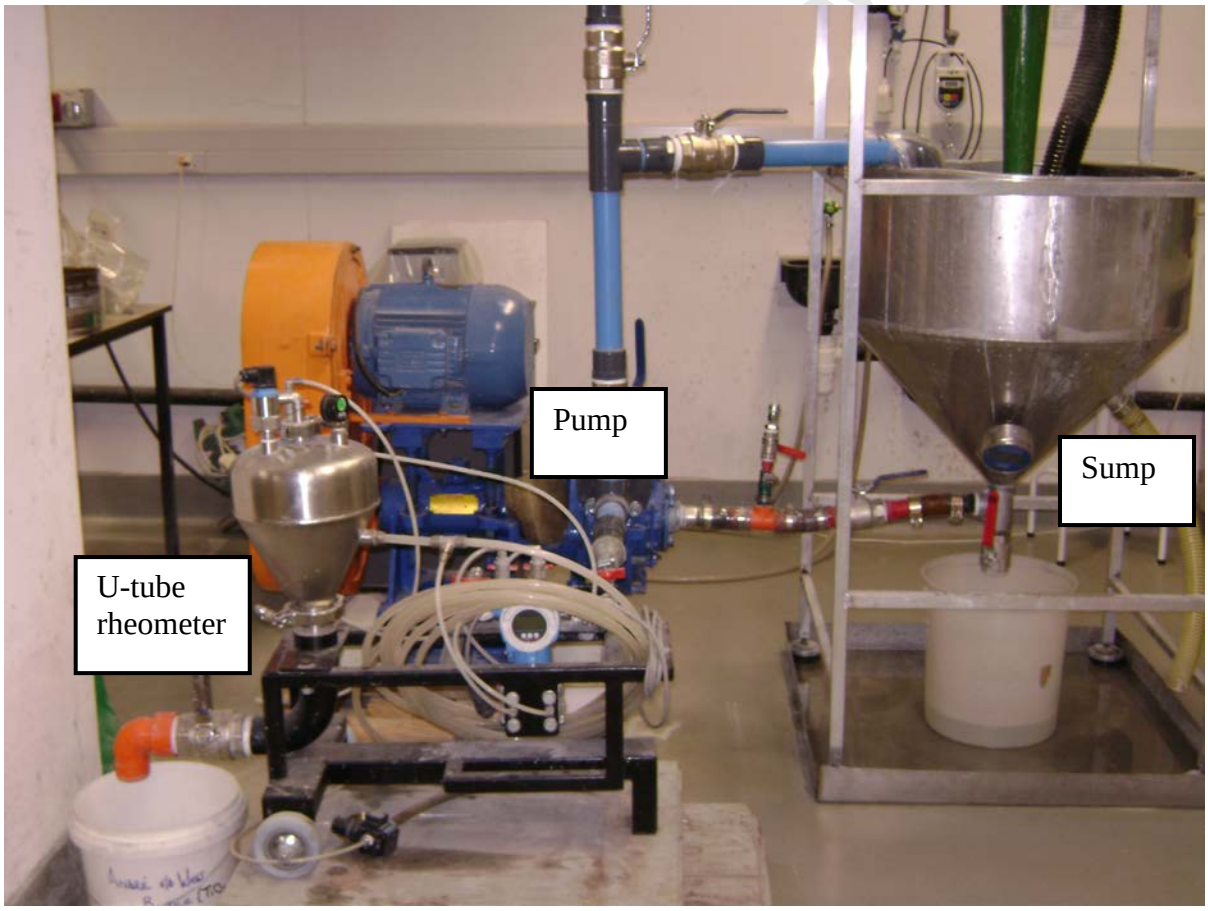

Figure 3-4: The rheometer experimental set-up used to conduct the rheology tests using mineral ore-water suspensions.

The rheometer was used to obtain the rheograms for the slurry at different solids concentrations. It measured the shear stress at a range of shear rates. The tube

rheometer is a type of pressure vessel rheometer (He et al, 2004). The inlet of this rheometer is attached to a recirculating fluid line and the other end is connected to a conical sealed chamber. A ball valve is attached to the base of the vessel to drain fluids or slurries after each test. An absolute pressure transducer measured the pressure of the air inside the vessel and a differential pressure transducer measured the pressure difference across the inlet tube. Data from both pressure transducers is collected by a digital computer. Table 3-5 shows the dimensions of the tube rheometer the specifications of the sump and pump used to conduct the rheology experiments.

Table 3-5: Tube rheometer, pump and sump dimensions

Active volume (L)	5.72
Internal tube diameter (mm)	9.90
Measuring tube length (m)	9.64
Pipe roughness	30
Sump volume (L)	45
Maximum pump speed (Hz)	50
Pump Power (Kw)	50

The tube rheometer works on a principle of measuring the pressure drop across a measured length of tube. The pressure drop determines the pseudo shear stress. The slurry flow rate in the tube determines the shear rates. These results are used to plot a pseudo rheogram of shear stress of tube wall versus the bulk shear rate (Kahn, 2005).

Equations (3.1), (3.2) and (3.3) show how the pseudo shear rate and shear stress were calculated for this rheometer. These equations were supplied by the manufacturers of the rheometer.

$$u = \frac{V}{XSA} \tag{3.1}$$

Where: u =slurry velocity ($m.s^{-1}$)
V =volumetric flow rate of the slurry velocity ($m^3.s^{-1}$)
XSA = cross sectional area across the tube (m^2)

$$\gamma = \frac{u}{\Delta x} \tag{3.2}$$

Where : γ = pseudo shear rate (s^{-1})
u = slurry velocity ($m.s^{-1}$)
Δx = distance from the tube wall (m)

The shear stress of the bulk fluid through the tube rheometer is calculated using equation (3.3)

$$\tau = \frac{(P1 * XSA) - (P2 * XSA)}{ISA} \tag{3.3}$$

Where: τ = shear stress
$P1$ = pressure at the entrance end of the tube (Pa)
$P2$ = pressure at the exit end of the pipe (Pa)
XSA = cross sectional area across the tube (m^2)
ISA = internal surface area between the two ends of the tube (m^2)

3.4.1. The water curve calibration on the Paterson and Cooke U-tube rheometer

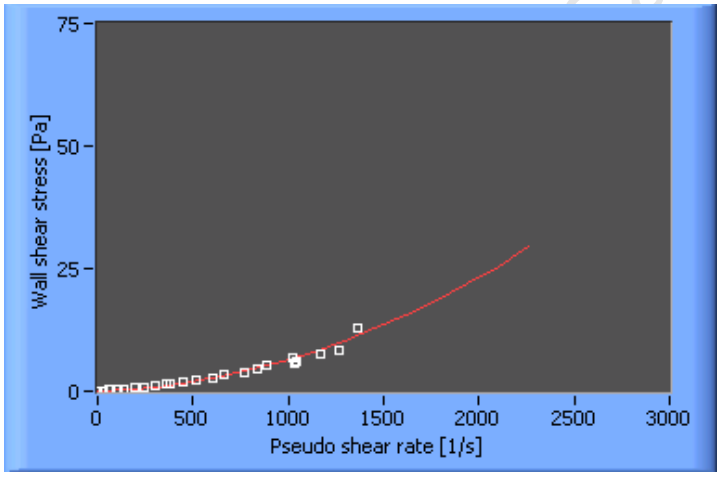

Figure 3-5: Rheogram of the water calibration curve obtained from the tube rheometer

The calibration water curve obtained from the Paterson and Cooke rheometer is shown in Figure 3-5. It shows dilatant behaviour instead of the expected Newtonian behaviour for water at room temperature. This is because the instrument calculates shear rates using equation (3.2). Equation (3.2) assumes that Δx =d/8 (d is the tube diameter). This is valid at lower shear rates in the laminar regime. At higher shear rates, Δx at the tube wall decreases and this is not accounted for in equation (3.2). This leads to an underestimation of the higher pseudo shear rates on the rheogram.

This assumption leads to the dilatant curve. A correction factor was applied to all measured data during data analysis to eliminate this systematic error generated by the rheometer. This correction methodology is discussed in detail in section 4.2.

3.4.2. The Rheology Experimental Programme

Table 3-6 shows the experimental programme used to conduct the rheology tests. The solids concentration ranged from 10% to 60% by weight and the particle size fraction used in the slurry tests was the -75+53 microns. All other factors which affect slurry rheology were kept constant to simplify the analysis. These include surface chemistry, ore type and particle size distribution. The slurry temperature was measured throughout all the experimental runs.

Table 3-6: The experimental programme for rheology tests

Solids Concentration (wt%)	**Solids Concentration (v%)**
10	3.8
20	8.2
30	13.3
40	19.2
50	26.3
60	34.9

3.4.3. Rheology tests sampling procedure

A fixed volume of 9.62L of water was measured in the sump. The water temperature of the slurry was recorded using a temperature probe on the sump. Water tests were conducted to establish a measurement reference for subsequent slurry rheology tests. Each reading was repeated three times to assess the reproducibility of the results. The experimental results were obtained in a form of a rheogram.

The El Soldado slurry was then prepared to a specified solids concentration. The stirrer was switched on and the required amount of ore was added to attain the targeted solids concentration. The different ore amounts added to obtain the required solids concentrations are shown in Table A in appendix A. The slurry temperature was recorded using a temperature probe on the sump for each test conducted. The El Soldado slurry was pumped through the system and recycled back into the sump to

ensure good mixing and homogeneity of the slurry. It was ensured that the discharge valve of the rheometer was properly shut.

Sampling was started when instructed to open the feed valve by the computer system. At higher solids concentration, when the feed valve was opened the recycle valve was half opened instantaneously to increase the pressure in the system. When sampling was complete, the discharge valve of the rheometer was opened to drain it. The discharge sample was poured back into the sump. The system was flushed with water before continuing with the next test. The water was then decanted and the solids placed back into the sump for further tests. A total of 36 slurry tests and 6 water tests were conducted for the range of solids concentration shown in Table 3-6.

After the tests were conducted, the rig was shut down using this procedure. The tap at the bottom of the sump was opened while still running the agitator and the pump to drain out the sump. The slurry was collected into buckets and the water decanted out. The recycle valve was opened to flush out all solids from the system using water. The agitator was stopped followed by the pump. The plug was then disconnected from the switch.

4. RHEOLOGY RESULTS AND DISCUSSION

***Overview**:*

This chapter presents and discusses the rheology results which were obtained from using the Paterson and Cooke U-tube rheometer.

4.1. Presentation of rheology experimental data

Rheology tests were conducted to determine the rheological characteristics of the El Soldado ore slurry used in the test work. The investigated range of solids concentrations varied from 10wt% to 60wt% (4vol% - 35vol %). The experimental results were obtained in a form of a rheogram.

4.1.1. Rheograms at different solids concentrations

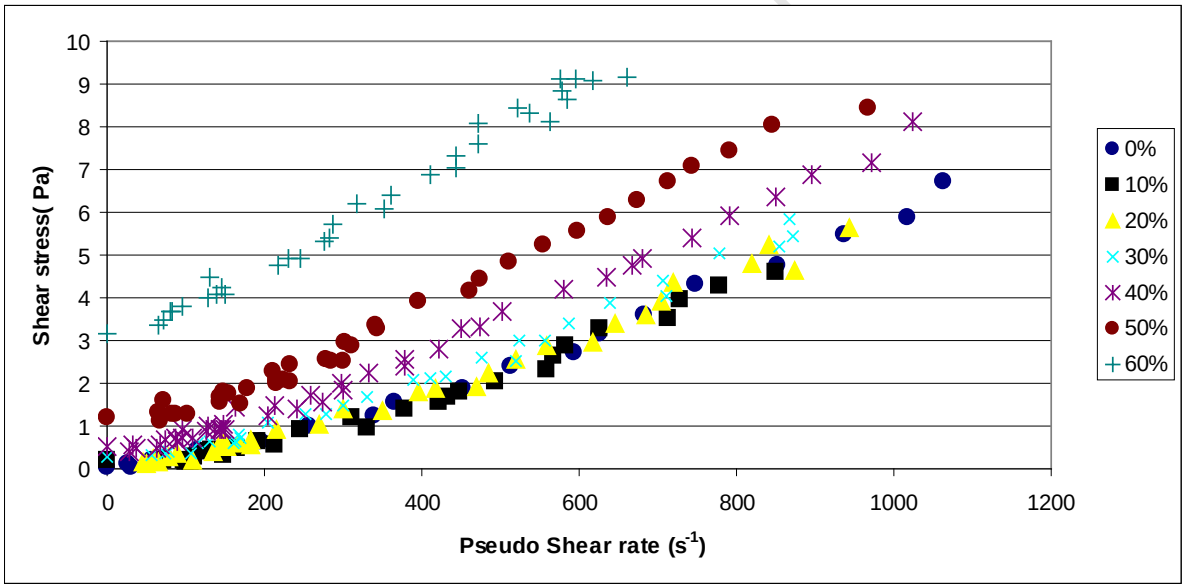

Figure 4-1: Rheograms for the -75+53 microns size fraction at different solids concentrations.

Figure 4-1 shows the rheograms obtained for water and El Soldado slurries at solids concentrations ranging from 10wt% to 60wt% for the slurry composed using El Soldado ore with the particle size fraction of -75+53μm. The rheograms show that for the measured range of shear rates up to 1200s^{-1}, shear stress increased with solids concentration.

4.2. Correction of systematic error in rheological measurements

The calibration water rheogram obtained from the Paterson and Cooke rheometer presented in Figure 3-5 shows a dilatant behaviour instead of the expected Newtonian behaviour for water at room temperature. A correction factor had to be applied to all the measured rheological data to eliminate this systematic error generated by the rheometer before fitting of rheological models was done. The experimental data points used were from all three repeat tests done at each solids concentration. Measurements at each solids concentration were repeated to show the reproducibility of the test results. Appendix A shows these repeated test measurements and their associated errors. The correction to measured rheological data was obtained by subtracting the theoretical rheogram curve for water at room temperature $\tau=(1\times10^{-3})\gamma$, from the best fitting curve of the measured water data. For the range of solids concentrations tested, the best fitting curve for the measured water data was a quadratic polynomial. In this regard, the following procedure was applied:

a) A straight line and quadratic polynomial were fitted to the water rheogram data and the "goodness of fit" was compared. The quadratic polynomial fit proved to be the best fit since it had the highest R^2 adjusted value of 0.99.

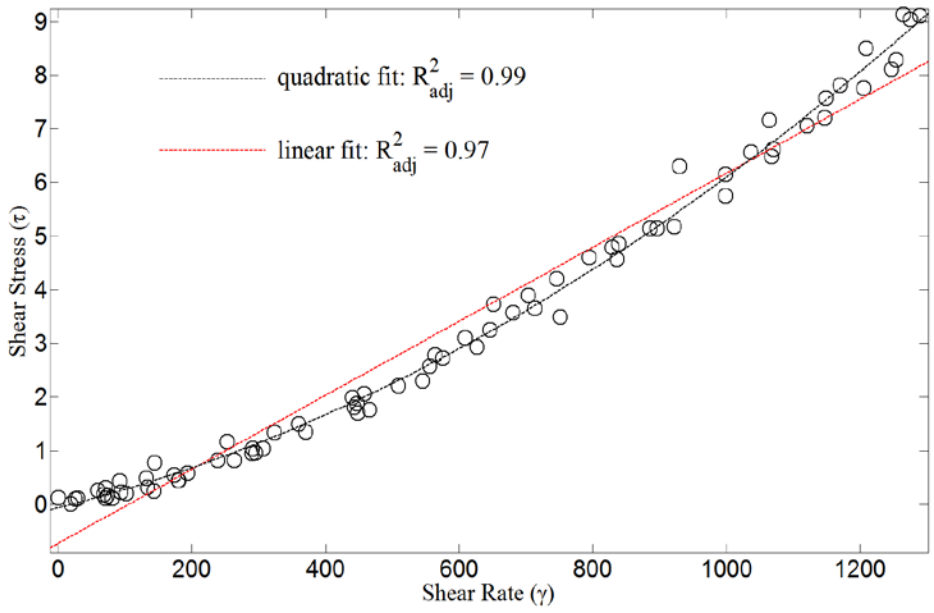

Figure 4-2 Water rheogram data fitted to a straight line and a quadratic polynomial

b) The theoretical water rheogram curve $\tau=(1 \times 10^{-3})\dot{\gamma}$, was subtracted from the best fitting curve, $a\dot{\gamma}^2 + b\dot{\gamma} + c$ .This yielded the correction factor (τ_c) required:

$$\tau_c = a\dot{\gamma}^2 + b - (1 \times 10^{-3})\dot{\gamma} + c \qquad (4.1)$$

c) Provided that the trend of the measured shear stress (τ_m), for *m* = 0%, 10%, 20%, 30%, 40%, 50% and 60% solids concentration, does not deviate significantly from quadratic fit, the measured shear stress values can be corrected by simply subtracting the corresponding correction (τ_c)

$$\tau_n = \tau_m - \tau_c \qquad (4.2)$$

where τ_n is the corrected shear stress

Figure **4-3** shows the rheogram data at various solids concentrations after the correction factor was applied to the measured rheogram data obtained using the Paterson and Cooke rheometer.

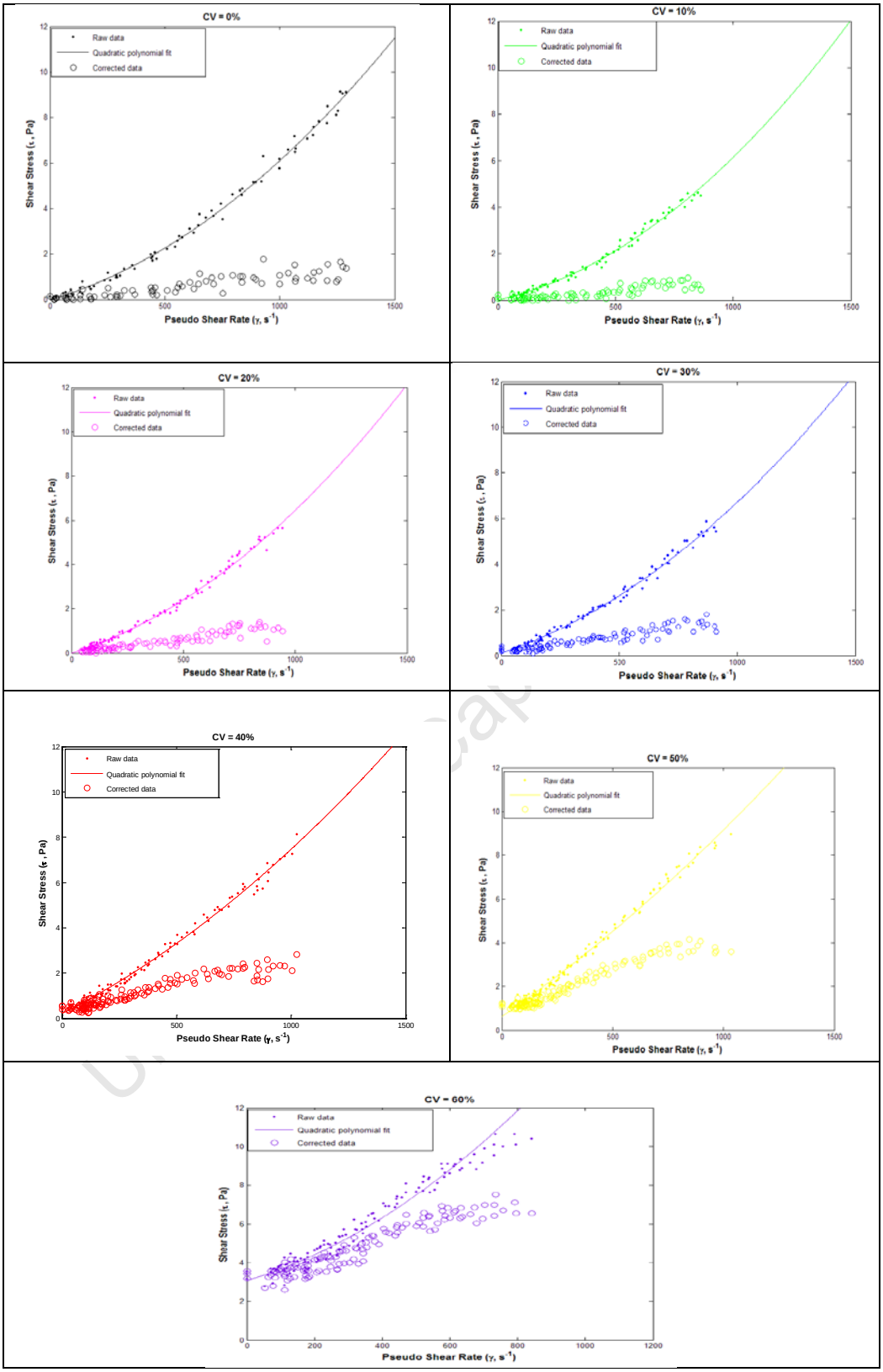

Figure 4-3: Corrections to rheogram data for the d=-75+53 size fraction at different solids concentration

4.3. Fitting rheology models to experimental data

Different rheological models were fitted to the corrected rheogram data obtained from conducting the rheology experiments. This was done with the objective of finding a model which best describes the El Soldado slurry in terms of its rheological characteristics. The three models which were tested are the Bingham, Casson and the Herschel-Bulkley models. These models were chosen because they have a power form and contain a yield stress parameter. They were thus perceived to be the most suitable for the trends observed in the experimental data collected in this thesis.

Figure 4-4 to Figure 4-6 show the fitting of the three chosen rheological models onto rheogram data measured at different solids concentrations for the -75+53 microns El Soldado slurry particle size fraction. These rheogram curves can be described as Newtonian and Bingham when compared to the rheogram curves presented in Figure 2-6. The shear stress increases linearly with shear rate at all investigated solids concentrations.

Table 4-1 to Table 4-3 show the fitted model parameters for the three rheological models at each solids concentration. τ_B is the yield stress parameter and $\Delta\tau_B$ is the standard error associated with yield stress. η_B is the viscosity parameter and $\Delta\ \eta_B$ is the standard error associated with viscosity. P is the power law index associated with the Herschel-Bulkley model. When the power index (P) is greater than 1 it means the flow curves are dilatant and when it is less than 1 it means the flow curves are pseudoplastic. The R^2 adjusted value was used to assess the goodness of fit for the different models tested. A comparison of R^2 adjusted values for all fitted models showed that the Bingham model is best rheology model which describes the rheology of El Soldado slurry since it had the overall highest R^2 adjusted values across all tested solids concentrations compared to the Casson and Herschel Bulkley models. As shown in Table 4-3 the fitted Herschel Bukley power index (P) is approximately 1 across all solids concentrations up to 60wt% which further supports that the flow curves are Bingham.

Table 4-1 to Table 4-3 also show that the yield stress (τ_B) and viscosity (η_B) parameters increased with solids concentrations for the Bingham and Casson

rheological models. For the Herschel Bulkley model yield stress parameter also increases with solids concentration across the tested range. However, the viscosity increased with solids concentration up to 30wt%. At higher solids the viscosity trend could not be clearly defined. This was attributed to the measurement limitation of the U-tube rheometer used. Lower shear rates could not be measured at these high solids concentrations. As shown in Figure 4-6 shear rates start above $50s^{-1}$.

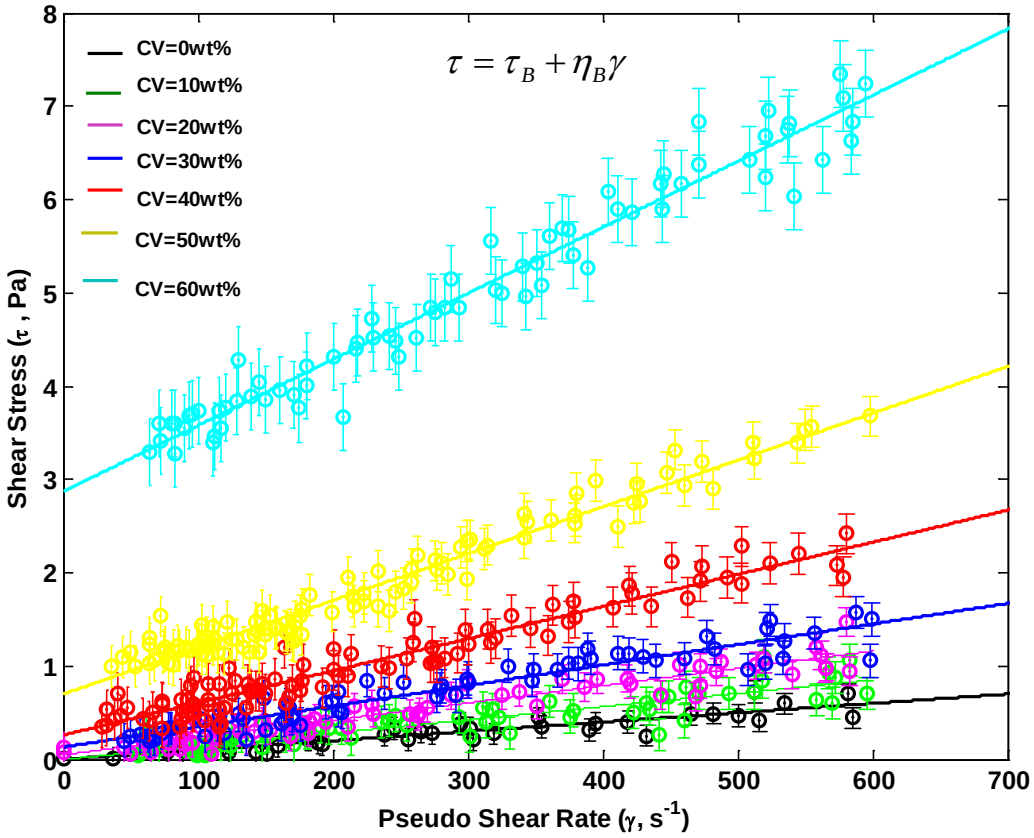

Figure 4-4: Bingham Model fit to -75+53 microns El Soldado slurry rheograms at different solids concentrations

Table 4-1: Bingham Model Parameters at different solids concentrations for the -75+53microns particle size fraction.

Solids concentrations (wt%)	R^2adjusted	$\eta_B \pm \Delta \eta_B$ (Pa.s)	$\tau_B \pm \Delta\tau_B$ (Pa)
0	0.8203	0.001±0.0001	0
10	0.8412	0.001±0.0001	0
20	0.9147	0.001±0.0001	0
30	0.9298	0.002±0.0002	0.11±0.0481
40	0.9231	0.003±0.0002	0.25±0.0532
50	0.9557	0.005±0.0002	0.69±0.0543
60	0.9611	0.007±0.0003	2.86±0.1130

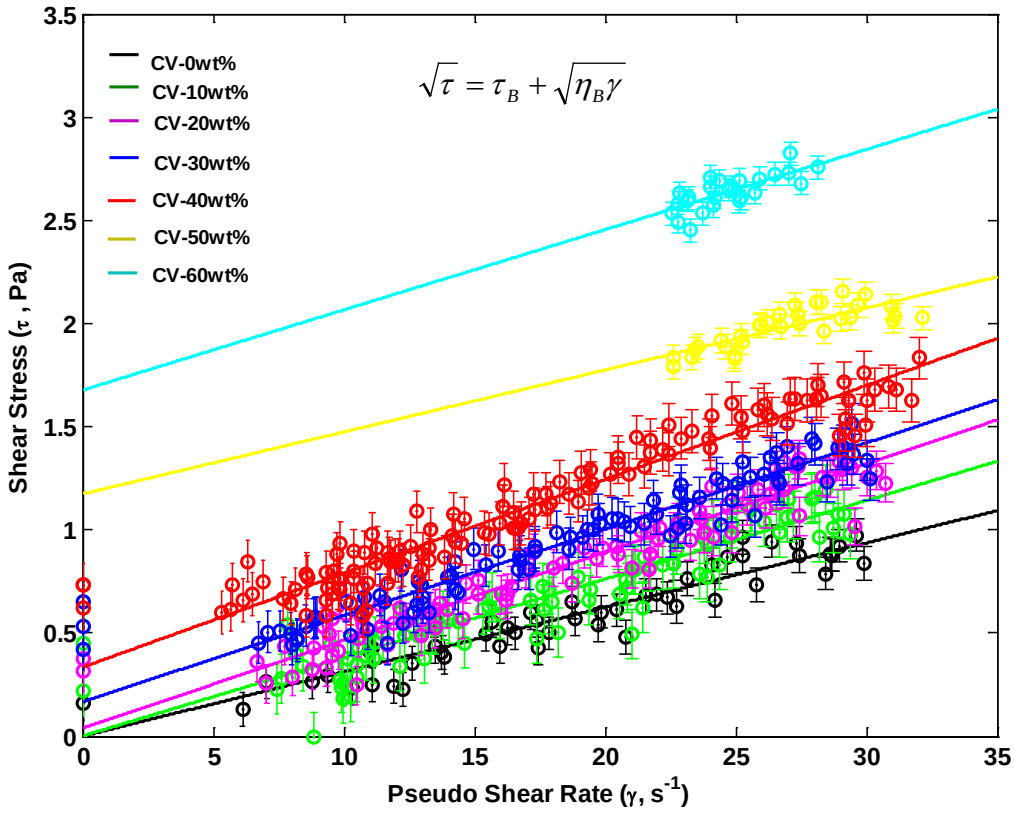

Figure 4-5: Casson Model fit to -75+53 microns El Soldado slurry rheograms at different solids concentrations.

Table 4-2: Casson Model Parameters at different solids concentrations for the -75+53microns particle size fraction.

Solids concentrations (wt%)	R^2adjusted	$\eta_B \pm \Delta \eta_B$ (Pa.s)	$\tau_B \pm \Delta\tau_B$ (Pa)
0	0.7840	0.001±0.0016	0
10	0.5895	0.001±0.0019	0
20	0.8553	0. 001±0.0011	0
30	0.8201	0.001±0.0030	0.06±0.0584
40	0.8779	0.001±0.0024	0.15±0.0445
50	0.9062	0.002±0.0024	0.45±0.0423
60	0.7566	0.002±0.0046	1.92±0.085

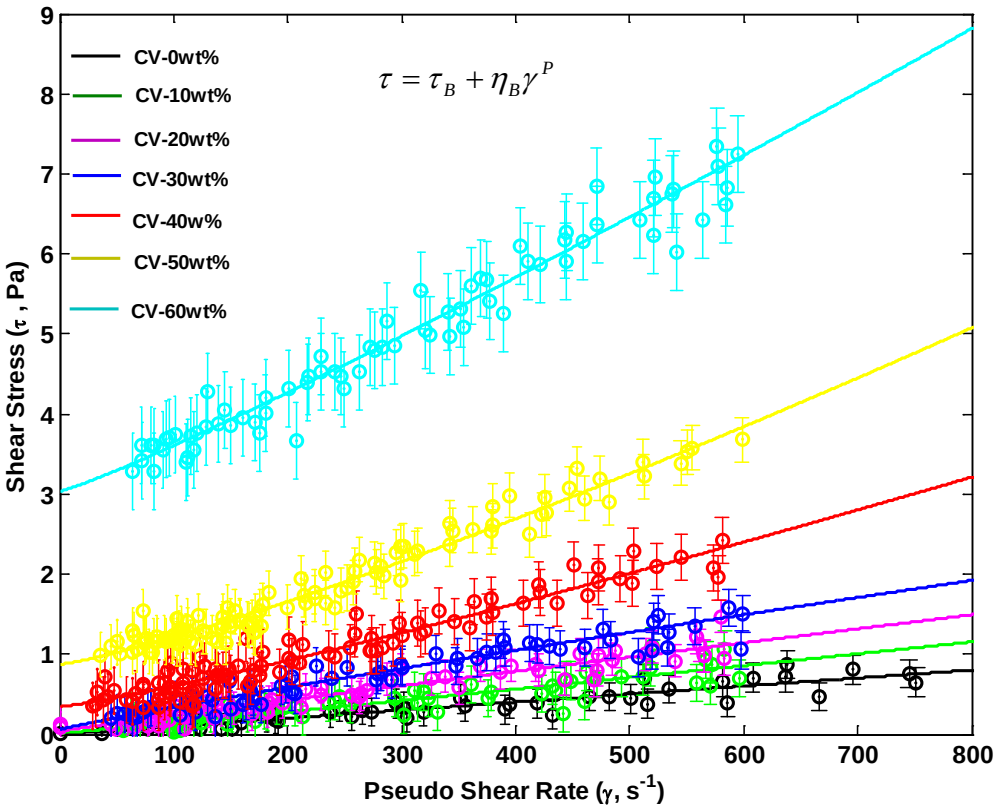

Figure 4-6: Herschel-Bulkley Model fit to -75+53 microns El Soldado slurry rheograms at different solids concentration.

Table 4-3: Herschel-Bulkley Model Parameters at different solids concentrations for the -75+53microns particle size fraction.

Solids concentration (wt%)	R^2 adjusted	$\eta_B \pm \Delta \eta_B$ **(Pa.s)**	$\tau_B \pm \Delta\tau_B$ **(Pa)**	**p**
0	0.8415	0.001±0.0028	0	0.99±0.3760
10	0.8062	0.001±0.0034	0	1.05±0.5163
20	0.9134	0.002±0.0036	0.04±0.1036	0.96±0.2330
30	0.9257	0.004±0.0068	0.06±0.1604	0.91±0.2398
40	0.9249	0.001±0.0016	0.34±0.1145	1.16±0.2010
50	0.9589	0.001±0.0012	0.87±0.1165	1.21±0.1500
60	0.9624	0.003±0.0043	3.03±0.2900	1.11±0.1890

4.4. The computation of viscosity at different solids concentrations

The Bingham model was used to compute the apparent viscosity from the slope of the rheogram using equation (4.3).

$$\tau = \tau_C + \eta_B \gamma \qquad (4.3)$$

Where: η_B is apparent viscosity; τ is Bingham shear stress, τ_C is the Bingham yield stress and γ, the shear rate.

The rheological behaviour of El Soldado slurry with a particle size fraction of -75+53 microns can be described as Bingham. This means that the viscosity is constant and does not vary with shear rate. This is demonstrated in Figure 4-4 by the constant slope of the El Soldado slurry rheograms with shear rate across the tested range of solids concentrations.

Figure 4-7 shows the Bingham viscosity plots obtained as a function of solids concentrations for the -75+53 microns El Soldado slurry particle size class. The trend which is observed is that viscosity increases with solids concentration. At low solids concentrations up to 20wt%, the viscosity values obtained are equivalent to that of water at room temperature at 0.001 Pa.s. At higher solids concentrations up to 60wt%, the viscosity increases to 0.007 Pa.s for the tested shear rate range. The viscosity

trend obtained at the various solids concentrations can be best mathematically described using the exponential expression shown in equation (4.4).

$$y = 0.0006067\exp(0.04096x) \quad (4.4)$$

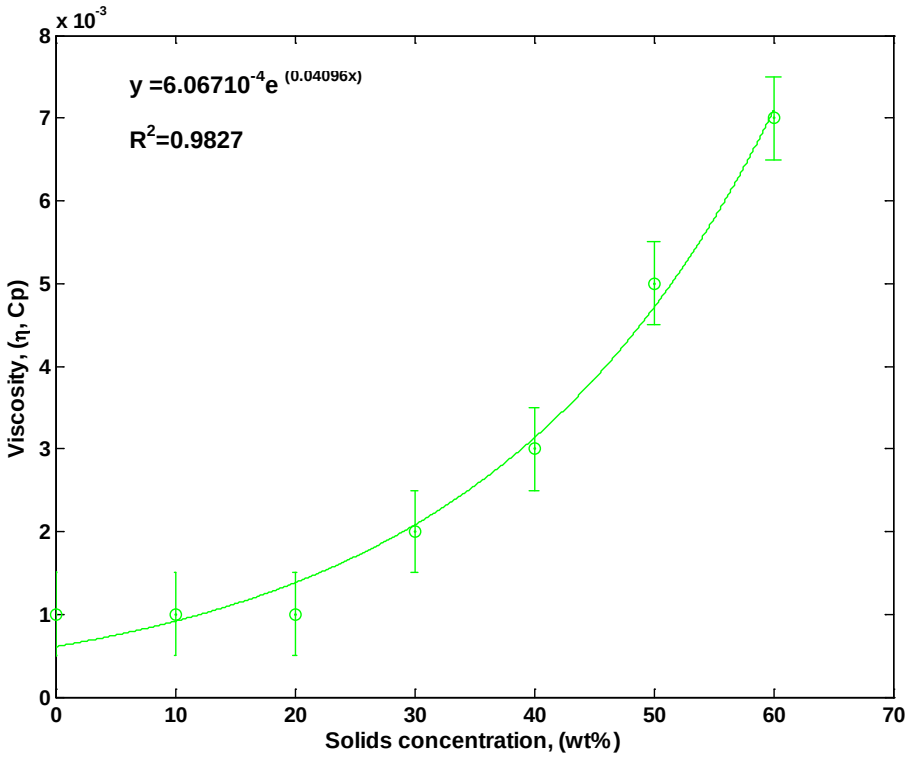

Figure 4-7: Apparent viscosity for d=-75+53 El Soldado slurry at different solids concentrations.

Figure 4-8 shows the yield stress trend obtained at different solids concentrations for the same El Soldado slurry. The yield stress was observed for solids concentrations above 10wt%. It was observed that as solids concentration increases, the yield stress also increased. The lowest and highest yield stress values attained were 0.11Pa and 2.86Pa at 30wt% and 60wt% respectively. The extrapolated yield stress values from the Bingham model are also shown in Table 4-1 for different solids concentrations. The yield stress trend obtained at the various solids concentrations can be mathematically best described using the exponential expression shown in equation (4.5).

$$y = 0.001576\exp(0.1249x) \quad (4.5)$$

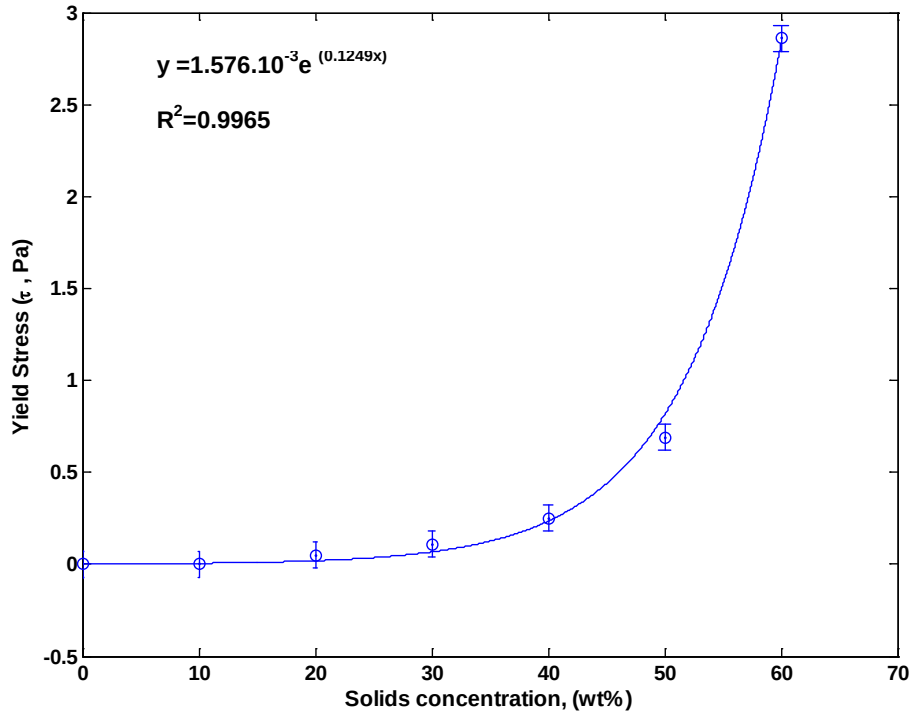

Figure 4-8: Yield stress for d=-75+53 El Soldado slurry at different solids concentrations

4.5. Discussion of results

This section presents a discussion of the results which were obtained from performing the rheology experiments.

4.5.1. Effect of solids concentration on viscosity

The Bingham model fit to experimental data was found to be the best rheological model which describes the rheology of El Soldado slurry as shown by Figure 4-4. It had the best goodness of fit as indicated by the highest R^2 adjusted values obtained overall across all tested solids concentrations compared to the Casson and Herschel-Bulkley models. Figure 4-4 also shows that the behaviour of El Soldado slurry can be described as Bingham from the constant slope of the rheogram curves across the range of tested solids concentrations. The rheology of the El Soldado slurry exhibits Newtonian behaviour with no yield stress at low solids concentrations below 30wt%. At solids concentrations from 30wt% up to 60wt% the rheological behaviour of the El Soldado slurry is Newtonian with yield stress which is also known as Bingham. This is in agreement with the rheological behaviour witnessed for quartz slurries (Tangsathitkulchai, 2003); galena slurries (Prestige, 1997) and coal slurries

(Tangsathitkulchai and Austin, 1988). They all found that the Bingham model best described the rheological data of these slurries at low solids concentrations.

To determine the effect of solids concentration on viscosity, rheological measurements of El Soldado slurry were conducted at different solids concentrations ranging from 10wt% to 60wt%. Figure 4-7 shows the relationship between viscosity and solids concentration. It shows that apparent viscosity increases exponentially with increasing solids concentration at the measured range of shear rates up to $600s^{-1}$. This is due to the increased particle-particle interactions. Cheng, (1980) also reached a similar conclusion. According to Cheng, this trend can be attributed to increased particle-particle interactions in the fluid. At low to medium solids concentrations, the effect of hydrodynamic interactions prevails and they give rise to the viscous dissipation of the liquid. As a result the viscosity increases with concentration. This is also observed at high solids concentrations but the particle-particle contact effect dominates over the hydrodynamic effect. This particle-particle contact brings into play frictional interactions. The frictional interactions per unit volume increase with solids concentration thereby increasing the viscosity of slurry. Cheng did not quantify what low, medium or high solids concentration were thus the observed phenomenon in his study could be due to either hydrodynamic interactions or particle-particle contact. He et al., (2006) also made similar observations when they conducted rheological measurements on limestone slurry (<100μm) using a Bohlin Visco 88 BV rotational viscometer. They investigated solids concentrations up to 78.5 wt%.

Figure 4-7 also shows that at low solids concentrations from 0wt% to 20wt%, viscosity is constant and is independent of shear rates. The viscosity is also equivalent to that of water which is 0.001Pa.s at room temperature. At increasing solids concentrations from 20wt% up to 60wt%, the formation of yield stress starts to appear. This is characteristic of the Bingham rheological behaviour. The yield stress increases with increasing solids concentrations as shown by Figure 4-8.

Figure 4-8 shows the relationship between yield stress and solids concentration. The yield stress increased for solids concentration values above 20wt%. The extrapolated Bingham yield stress also increases exponentially with solids concentration. An increase in yield stress means that more energy is required before the slurry starts to

flow. A similar conclusion was made by Tseng and Chen, (2003). This trend was attributed to the fact that in concentrated slurry the inter-particle distance is smaller thus there is an increased attractive potential and a larger probability of collisions between particles. This also means there are stronger interactions between particles which form loosely packed flocs and trap some water within them which is indispensable to flow. A shearing force is required to overcome the internal friction between the particles to allow the slurry to flow again by breaking down the flocs and gradually releasing the entrapped water with increasing shear rate. This trend is also in agreement with work done by Mingzhao et al., (2004) which identified that as the concentration increases the rheological behaviour of the slurry becomes more strongly non-Newtonian with a steeply increasing viscosity as the shear rate decreases. This is indicative of a possible appearance of a yield stress.

5. PEPT RESULTS AND DISCUSSION

Overview

This chapter presents and discusses the results obtained from conducting PEPT experiments. PEPT experiments were used to quantify in-situ shear rates inside the tumbling mill. A description of the methodology used to compute absolute velocity, tangential velocity and shear rates from PEPT experiments is presented.

5.1. Introduction to PEPT data analysis

PEPT experiments were conducted to quantify and characterize in-situ shear rates in a laboratory scale tumbling mill. Positron emission particle tracking (PEPT) is a method used for detecting the position of particles in vessels over a period of time (Waters et al., 2008). It was used to map the trajectory of a radioactive 1mm blue stone particle (the "tracer") as it circulated in the tumbling mill. PEPT experiments were conducted using the positron camera from Birmingham University in the United Kingdom. Experiments were performed using the -75+53μm El Soldado ore slurry at different solids concentrations and mill speeds as detailed in Table 3-3 .The information about the trajectory of the ore particle over time enabled the computation of other physical properties of charge kinematics such as velocity and shear rates from taking the appropriate partial derivative of the position data.

The raw data from the PEPT positron camera consists of lines of response (LoR's) that are triangulated using the Birmingham triangulation code (Parker et al., 1996). The result is a set of 3D Cartesian coordinates in the form of *x*, *y*, *z* and time *t*. The converted PEPT data consisted of the tracer positional data relative to the detector origin which was recorded sequentially from the start to the finish of the experimental run.

Figure 5-1 shows an example of the PEPT raw data file. The data file consisted of a header detailing the experimental and processing conditions of the PEPT experiment. The first four columns show the position Cartesian coordinates of the tracer particle (mm) as a function of time in ms. The 5thcolumn shows an error measurement which is an indication of the reliability of the tracer location. The error measurement is the

root mean square (RMS) which is predefined as part of the convergence criteria during triangulation as described in section 2.11. The 6th and 7th columns show the recorded shaft angle and torque measurements respectively which were not applicable to this tumbling mill system being studied. The 8th column shows the number of events used in calculating the tracer location. An event is when the gamma rays from the decaying tracer are simultaneously detected by both detectors. The accurate location of the tracer is determined from the detection and triangulation of these gamma rays as detailed in section 2.11.1.

```
Processed on: 9-JULY-06
Words per event :    4        Reads :    2680        Camera sep :   300.00mm
First event :         1         Last event :   6855844
f(opt) :   0.190       Displacement parameters :   180.0, 450.0, 450.0
Number of Locations :     37685
Experiment time :       3692.84
P-code : 1.2_1.2_1.4_1.4_256_256_128_128_2F2F_ 2000_10000_ 1000_     0_ 5_V
```

Time (ms)	X (mm)	Y (mm)	Z (mm)	Error	Angle	Torque	No. of Events
215.7	161.6	264.5	177.8	5.0	0.0	0.00	-188
405.2	163.3	259.1	175.8	5.4	0.0	0.00	287
534.0	164.7	255.0	176.6	5.4	0.0	0.00	272
645.9	166.7	251.4	175.7	5.4	0.0	0.00	258
768.0	168.7	248.2	173.8	5.4	0.0	0.00	245
827.0	169.2	247.1	173.7	6.5	0.0	0.00	286
881.4	170.4	245.6	173.6	6.4	0.0	0.00	232
924.8	171.9	244.7	172.0	6.4	0.0	0.00	178
963.5	173.7	245.8	171.3	6.4	0.0	0.00	139
993.7	174.2	246.4	170.0	6.4	0.0	0.00	97
1013.5	174.9	247.2	169.8	6.6	0.0	0.00	67
1034.2	175.5	248.6	168.4	6.6	0.0	0.00	44
1047.5	178.3	249.3	169.4	6.5	0.0	0.00	32
1057.7	179.4	252.7	167.8	6.6	0.0	0.00	29
1067.4	177.2	254.2	168.2	6.5	0.0	0.00	20

Figure 5-1: An example of the raw data file generated from PEPT.

The PEPT position-time data was then imported into the MATLAB program which was used to perform all the analyses in this work. The methodology used to process the data and extract the relevant velocity and shear rate data is given in the sections that follow.

5.2. Computing absolute velocity profiles from PEPT data

The positional coordinates of the tracer particle with time is unevenly spaced. The triangulation technique for determining the tracer location in the mill uses consecutive groups of Lines Of Response (LOR) for each triangulation. As a result of the random nature of radioactive decay, the time spacing between each LOR is not the same. Each group of LORs span different times. Consequently the time spacing between each triangulated point is not the same. A 2nd order Lagrange Interpolation polynomial was fitted between the positional coordinates to generate a continuous and smooth trajectory from which the velocity can be computed by differentiation. The Lagrange interpolating polynomials used are denoted by the general form shown in Equation (5.1) and Equation (5.2).

$$f_n(x) = \sum_{i=0}^{n} L_i(x) f(x_i) \tag{5.1}$$

where 'n' in $f_n(x)$ denotes the n^{th} order polynomial that approximates the function $y = f(x)$ given at $(n+1)$ data points as $(x_0, y_0), (x_1, y_1), ..., (x_{n-1}, y_{n-1}), (x_n, y_n)$ and

$$L_i(x) = \prod_{\substack{j=0 \\ j \neq i}}^{n} \frac{x - x_j}{x_i - x_j} \tag{5.2}$$

$L_i(x)$ is a weighting function that includes a product of $(n-1)$ terms with terms of $j = i$ omitted. In its expanded Equation 5.1 becomes;

$$f_n(x) = \frac{(x-x_2)(x-x_3)...(x-x_n)}{(x_1-x_2)(x_1-x_3)...(x_1-x_n)} y_1 + \frac{(x-x_1)(x-x_3)...(x-x_n)}{(x_2-x_1)(x_2-x_3)...(x_2-x_n)} y_2 + ... + \frac{(x-x_2)(x-x_2)...(x-x_{n-1})}{(x_n-x_1)(x_n-x_2)...(x_n-x_{n-1})} y_n$$

When selecting the order of the interpolation function it was necessary to take cognisance of the trade-off between obtaining a better fit and a smooth well-behaved fitting function. Using more data points resulted in a higher degree polynomial with greater oscillation between data points. Interpolation using a higher degree polynomial increases fitting accuracy but at the expense of poor prediction by the function between data points. A 2nd order interpolation polynomial, finite differencing

scheme was used and was previously shown by Wolfram et al., (2008) and Chapra and Canale, (1989) to be a suitable approach for determining the velocity.

In this work, the cross section of the mill inner volume was uniformly discretised into a fine rectangular grid of 50× 50 cells. Each cell represented a bin. The positional data and the subsequent velocity calculations were binned into these equal size cells to aid the analysis of the axially-averaged charge behaviour per cell. The mill system was assumed to be ergodic to ensure that the tracked tracer particle was representative of the entire system. Ergodicity means the time and ensemble averages of a given quantity are equal (Wildman, 2000). This implies that the time averaged behaviour of the single tracked tracer particle was assumed to be representative of the system's behaviour of the same size class at steady state.

The time-averaged tracer velocities per bin were computed as the first derivative of the Langrange polynomial at the data points. The same binning technique was used to characterise the absolute and tangential velocities across the mill. Figure 5-2 and Figure 5-3 show the absolute velocity and vector velocity profile plots obtained when tracking a 1mm bluestone slurry particle in mill charge containing 30wt% slurry and the mill operating at 60% and 75% critical speeds.

5.2.1. Absolute velocity profiles trends at different solids concentrations and mill speeds.

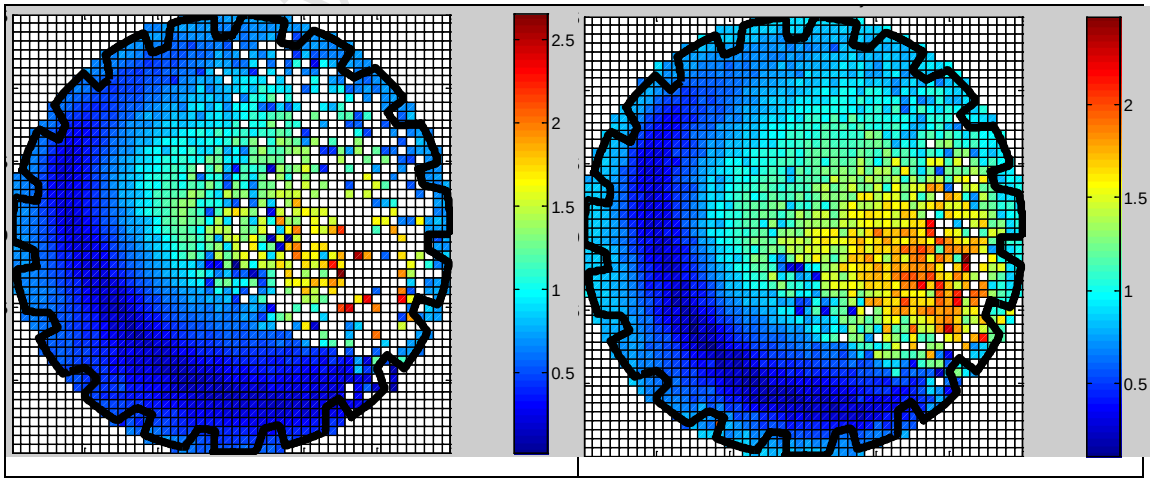

Figure 5-2: Magnitude plot of absolute velocity profile for a1mm bluestone slurry particle at 30%wt solids concentration at 60% (left) and 75% (right) critical mill speeds.

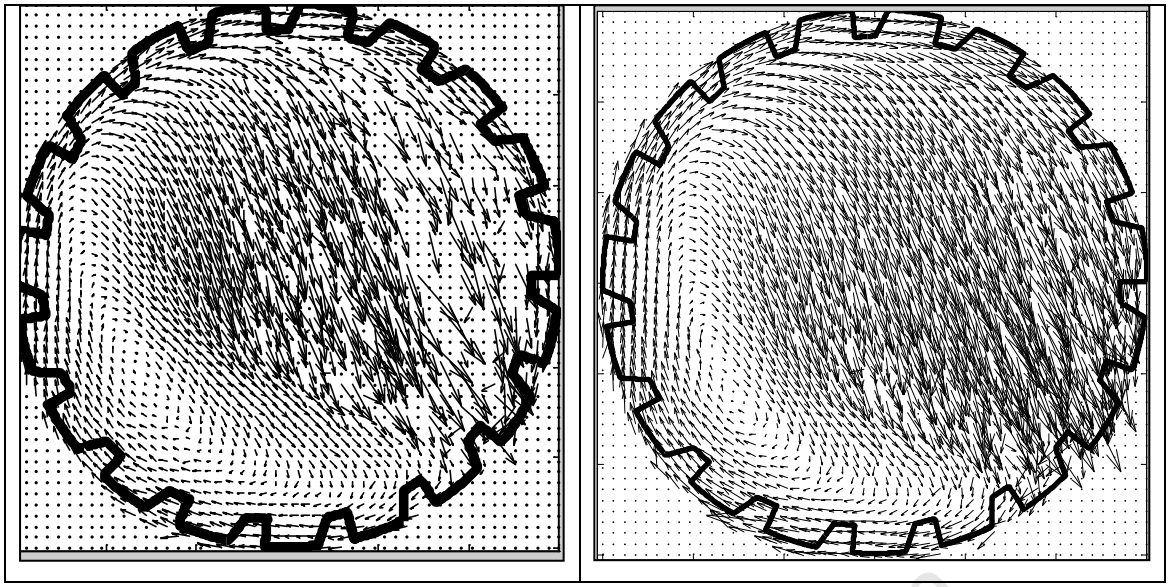

Figure 5-3: Velocity vector profile for a1mm bluestone slurry particle at 30%wt solids concentration at 60% (left) and 75%(right) critical mill speeds.

Section B2 and section B2.1 in Appendix B show the magnitude and velocity field profile plots for all PEPT slurry experimental runs conducted at solids concentrations ranging from 20%wt to 40%wt at different mill rotational speeds of 60% and 75% of the critical mill speed. These velocity profile plots are similar to Figure 5-2 and Figure 5-3 and show a two dimensional view of the mill oriented horizontally. The colour scale of these plots represents the magnitude of the absolute velocities. The colour scale shown in Figure 5-2 ranges from navy blue which indicates low absolute velocities to red which indicates high absolute velocities in $m.s^{-1}$. The white colour indicates regions of no tracer occupancy. With reference to Figure 5-2 a varying velocity profile can be observed across the mill plane. The absolute velocity increases from the rising region to the cataracting region of the charge towards the mill centre. The lowest absolute velocities are obtained in the rising and cascading region of the charge. The velocity gradually increases radially from the cascading region and is the highest in the cataracting region with absolute velocities ranging between $1.5m.s^{-1}$ and $2.5m.s^{-1}$ .Section B2 and section B2.1 in Appendix B also shows the time- averaged velocity field profiles for the same selection of runs. The relative magnitude and direction of the velocity of the particle for each location is represented by an arrow. The length and direction of the arrow indicates the tracer velocity averaged over all tracer locations falling within the bin over the duration of the entire run. These velocity plots show the flow of the charge inside the tumbling mill. The clockwise

rotation of the charge, the centre of circulation (CoC) and other regions of the charge such as the equilibrium surface, shoulder and toe positions can be identified. A distinction between the active rising charge and passive cascading charge can also be observed. Similar PEPT velocity trend profiles were observed by Parker et al., (1996) who used PEPT to conduct studies using 1.5mm and 3mm spherical glass beads rotating in a drum at different mill speeds ranging from 10rpm to 65rpm. Conway-Baker et al., (2002); Barley et al., (2004) and Bakalis et al., (2006) also applied the PEPT technique to different systems to conduct velocity measurements. They used a similar PEPT data analysis methodology as described in section 5.2.

5.3. Computing the tangential velocity profiles in the tumbling mill from PEPT data

The computation of the tangential velocity is the key component in the formulation of the shear rate estimation methodology used in this thesis. Tangential velocity is the tangential component of the linear velocity of the tracer particle in the rotating mill at a distance *r* from the axis of rotation. The axis of rotation is the centre of the mill. The tracer particle's tangential velocity was calculated using Equation (5.3). The tangential velocity profiles were then obtained from averaging the tangential velocities for all tracer locations within each bin.

$$\vec{V}_t = \vec{V} - \left(\frac{\vec{V} \cdot \vec{r}}{|\vec{r}|^2} \right) \vec{r} \qquad (5.3)$$

where $\vec{r}$ is the position of the particle, $\vec{V}$ is the velocity, and $\vec{V}_t$ is the tangential velocity.

Figure 5-4 shows the magnitude and vector plot of the calculated tracer tangential velocities at each radial position along a diametrical line passing through the mean centre of circulation (CoC) for a PEPT experiment run at 30wt% slurry and at 60% and 75% critical mill speeds. The CoC was chosen because it is a unique location in the charge which is characteristic of the milling configuration. The colour scale in $m.s^{-1}$ represents the magnitude of the tangential velocity across the plane of the mill. The navy blue colour represents low tangential velocities while the red colour represents high tangential velocities. The magnitude and direction of the tangential

velocity of the tracer particle for each location is represented by an arrow. The arrow also indicates the tracer tangential velocity averaged over all tracer locations falling with the bin over the duration of the entire run.

Section B3 and section B3.1 in Appendix B presents the tangential velocity profile plots for a selection of PEPT slurry experimental runs at solids concentrations ranging from 20wt% to 40wt% and operated at critical mill speeds of 60% and 75% in a laboratory tumbling mill. The observed trend shows a variation in the tangential velocities across the mill. The tangential velocities decrease linearly to very low magnitudes from the mill shell towards the equilibrium surface. Beyond the equilibrium surface towards the centre of the mill, the tangential velocities start increasing again. The tangential velocities are highest in the cascading region near the mill shell and the cataracting region towards the centre of the mill as shown in Figure 5-4.

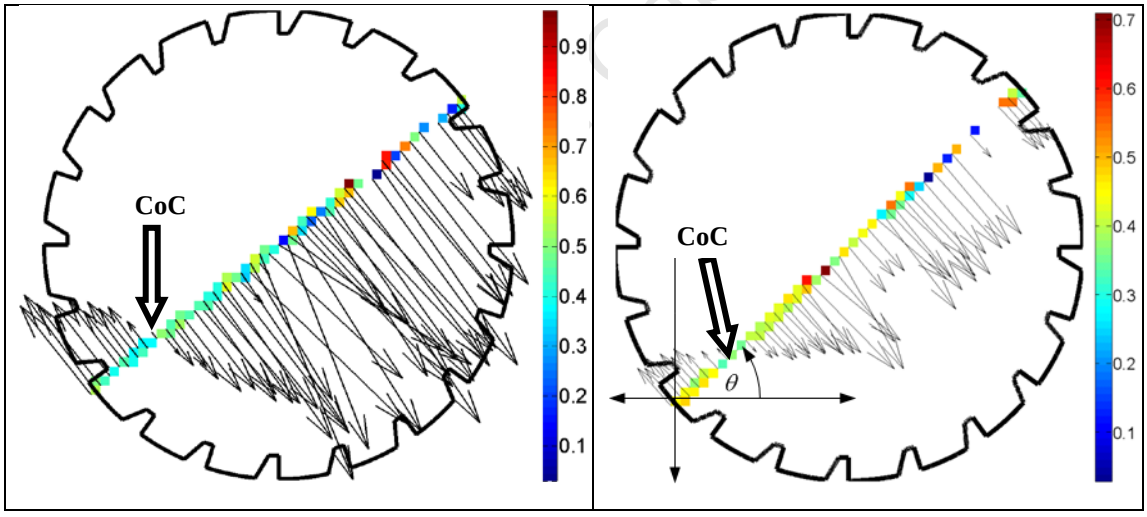

Figure 5-4: Magnitude plot of the tangential velocity profile for a1mm bluestone slurry tracer particle in 30%wt slurry at 60% (left) and 75% (right) critical mill speed.

5.3.1. Tangential velocity profile trends at different solids concentrations and mill speeds

A best fit function shown in Figure 5-5 was fitted to the derived tangential velocity data. It is of the form shown by Equation (5.4).

$$V(r,\theta) = a_1 \sin(b_1 r + c_1) + a_2 \sin(b_2 r + c_2) \quad (5.4)$$

where $V(r, \theta)$ is the tangential velocity at polar coordinates (r, θ) along the diametrical line with r measured from the bottom of the line and a_i, b_i, c_i are coefficients to be fitted.

The circles represent the calculated tangential velocity data and the solid line represents the fitted model shown in Equation (5.4). The red line shows the 'no slip 'tangential velocity trend which would be expected if the tumbling charge in the mill was rotating as a solid body. The no slip tangential velocity is calculated using Equation 5.5.

$$V_t = \omega r \quad (5.5)$$

where r is the mill radius and ω is the rotation rate of the mill shell.

However; due to the dynamic and complex motion of the charge in a tumbling mill the tangential velocity profile along the diametrical line passing through the mean CoC is not linear. The sinusoidal function shown in Equation 5.4 was found to be the best fit function for all the milling configurations tested at different solids concentrations and mill speeds. This model best described the tangential velocity trends up to the free surface at approximately r =0.12.

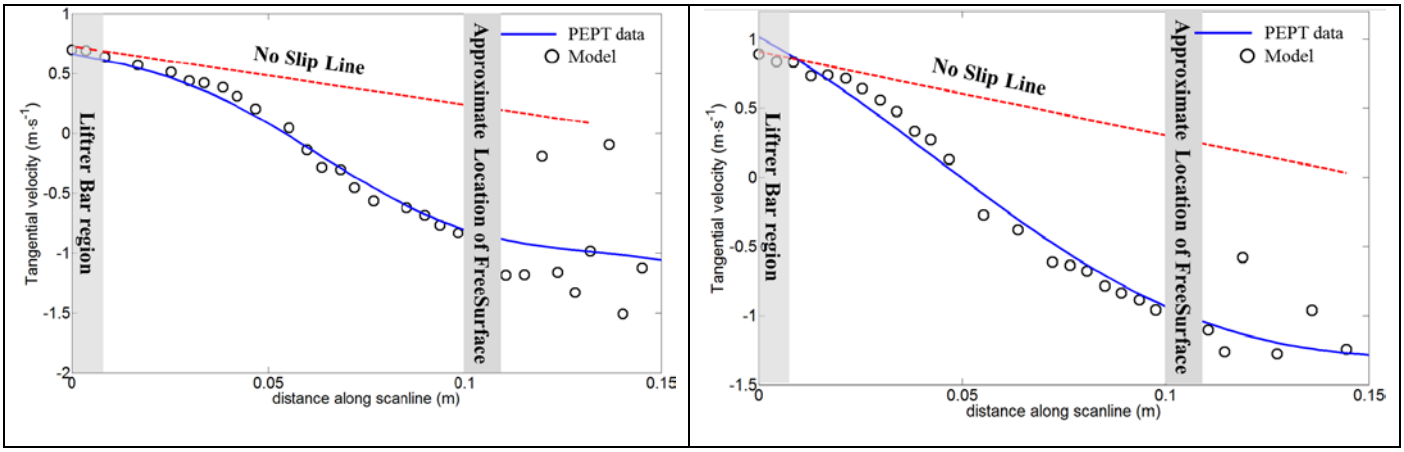

Figure 5-5: Variation of tangential velocity along a diametrical line passing through the mean CoC for a1mm bluestone tracer particle in 30%wt slurry at 60%(left) and 75% (right) critical mill speed.

At the region near r = 0 up to the lifter bar height, the red line and the PEPT data are statistically equivalent. At radii greater than the lifter bar, the PEPT tangential velocity data drops off from the red line. This means the tracer particle tangential velocity is decreasing more than the tangential velocity of the solid body. The variation in tangential velocities across the mill indicated that there is a velocity gradient in the rising and cascading charge regions as you move towards the region of the free surface. This is an indication of slip occurring. The greater the vertical difference between the red line and the blue line, the greater the slip. Beyond the free surface, the concept of slippage between layers becomes meaningless because particles are cataracting through the mill. This is the reason why the tangential velocity profiles were analysed up to the region of the free surface at r= 0.12m. Figure 5-5 has been truncated at the mill centre to exclude the cataracting charge. A similar trend shown in Figure 5-4 and Figure 5-5 was observed by (Yamane et al., 1998). According to (Yamane et al., 1998) with further radial increase from the mill shell, the charge particles start to slip and the velocity deviates from linearity. This defines the lower boundary of the sliding layer. The sliding area is a breakage region within the body of the charge as it is lifted by the rotation of the mill. In this region the charge does not move as a solid body but comprises of a series of layers which slip over one another. This gives rise to an angular velocity gradient in the charge (Napier-Munn et al., 1996). As you move further towards the "free surface" of the charge the tangential velocity decreases further to zero. At this point the sliding

velocity is equal to the mill rotational speed. Beyond the mill centre, the tangential velocity oscillates into the cataracting region of the mill and cannot be accurately predicted.

Slippage between layers in the en-masse region of the charge also suggested that there was shearing taking place. Shear rate profiles were analysed up to r= 0.12m. The advantage of having a good fitting function is that it resulted in a better derivative for computing the mill shear rates.

5.4. Computing shear rate profiles in a tumbling mill using PEPT data

Mill shear rates were computed from the first derivative with respect to *r* of the tangential velocity model shown in Equation (5.4). The resulting shear rate model equation was of the form shown by Equation (5.6).

$$\gamma(r,\theta) = a_1 b_1 \cos(b_1 r + c_1) + a_2 b_2 \sin(b_2 r + c_2) \qquad (5.6)$$

where θ is constant along the diametrical line going the mean CoC.

Due to the S-shaped obscured free surface in tumbling mill flows caused by the cascading and cataracting motions, a simple choice for θ that allows for comparison across the different operating conditions is not as clear as the perpendicular bisector used by (Nakagawa et al., 1997). A consistent choice would be a diametrical line passing through the centre of circulation (CoC) of the charge. McBride et al., (2003) and Govender et al., (2004) described a clear definition and calculation of the CoC. Further to this definition, the authors note that the CoC is not a point but a region. Accordingly an angular range (θ_{CoC} ± 20°) about the mean CoC was used. Equation 5.6 was applied to the tangential velocity profile illustrated in Figure **5-5** to obtain the shear rate profile along diametrical line passing through the centre of circulation (CoC) of the charge. The shear rate profiles were only computed up to the approximation of the end of the charge bed. This was approximated to be at r=0.12m.

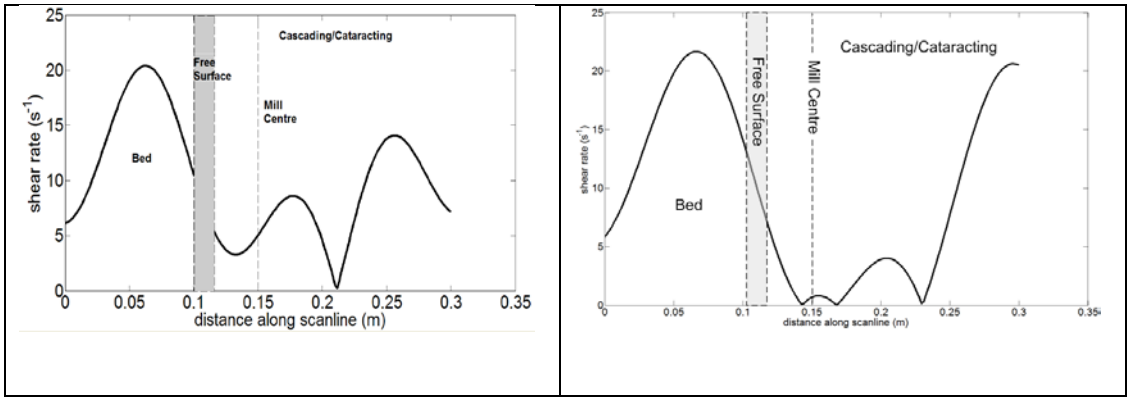

Figure 5-6: Magnitude plot of shear rate profile for a1mm bluestone slurry particle at 30%wt solids concentration at 60% (left) and 75%(right) critical mill speeds.

Figure 5-6 shows the variation of shear rates along the diametrical line passing through the mean CoC. The chosen region of interest for extracting shear rates was the rising and cascading regions of the mill charge. Maximum charge pressure is expected in these regions and thus more shear stress and slip between layers was anticipated in this region. The variation of shear rates in the charge bed was the focus for further analysis. The general trend shows that the shear rates increase with radial position from the mill shell to some maximum value and then they start decreasing. This trend was observed across all tests solids concentrations and mill speeds as shown in Appendix B. Figure **5-7** shows the computed shear rate profiles at different angular positions at 20 degrees above and below the CoC. For comparison across the different speeds and slurry solids concentrations ranges investigated, the maximum shear rate was extracted.

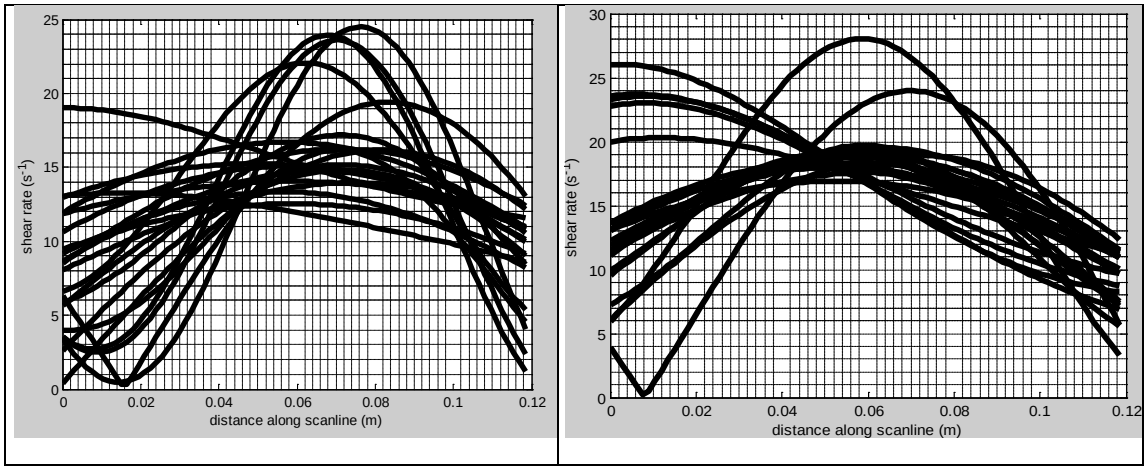

Figure 5-7: Mill shear rates at different angular positions for a 1mm bluestone slurry particle at 30%wt solids concentration and 60%(left) and 75%(right) critical mill speeds.

5.5. Shear rate Discussion

Mill shear rates were computed at different solids concentrations and mill speeds. The maximum shear rates were computed at an angular position range $-20^{o} < \theta < 20^{o}$. Figure 5-8 shows the variation of maximum shear rates obtained at across the investigated solids concentrations and critical mill speeds at 60% and 75%. The highest shear rates were obtained at the lowest solids concentration for both mill speeds. It was $30s^{-1}$ at 60% critical mill speed and $36s^{-1}$ at 75% critical mill speed. This is in the lower range compared to the shear rate range estimations made by Shi and Napier-Munn, (1999) on ball mill shear rates being between $13s^{-1}$- $730s^{-1}$. The high end of this range seems unlikely in the context of the mill system and operating conditions being studied.

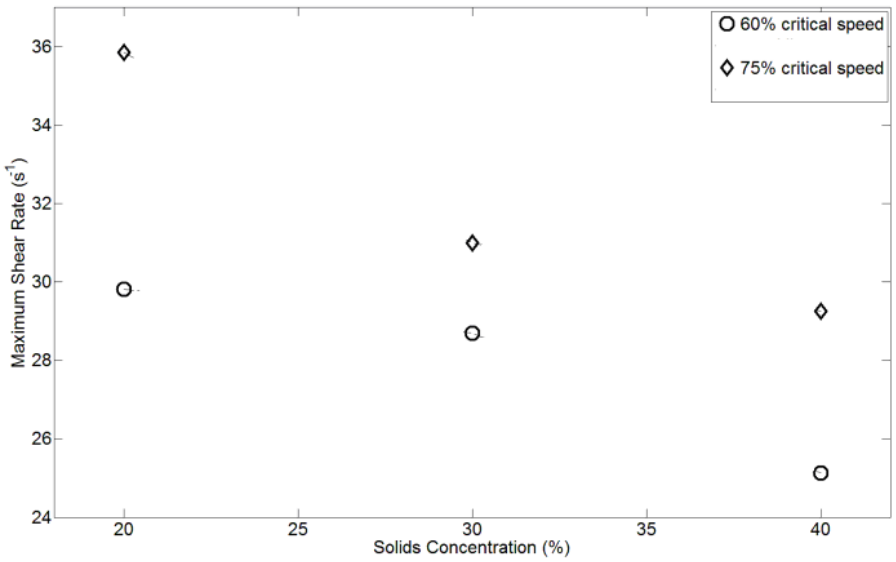

Figure 5-8: Maximum shear rates at different solids concentrations and mill speeds.

Figure 5-8 also shows that mill shear rates decrease with increasing slurry solids concentration. This is because as the solids fraction is increased, the particle packing per unit volume also increases. This reduces voidage, this implies there is less volume available for particle shearing (Cheng, 1980). This could be attributed to increased particle-particle interactions as solids concentration is increased. Consequently a decrease in shear rates is observed.

The magnitude of the maximum shear rate is higher for the 75% critical mill speed at all slurry solids concentrations. This is because at higher speed the mill charge is fairly dilated by the strong centrifugal effects that oppose the natural packing structure which results in an overall decrease in bulk density (Liddell and Moys, 1988). The increased voidage allows more volume for relative motion, producing an overall increase in shear rate.

6. COMPUTATION OF VISCOSITY PROFILES IN TUMBLING MILLS

Overview

This chapter presents the proposed methodology for combining PEPT in-situ shear rates and Rheology information to obtain viscosity distributions for regions of interest in the tumbling mill. Viscosity distributions in the mill can be used to determine regions in the mill were transport is dominant.

6.1. Summary of results

The objective of this thesis was to develop a quantitative methodology for computing and characterising viscosity profiles in a tumbling mill from combining in-situ shear rates obtained from PEPT experiments and rheology data obtained from rheometer experiments. The complex environment in the tumbling mill makes the existing flow models such as the Ergun equation insufficient to fully describe the transport of both fluid and particles in these systems. The Ergun equation shows that viscosity has a significant influence on the transport of slurries in packed bed systems. The transport of material in the tumbling mill is influenced by the rheological properties of the solid-liquid mixture that forms the slurry. The optimization of the rheological behaviour of slurries during grinding can increase throughput, product fineness and energy efficiency. The aim of this study was to develop a methodology for characterising in-situ viscosity profiles in tumbling mills that could be incorporated in transport models.

PEPT experiments were conducted to quantify the typical in-situ shear rates and distributions that occur at various regions in the tumbling mill. Rheometer experiments were conducted to rheologically characterise the El Soldado slurry viscosity at a wide range of shear rates. This enabled the quantification of viscosity distributions from the slope of the rheogram at typical shear rates found in the tumbling mill.

6.1.1. Key findings from rheology experiments

Rheology experiments were performed to determine the rheological characteristics of El Soldado slurry at different solids concentrations. The investigated slurry solids concentration range was between 10wt% to 60wt% (4vol% – 35vol %). The slurry particle size range was -75+53 microns. Rheometer experiments were conducted using a U-tube rheometer and the results were generated in a form of a rheogram.

Different rheological models were then fitted to the rheogram data to find a model which best described the rheological characteristics of the El Soldado slurry. The Bingham rheological model was found to best describe the rheology of El Soldado slurry since it had the highest R^2 adjusted values ranging from 0.82 to 0.96 at all tested solids concentrations ranges compared to the Casson and Herschel Bulklely models. The rheological behaviour of El Soldado slurry with a particle size fraction of -75+53 microns can be described as Newtonian at low solids concentration up to 20wt%, there is no yield stress. At higher solids concentrations above 20wt% up to 60wt% it displayed Bingham characteristics. This means that the viscosity is constant with yield stress and does not vary with shear rate.

The fitted Herschel Bukley power index (P) is approximately 1 across all solids concentrations up to 60wt%. The power indices range between 0.91-1.21. This further supports that the flow curves are Bingham. Typical industrial tumbling mill slurries are operated between 68wt% and 80wt%. Rheological measurements could not be taken at this high solids concentrations range due to the limitations imposed by the U-tube rheometer. However; it seems with further extrapolation, an increase in solids concentration above the measured 60wt% (35vol%) the power index is increasingly becoming greater than 1. This is characteristic of dilatant behaviour which means with higher solids concentrations viscosity will also start to increase with shear rates. Many coal and mineral slurries also show dilatant characteristics at low slurry concentration less than 40-45% solids by volume for a particular size distribution (Klimpel, 1984).

The model fitting yielded the viscosity (η_B) and yield stress (τ_B) parameters for different rheological models which were tested. The extracted model parameters are shown in Table 4-1 to Table 4-3. The observed trend showed that yield stress

increased with solids concentration for all tested rheological models tested. The viscosity also increased with solids concentration for the Bingham and Casson models. For the Herschel-Bulkley the viscosity increased with solids concentration up to 30wt%. At higher solids the viscosity trend could not be clearly defined. This was also an indication of the unsuitability of the Herschel-Bulkley model to be applied to the obtained rheogram data at the tested low range of solids concentration. The Bingham rheological model was then used for further viscosity and yield stress analysis.

The Bingham viscosity and yield stress increased in an exponential form with solids concentration. At lower solids concentrations up to 20wt% the El Soldado slurry viscosity is equivalent to that of water at room temperature at 0.001Pa.s. This further supports that the rheological characteristic of the El Soldado slurry at these low solids concentration is Newtonian. Viscosity is constant and does not vary with shear rate. At higher solids concentrations up to 60wt% the viscosity increases up to 0.007Pa.s. The yield stress was observed for solids concentrations above 20wt%. The lowest and highest yield stress values obtained were 0.11Pa and 2.86Pa at 30wt% and 60wt% respectively. Solids concentration has a significant effect on slurry viscosity yield stress and consequently the rheological characteristics of slurry.

6.1.2. Key findings from PEPT experiments

PEPT experiments were conducted to quantify the in-situ shear rate distributions in a laboratory scale tumbling mill at different solids concentrations and mill speeds. The investigated slurry solids concentration ranged between 20wt% to 40wt% (8vol% – 19vol %). The mill speed was operated at 60% and 75% of the critical speed.

The computation of the tangential velocity was the key component in the formulation of the shear rate estimation methodology used in this thesis. Tracer tangential velocities were calculated at each radial position along a diametrical line passing through the mean centre of circulation (CoC). A best fit sinusoidal function shown in Equation 5.4 was fitted to the derived tangential velocity data. This model best described the tangential velocity trends up to the free surface of the charge at approximately r =0.12m. At radii above equilibrium surface at r= 0.12m, the charge

behaviour indicated the start of the cataracting region in the mill where the charge particles were being flung from the shoulder to the toe position of the charge and the tangential velocity oscillates and cannot be accurately predicted. There are no particle- particle interactions and thus no shearing taking place in this region. The tangential velocities decreased to very low magnitudes close to zero with radial increases from the mill shell up to the CoC. This was attributed to the charge particles starting to slip and the velocity deviating from linearity. In this region the charge does not move as a solid body but comprises of a series of layers which slip over one another. At the CoC the sliding velocity is equal to the mill rotational speed. Beyond the CoC towards the equilibrium surface the tangential velocities start increasing again. The variation in tangential velocities across the mill indicated that there is a velocity gradient in the rising and cascading charge regions as you move towards the region of the free surface. This was an indication of slip occurring in this region which suggested that shearing was taking place.

Shear rate characterization in the mill was computed from average tangential velocity distributions and displacement data obtained from performing tumbling mill PEPT experiments. Mill shear rates decreased with increasing slurry solids concentration. The highest shear rates were obtained at the lowest solids concentration for both mill speeds. It was $30s^{-1}$ at 60% critical mill speed and $36s^{-1}$ at 75% critical mill speed. This was attributed to increased particle-particle interactions and reduced voidage. There is less volume available for particle shearing. The magnitude of the maximum shear rate is higher for the 75% critical mill speed at all slurry solids concentrations. At a higher speed the mill charge is fairly dilated by the strong centrifugal effects that oppose the natural packing structure which results in an overall decrease in bulk density. The increased voidage allows more volume for relative motion, thus producing an overall increase in shear rate. These trends are shown in Figure 5-8. The calculated shear rate ranges are $24.8s^{-1}$ to $30s^{-1}$ at 60% critical mill speed and $29.4s^{-1}$ to $36s^{-1}$ at 75% critical mill speed across the investigated solids concentrations. This is a narrow shear rate range showing an insignificant variation in the shear rate profile in the en-masse region of the tumbling mill at the investigated critical mill speeds.

6.1.3. Viscosity profiles in the tumbling mill.

Viscosity profiles in the en-masse region of the laboratory tumbling mill were computed from combining the tumbling mill in-situ shear rate ranges obtained from PEPT experiments with the rheology data from rheometer experiments. PEPT and rheological measurements could only be performed up to solids concentrations of 40wt% and 60wt% by mass respectively. This was due to the measurement limitations imposed by the equipment. A wider range of solids concentrations could be tested using the U-tube rheometer. Rheology experiments could not be conducted at solids concentrations above 60wt% because the slurry started settling and causing plugging in the rheometer. PEPT experiments were conducted at solids concentrations less than 40wt% because above 40wt% the tracer particle got stuck in certain regions of the tumbling mill particularly in the grate. Performing more experiments under these conditions could have resulted in PEPT data which was not representative of the charge behaviour in the tumbling mill.

The Bingham rheological model was found to best characterise the rheology of El Soldado slurry at a wide range of shear rate distributions from $0s^{-1}$ to $600s^{-1}$ across the tested solids concentration range of 10wt% to 60wt%. The measured in-situ shear rates encountered in the en-masse region of the tumbling mill charge along the diametrical line ranged between $24.8s^{-1}$ to $30s^{-1}$ at 60% critical mill speed and $29.4s^{-1}$ to $36s^{-1}$ at 75% critical mill speed. The measured in-situ shear rates in the laboratory scale tumbling mill using PEPT were found to be lower than the shear rate range measured by the U-tube rheometer.

The derived Bingham model shown in Equation 4.6 was used to compute the apparent viscosity from the slope of the Bingham curves show in Figure 6-1 and Figure 6-2. The corresponding viscosities shown in Table **6-1** were computed at a solids concentrations range of 20wt% to 40wt%. This solids concentration range was chosen as a basis for combining PEPT and rheology data since both experiments were able to be performed within this operating range. The Bingham viscosities are constant and independent of shear rates at each solids concentration. This means that in-situ viscosities do not vary with mill shear rates encountered in the en-masse region of the tumbling mill.

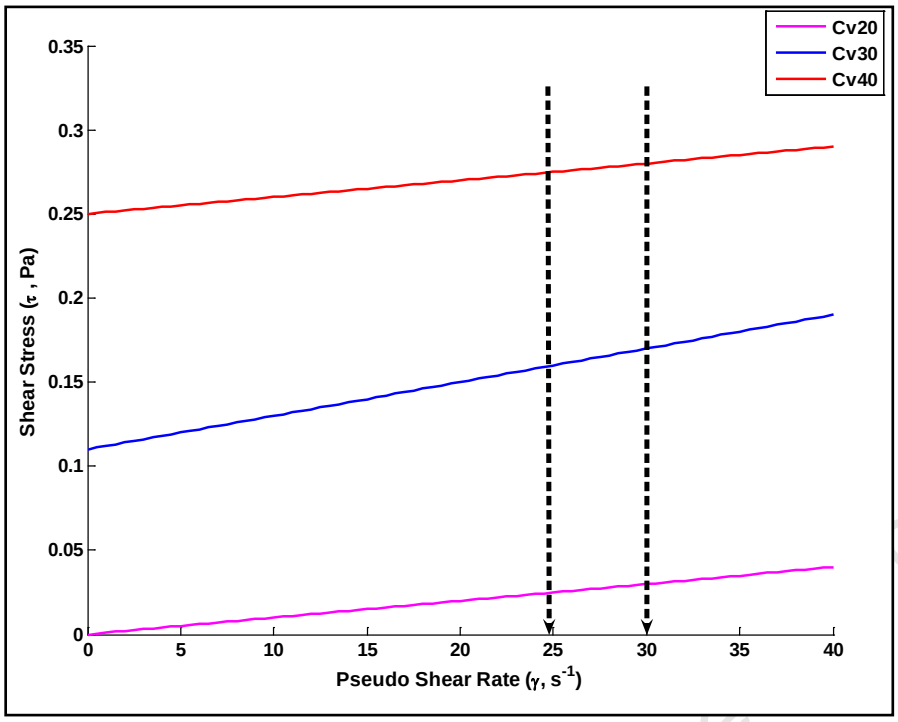

Figure 6-1 : El Soldado slurry rheograms for different solids concentrations at the measured in-situ shear rate ranges obtained at 60% critical mill speeds.

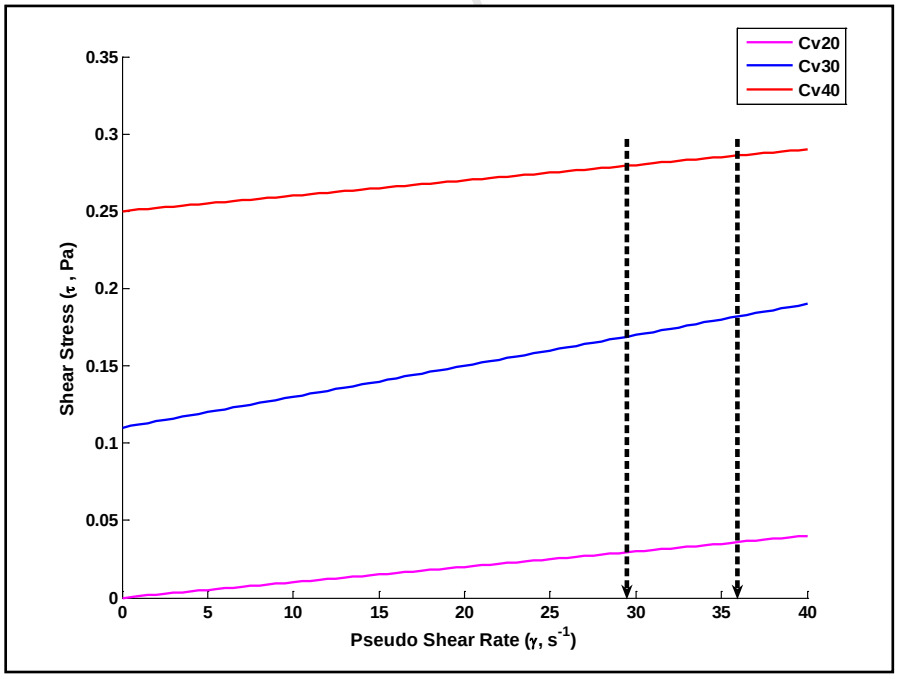

Figure 6-2: El Soldado slurry rheograms for different solids concentrations at the measured shear rate ranges obtained at 75%% critical mill speeds.

Table 6-1: Slurry viscosities obtained at 60% and 75% critical mill speeds

Solids concentrations (wt%)	R^2adjusted	$\eta_B \pm \Delta \eta_B$ (Pa.s)	$\tau_B \pm \Delta\tau_B$ (Pa)
0	0.8203	0.001±0.0001	0
20	0.9147	0.001±0.0001	0
30	0.9298	0.002±0.0002	0.11±0.0481
40	0.9231	0.003±0.0002	0.25±0.0532

Viscosity does not vary significantly in the different regions of the mill since the shear rate range is narrow and the rheological behaviour of the El Soldado slurry is Bingham like. However, operating the mill at different solids concentrations would result in significant changes in the viscosity. This is also shown in Figure 4-7 by the exponential increase of viscosity with increasing solids concentration. This implies that a single viscosity value can be used in the viscosity model to represent all regions in the tumbling mill for a given solids concentration.

7. CONCLUSIONS AND RECOMMENDATION

Overview

This chapter summarises the main conclusions from this thesis and presents recommendations for future work.

7.1. Conclusions

The objective of this thesis was to develop a methodology for characterising viscosity distributions inside a laboratory scale tumbling mill using in-situ shear rate distributions obtained from PEPT and rheological characteristics of the El Soldado slurry from rheometer experiments. Rheometer experiments were performed using a U-tube rheometer to rheologically characterise the El Soldado slurry at a wide range of shear rates. The PEPT experiments provided information about the typical shear rate ranges that occur inside the mill. This enabled the quantification of viscosity distribution from the slope of the rheogram curve at typical shear rates found in the tumbling mill. The two mill operation parameters which were varied are mill speed and solids concentration. The slurry solids concentration range investigated was between 10wt% to 60wt% while the mill was operated at 60% and 75% of the critical speed.

- The Bingham rheological model was found to best describe the rheology of Elsodado slurry since it had the highest R^2 adjusted values ranging from 0.82 to 0.96 at all tested solids concentrations concentration ranges. The rheological behaviour of El Soldado slurry with a particle size fraction of -75+53 microns can therefore be described as Newtonian. This means that the viscosity is constant and does not vary with shear rate.

- The Bingham viscosity and yield stress increased exponentially with solids concentration. At low solids concentrations up to 30wt%, the fitted viscosity values obtained are equivalent to that of water at room temperature at 0.001 Pa.s. At higher solids concentrations up to 60wt%, the viscosity increases to

0.007 Pa.s for the tested shear rate range. The yield stress was observed for solids concentrations above 20wt%. The lowest and highest yield stress values obtained were 0.11Pa and 2.86Pa at 30wt% and 60wt% respectively.

It can thus be concluded that solids concentration has a significant effect on slurry viscosity and consequently the rheological characteristics of a slurry.

PEPT experiments were conducted to quantify and characterise the in-situ shear rates in a laboratory scale tumbling mill. Shear rate characterization in the mill was calculated from average velocity distributions and displacement data obtained from performing tumbling mill experiments using PEPT.

- The absolute velocity increases from the rising region to the cataracting region of the charge towards the mill centre. The lowest absolute velocities are obtained in the rising and cascading region of the charge. The velocity gradually increased radially from the cascading region towards the cataracting region with absolute velocities ranging between 1.5m.s^{-1} and 2.5m.s^{-1}. This trend was observed at all mill speeds and solids concentrations.

- The tangential velocity decreased linearly with radial distance as you move towards the centre of the mill. With further radial increases towards the "free surface" of the charge, the tangential velocity decreased to zero. At this point the sliding velocity is equal to the mill rotational speed. Beyond the mill centre, the tangential velocity oscillates into the cataracting region of the mill and cannot be accurately predicted.

- The absolute and tangential velocities obtained at 75% critical mill speed were higher than those obtained at the lower speed of 60% critical speed.

- Mill shear rates decreased with increasing slurry solids concentration. The highest shear rates were obtained at the lowest solids concentration for both mill speeds. It was 30s^{-1} at 60% critical mill speed and 36s^{-1} at 75% critical

mill speed. This was attributed to increased particle-particle interactions and reduced voidage. There is less volume available for particle shearing.

- The magnitude of the maximum shear rate is higher for the 75% critical mill speed at all slurry solids concentrations. At a higher speed the mill charge is fairly dilated by the strong centrifugal effects that oppose the natural packing structure which results in an overall decrease in bulk density. The increased voidage allows more volume for relative motion, producing an overall increase in shear rate.

- Due to the narrow shear rate range, a single viscosity value can be used to represent all the regions in the mill assuming the solids concentration is similar.

7.2. Recommendations

Tumbling mills are usually industrially operated at solids concentrations ranging between 40% and 60% solids by volume. The rheological characterisation of El Soldado slurries in this study were performed with a maximum solids concentration of 35% by volume. Typical measurements for rheology characterization of slurries are performed using very fine particles at sub 75 microns. In this study the rheological characteristics of El Soldado slurry were evaluated using the -75 +53 microns particle size class. A size distribution should be used. This was due to the limitations imposed by the U-tube rheometer used to obtain the rheological measurements and properties of the slurry. A different type of rheometer or viscometer could be used to measure the rheological characteristics of the slurry at a finer size class at sub 75 microns and at higher solids close to what is used in industrial mills without resulting in particles settling out during measurements. This would be a more realistic representation of the milling operating conditions and will provide a good basis for implementing outcomes of this work to industrial operations.

PEPT experiments were performed using a 1mm bluestone tracer particle. The practical limitations of fine particle activation using the Birmingham cyclotron prevented the use of the -75+53 microns as it was too small and dissipated during

direct radiation. More work should be done to evaluate the behavior of different slurry particles. I recommend that a tracer particle which is equivalent to the slurry particle size range should be used for PEPT experiments to get a more accurate representation of the slurry movement behaviour in the tumbling mill system.

Viscosity is more significantly impacted by solids concentration than shear rate distributions in the tumbling mill. The solids concentration gradient in the various regions of the mill could be investigated to provide better insight on areas of active transport in a tumbling.

8. REFERENCES

Atzeni C., Massida L., Sanna, U., *Comparison between rheological models for Portland cement pastes.* Cement and Concrete Research, 1985. **15**: p. 511-519.

Austin, L.G., *A treatment of impact breakage of particles.* Powder Technology, 2002. **126**: p. 85-90.

Baguley, P.J., *Modelling and simulation of dense medium drum separators.* University of Queensland, 1998. Masters in Engineering Science Thesis.

Bailey,W.J., Weir, I.S., *Investigation of methods for direct rheological model parameter estimation.* Journal of Petroleum Science & Engineering, 1998. **21**: p. 1-13.

Bakalis, S., Fryer, P.J., *Measurement of velocity distributions of viscous fluids using PEPT*, 2001. 6th Congress of Chemical Engineering, Melbourne.

Bakalis, S., Fryer, P.J., Parker, D.J., *Measuring velocity distributions of viscous fluids using PEPT.* American Institute of Chemical Engineers Journal, 2004. **50** (7): p.1606 -1613.

Bakalis, S., Cox, P.W., Russell, A.B., Parker, D.J., Fryer, P.J., *Development and use of positron emitting particle tracking (PEPT) for velocity measurements in viscous fluids in pilot scale equipment.* Chemical Engineering Science, 2006. **61**: p1864 - 1877.

Bakshi, A.K., Eisele, T.C., Kawatra, S.K.., *Online viscometer for mineral slurries.* 1999. SME Annual Meeting, Denver,CO, Preprint 99-82 .

Barley, R.W., Conway-Baker, J., Pascoe, R.D., McLoughlin, B., Parker, D.J., *Measurement of the motion of grinding media in a vertically stirred mill using positron emission particle tracking (PEPT) Part II.*. Minerals Engineering.2004. **17**: p.1179-1187.

Bartos P., *Fresh Concrete: Properties and Tests*, 1992. Elsevier.

Bazin,C., and B- Chapleau,C., *The difficulty associated with measuring slurry rheological properties and linking them to grinding mill performance.* International Journal of Minerals Processing, 2004. **76**: p. 93-99.

Bbosa, L.S., *Estimating the Power Draw in a tumbling mill using PEPT*. Centre for Minerals Research, 2010. Department of Chemical Engineering. University of Cape Town.

Bridgwater, J., Broadbent, C.J., and Parker, D.J. *Study of the influence of blade speed on the performance of a powder mixer using positron emission particle tracking*. Institute of Chemical Engineers A, 1993. **71**: p. 675-681.

Broadbent, C.J., Bridgwater, J., Parker, D.J., Keningley, S.T., and Knight, P., *A phenomenal study of a batch mixer using a positron camera.* Powder Technology, 1993. **76**: p .317-329.

Broadbent, C.J., Bridgwater, J., and Parker, D.J., *The effect of fill level on powder mixer performance using a positron camera.* Chemical Engineering Journal. 1995. **56**: p.119-125.

Chapra, S.C., Canale, R.P., *Numerical Methods for Engineers*. 5th Edition, McGraw-Hill, 1989.

Conway-Baker, J., Barley,R.W.,Williams,X., Kostuch, J., McLoughlin, B., and Parker, D.J., *Measurement of the motion of grinding media in a vertically stirred mill using positron emission particle tracking (PEPT).* Minerals Engineering.2002. **15**: p.53-59.

Davis, E.W., *Fine crushing in ball mills.* A.I.M.E Transactions. 1919.**61:** p.250-296.

Ergun S., *Fluid Flow Through Packed Columns.* Chemical Engineering Progress, Carnegie Institute of Technology, 1952. **48**(2): p. 89-94.

Fan, X., Parker, D.J., Smith, M.D., *Enhancing ^{18}F uptake in a single particle for positron emission particle tracking through modification of solid surface chemistry.* Nuclear Instruments and Methods in Physics Research A, 2006. **558**:p. 542- 546.

Fuerstenau, D.W., Venkataramana, K.S., Velamakanni, B.V., *U-effect of chemical additives on the dynamics of grinding media in wet ball mill grinding.* International Journal of Mineral Processing, 1984. **15**: p. 251-267.

Fuerstenau, D.W., Lutch J.J., and De, A., *The effect of ball size on the energy efficiency of hybrid high-pressure roll mill/ball mill grinding.* Powder Technology, 1999. **105**: p. 199-204.

Fuerstenau, D.W. and Abouzeid, A.-Z.M., *The energy efficiency of ball milling in comminution.* International Journal of Mineral Processing, 2002. **67**: p. 161-185.

Gao, M., and Forssberg, E., *The influence of slurry rheology on ultrafine grinding in a stirred ball mill.* 18th International Mineral Processing Congress, 1993. Sydney, Conference Article, p. 237-244.

Govender, I., McBride A. T., Powell M. S., *Improved experimental tracking techniques for validating discrete element method simulations of tumbling mills*. Journal of Experimental Mechanics, 2004. **14**(10): p. 153-160.

Govender, I., *X-ray motion analysis of charge particles in a laboratory mill.*, Dept. of Mechanical Engineering, University of Cape Town, 2005.PhD thesis.

Govier, G.W., Aziz, K.., *The Flow of Complex Mixtures in Pipes*, Robert E. Krieger Publishing Company Inc. 1977.

Hawkesworth, M.R., O'Dwyer, M.A., Walker, J., Fowles, P., Heritage, J., Stewart, P.A.E., Witcomb, R.C., Bateman, J.E., Connolly, J.F ., Stephenson, R., *A positron Camera for industrial application.* Nuclear Instruments and Methods A, 1986. **253**: p. 145-157.

He, M., Wang, Y., Forssberg, E., *Slurry rheology in wet ultrafine grinding of industrial minerals: a review*. Powder Technology, 2004.**147**: pp 94-112.

He, M., Wang, Y., Forssberg, E., *Parameter studies in the rheology of limestone slurries*. International Journal Minerals Processing, 2006.**78**:p. 63-77.

Hogg, R., and Rogovin, Z., 1982. *Mass Transport in wet overflow ball mills.* In: XIV International Mineral Processing Congress, CIM, Paper no I-7, Toronto, Canada.

Ingram, A., Hausard, M., Fan, X., Parker, D.J., Seville, J.P.K., Fin, N., Evan, M., *Portable Positron Particle Tracking (PEPT) for industrial use*. ECI Conference on the 12 International Conference on Fluidization. 2007.

Jinescu, V.V., *The rheology of suspensions.* International Chemical. Engineering, 1974. **14**: p.397-420.

Kahn,R. , *A report on Paterson and Cooke rheometer*. 2005.

Kawatra, S.K., Bakshi, A.K., Shoop, K.J., Eisele, T.C., *Slurry rheology in autogenous grinding and classification.* Comminution Practices Chapter 21, Society for Mining Metallurgy and Exploration, 1997. Littleton, Columbia.

Kawatra, S.K., and Eisele, T.C., *Rheological Effects in grinding circuits.* International Journal Minerals Processing, 1988. **22**: p. 251-259.

Kawatra, S.K., Bakshi, A.K., *Online measurement of viscosity and determination of flow types for mineral suspensions.* International Journal of Mineral Processing, 1996**.** **47:** p. 275-283.

Kawatra, S.K., Bakshi, A.K., Miller, T.E., *Rheological Characterisation of minerals suspensions using a vibrating sphere and a rotational viscometer***.** International Journal of Mineral Processing, 1996. **44-45**: p. 155-165.

Kawatra, S.K, Bakshi, A.K., Eisele, T.C., *An online pressure vessel rheometer for slurries* .Powder Technology, 1999. **47**: p. 275-283.

Klimpel, R.R., *Laboratory studies of the grinding and rheology of coal-water slurries*. Powder Technology, 1982. **32**: p. 267-277.

Klimpel, R.R., *Slurry Rheology influence on the performance of mineral/coal grinding circuit. Part1*. Mining Engineering, 1982. **34**(12): p. 1665-1668.

Klimpel, R.R., *Slurry Rheology influence on the performance of mineral/coal grinding circuit. Part2*. Mining Engineering, 1983. **35**: p. 21-26.

Klimpel, R. R.., *Influence of material breakage properties and associated slurry rheology on breakage rates in wet grinding of coal/ores in tumbling media mills.* In M.J. Jones and R. Oblatt (Eds), Reagents in the Mineral Industry, IMM, 1984. London, 265-270.

Klimpel, R.R., Austin, L.G., Hogg, R., *The mass transport of slurry and solids in a laboratory overflow ball mill*. Mineral and Metallurgical Processing, 1989. **6**: p. 73-78.

Klimpel, R.R., *The impact on industrial grinding circuits of changing and/or controlling the slurry rheology.* Comminution Practices Chapter 21, Society for Mining Metallurgy and Exploration, 1997. Littleton, Columbia.

Klimpel, R.R., *The selection of wet grinding chemical additives based on slurry rheology control*. Powder Technology, 1999. **105**: p. 430-435.

Latchireddi, S., Morrell, S., *Slurry flow in mills: grate –only discharge mechanism (Part-1)*. Minerals Engineering, 2003. **16:** p. 625-633.

Liddell, K.S., Moys, M.H., *The effects of mill speed, filling and pulp rheology on the dynamic behaviour of load in a rotary grinding mill.* 1986. MSc Thesis, University of the Witwatersrand, S.A.

Liddell, K.S., Moys, M.H., *The effects of mill speed and filling on the behaviour of load in a rotary grinding mill.* Journal of the South .African Institute of Mining and Metallurgy, 1988. **88** (2): p. 49-57.

Logos, C., Nguyen, Q.D., *Effect of particle size on the flow properties of a South Australian coal-water slurry.* Powder Technology, 1996. **88**: p. 55-58.

McBride, A.T., Govender, I., Powell, M., Cloete, T.J., *Contributions to the experimental validation of the discrete element method applied to tumbling mills.* Engineering Computations, 2003. **21** (2/3/4): p. 119–136.

Morrell,S., *The prediction of power draw in wet tumbling mills.* University of Queensland 1993**,** Ph.D. Thesis

Morrell,S., Napier-Munn, T.J., and Andersen, J.,*The prediction of power draw in comminution machines.* In K. Kawatra (ed): Comminution Theory and practice, SME. 1992. Chapter 17: p. 235-247**.**

Morrell, S., and Stephenson, I., *Slurry discharge capacity of autogenous and semi-autogeneous mills and the effect of grate discharge design.* International Journal of Minerals Processing, 1986. **46** (1-2)**:** p. 53-72.

Moys, M.H., *The effect of grate discharge design on the behaviour of grate discharge mills.* International Journal of Minerals Processing, 1986. **18:** p. 85-105.

Moys, M.H.,*Slurry Rheology- The key to a future advance in grinding mill control: Advances in autogeneous and semi-autogeneous grinding technology* Mining and Mineral Processing Engineering, 1989. University of Columbia, **2:** p. 713-728.

Muster, T.H., Prestidge, C.A., *Rheological investigations of sulphide mineral slurries.* Minerals Engineering,1995. **8**: p.1541-1555.

Nakagawa, M., Altobelli, S.A., Caprihan, A., Fukushima, E., *NMR measurement and approximate derivation of velocity depth – Profile of granular flow in rotating, partially filled, horizontal cylinder.* Powder and grains, 1997. Edited by R.P. Behringer and T.J. Jenkins (Balbema, Rotterdam), p. 447-450.

Napier-Munn, T.J., *The mechanism of separation in dense medium cyclones.* University of London.1983. Ph.D. Thesis.

Napier-Munn, T.J., Morrell S., Morrison R.D., and Kojovic T**.,** *Mineral Comminution Circuits-Their Operation and Optimisation*. JKMRC, University of Queensland, 1996.

Ottino, J.M., Khakhar, D.V., *Mixing and segregation of granular materials.* Annual Reviews of Fluid Mechanics, 2000. **32**: p. 55-91.

Parker, D.J., Broadbent, C.J., Fowles, P., Hawkesworth, M.R.,McNeil, P.A.1993. *Positron Emission Particle Tracking- a technique for studying flow within engineering equipment*. Nuclear Instruments and Methods in Physics Research A, 1993. **236**: p. 592-607.

Parker, D.J., Hawkesworth, M.R., Broadbent, C.J., Fowles, P., Fryer, T.D., McNeil, P.A., *Industrial positron-based imaging: principles and applications.* Nuclear Instruments and Methods in Physics Research A, 1994. **348**: p. 583-592.

Parker, D.J., Dijkstra, A.E., Martin, T.W., Seville, J.P.K., *Positron Emission Particle Tracking studies of spherical particle motion in rotating drums.* Chemical Engineering Science, 1997.**52** (13): p.2011-2022.

Parker, D.J., Allen, D.A., Benton, D.M., Fowles, P. McNeil, P.A., Min,T., Beynon, T.D., *Developments in particle tracking using the Birmingham Positron Camera.* Nuclear Instruments and Methods in Physics Research A, 1997. **392:** p. 421-426.

Powell, M.S., Nurick, G.N., *A study of charge motion in rotary mills: Part1-Extension of the theory.* Minerals Engineering, 1995. **9**(2): p. 259-268.

Powell, M.S., Nurick, G.N., *A study of charge motion in rotary mills: Part2-Experimental work.* Minerals Engineering, 1996. **9**(3): p. 343-350.

Prestidge, C.A., *Rheological investigations of ultra-fine galena particle studies under flotation-related conditions.* International Journal Minerals Processing, 1997. **51**: p.241.254.

Prestidge, C.A., *Rheological investigations of galena particle interactions.* Colloids and Surfaces A, Physicochemical and Engineering Aspects, 1997. **126**: p.75-83.

Radziszewski, P., Quan, Y.Y., Poirier, J., *Design parameters affecting tumbling mill natural frequencies.* Department of Mechanical Engineering, McGill University.2011

Sadrmomtaz, A., *Adjustment of a PET Scanner for PEPT*. Proceedings of world academy of Science, Engineering and Technology, 2008. **31**: p. 777-779.

Shi, F., *Slurry rheology and its effects on grinding*. Julius Kruttschnitt Mineral Research Centre, University of Queensland., 1994. PhD Thesis.

Shi., F., Napier-Munn, T.J., *A model of slurry rheology*. International Journal of Mineral Processing, 1996. **47**: p. 167-183.

Shi, F., Napier-Munn, T.J.,*Estimation of shear rates inside a ball mill.* International Journal of Mineral Processing, 1999. **47:** p. 167-183.

Shi, F., Napier-Munn, T.J., *Effects of slurry rheology on industrial grinding performance*. International Journal of Mineral Processing, 2002. **65:** p. 125-140.

Skudanov, P.V., Ling, J., Lin, C.X., and Ebadian, M.A., *Numerical Investigations of liquid-solid slurry flows in a fully developed turbulent flow region.* International Journal of Heat and Fluid flow, 2001. **24(**3): p. 389-398.

Slatter, P.T., *The rheological characterisation of sludges.* Water Science and Technology, 1997. **36** (11): p.9-18.

Somasundaran, P., Moudgil, B.M., *Grinding aids based on slurry rheology control*, *Reagents in Mineral Technology* . Surfactant Science Series, 1988.**27**: p.179-193.

Steane, H.A., *Coarser grind may mean lower metal recovery but higher profits.* Canadian Minerals Journal, 1976. **97**: p.44-47

Stellema, C.S., Vlek, J., Mudde, R.F., de Goeji, J.J.M.,van den Bleek., C.M., *Development of an improved positron emission particle tracking system*. Nuclear Instruments and Methods in Physics Research A, 1998. **404**: p. 334-348.

Taberlet, N., Richard, P., Hinch, E.J., *S shape of a granular pile in a rotating drum.* Physical Review E, 2006. **73:** p. 1-4.

Tangsathitkulchai, C., and Austin, L.G., *Rheology of concentrated slurries of particles of natural size distribution produced by grinding.* Powder Technology, 1988. **56**: p. 293-299.

Tangsathitkulchai, C., *The effect of slurry rheology on fine grinding in a laboratory ball mill.* Powder Technology, 2002. **1587**: p. 1-19.

Tanner, R..I., *Engineering Rheology*. 2nd edition, Oxford University Press, New York, 2000,p.1-29.

Tattersall G.H., *The workability of concrete*, A viewpoint Publication, PCA, 1976.

Tseng, W.J., Chen, C., *Effect of polymeric dispersant on rheological behaviour of nickel-terpineol suspensions.* Material Science Engineering A, 2003**. 347**: p .145-153.

Tucker, P., *Rheological factors that affect the wet grinding of ores.* Transactions of the Institution of Mining and Metallurgy. Section C **91 :** p: 117-122.

Turian, R.M., Ma, T.W., Hsu, F.L.G., Sung, D.J., *Characterization, settling, and rheology of concentrated fine particulate mineral slurries*. Powder Technology, 1997. **93**: p. 219-233.

Van Wazer, J.R., Lyons, J.W., Kim, K.K.Y.,Colwell, R.E., *Viscosity and flow measurement.* Interscience Publishers. London, 1963.

Velamakanni, B.V., Fuersteanau, D.V., *The effect of the adsorption of polymeric additives on the wet grinding of minerals: Dispersion and fine grinding of concentrated suspensions.* Powder Technology, 1993.**75**. p. 11-19.

Vermeulen, L.A., and Howat, D.D., *Effects of lifter bars on the motion of en masse grinding media in milling.* International Journal of Mineral Processing, 1988. **24:** p. 143-159.

Wang, Y., Forssberg, E., *Dispersants in stirred ball mill grinding.* Kona, 1995. **13**: p. 67-77.

Waters, K.E., Rowson, N.A., Fan, X., Parker, D.J., Cilliers, J.J., *Positron emission particle tracking as a method to map the movement of particles in the pulp and froth phases.* Minerals Engineering, 2008. **21**, p. 877-882.

Whorlow, R.W., *Rheological Techniques*, 2ND Edition. Ellis Horwood, West Sussex, 1992, p.1-40.

Wildman, R.D.,Huntley, J.M., Hansen, J.P., Parker, D.J., Allen, D. A., *Single-particle motion in three-dimensional vibrofluidized granular beds.*Physical Review E, 2000. **62**(3) : p. 3826-3835.

Wills, B.A., Napier-Munn, T.J., *Minerals Processing Technology- An introduction to the practical aspects of ore treatment and mineral recovery.* Elsevier Science & Technology Books. 2006.

Wills, B.A., Atkinson, K., *Some observations on the fracture and liberation of mineral assemblies,* Minerals Engineering, 1993. **6**(7): p. 697-671.

Wolfram, H., Matthias, K., *The analytical solution of two interesting hyperbolic problems as a test case for a finite volume method with a new grid refinement technique*. Journal of Computational and Applied Mathematics, 2008. **214**: p. 509-532.

Yamane, K., Nakagawa, M., Altobelli, S.A ., Tanaka, T., Tsuji, Y., *Steady particulate flows in a horizontal rotating cylinder*. Physics of Fluids, American Institute of Physics, 1998. **10(**6): p. 1419-1427.

Yang, H.L., Li, C., Gu, H., Fang, T., *Rheological behaviour of titanium dioxide suspensions.* Journal of Colloid Interface Science, 2001. **236**: p. 96-103

Yang, Z., Parker, D.J., Fryer, P.J., Bakalis,S.,Fan,X., *Multiple particle tracking-an improvement for positron particle tracking.* Nuclear Instruments and Methods in Physics Research A, 2006. **564**: p. 332-338.

Zik, O., Levine, D., Lipson, S.G., Shtrikman, S., Stavans, J., *Rotationally induced segregation of granular materials.* Physical Review Letters, 1994. **73**, pp. 644-647.

APPENDIX A: RHEOLOGY RESULTS

Section A1: The quantities of ore and water mixed to obtain the target solids concentration.

Table A1-1: El Soldado ore and water quantities used to obtain the target solids concentrations

Vol frac	%Solids required	Ore density (kg/m^3)	Pulp density (kg/m^3)	Pulp mass (kg)	Ore mass (kg)	Pulp volume (L)	Water volume (L)	Ore added (kg)
0.04	10	2.8	1.07	10.69	1.07	10	9.62	1.07
0.08	20	2.8	1.15	12.02	2.40	10.48	9.62	0.71
0.13	30	2.8	1.24	13.74	4.12	11.09	9.62	0.92
0.19	40	2.8	1.35	16.03	6.41	11.91	9.62	1.23
0.26	50	2.8	1.47	19.24	9.62	13.05	9.62	1.75
0.35	60	2.8	1.63	24.05	14.43	14.77	9.62	2.67

Section A2: Bingham Model fittings to rheogram data for the -75+53microns particle size fractions at different solids concentrations.

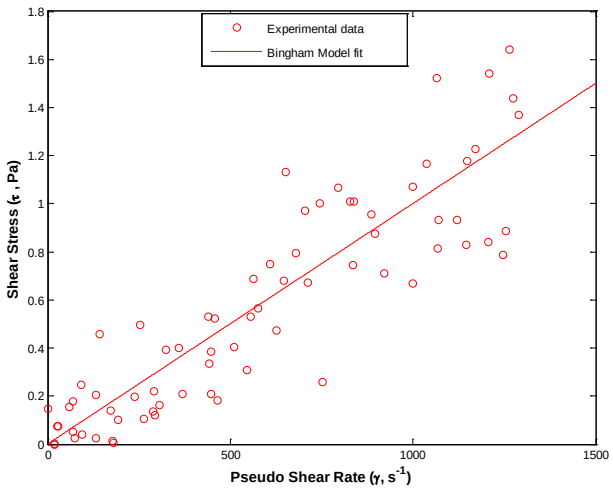

Figure A-1: Bingham Model fit to water rheogram data at Cv=0%

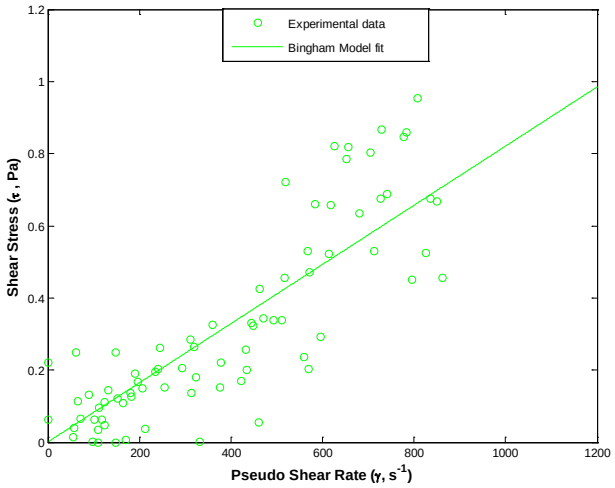

Figure A-2: Bingham Model fit to -75+53microns El Soldado ore rheograms at Cv=10%

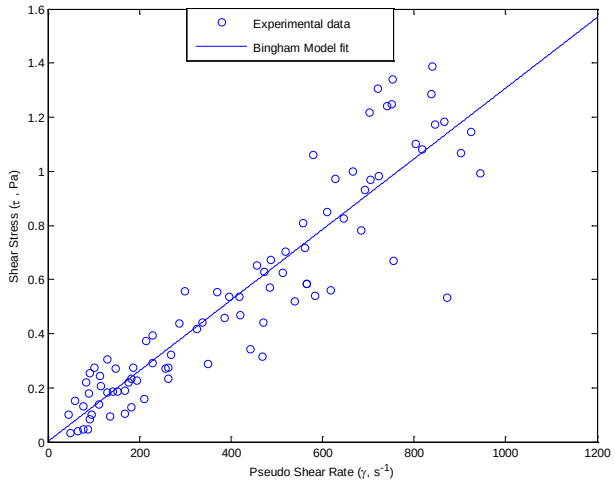

Figure A-3: Bingham Model fit to -75+53microns El Soldado ore rheograms at Cv=20%

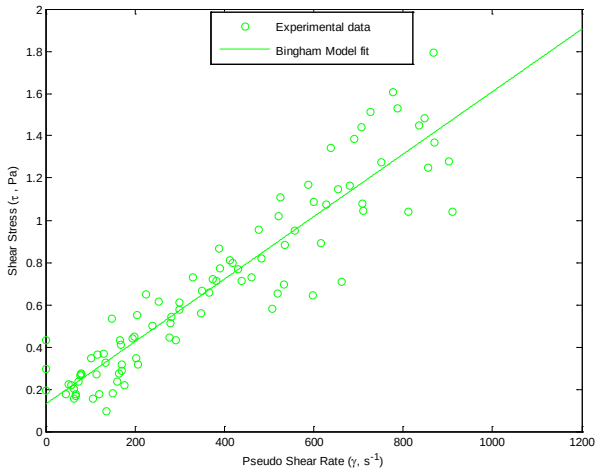

Figure A-4 Bingham Model fit to -75+53microns El Soldado ore rheograms at Cv=30%

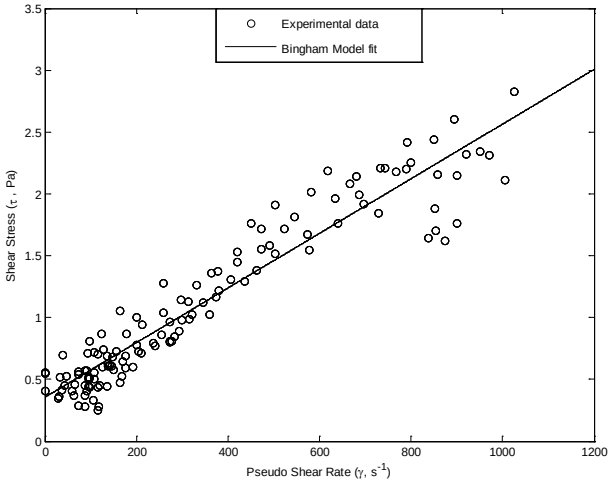

Figure A-5: Bingham Model fit to -75+53microns El Soldado ore rheograms at Cv=40%

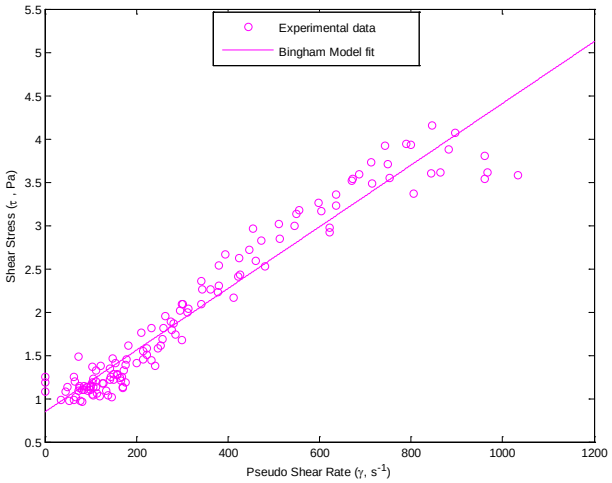

Figure A-6: Bingham Model fit to -75+53microns El Soldado ore rheograms at Cv=50%

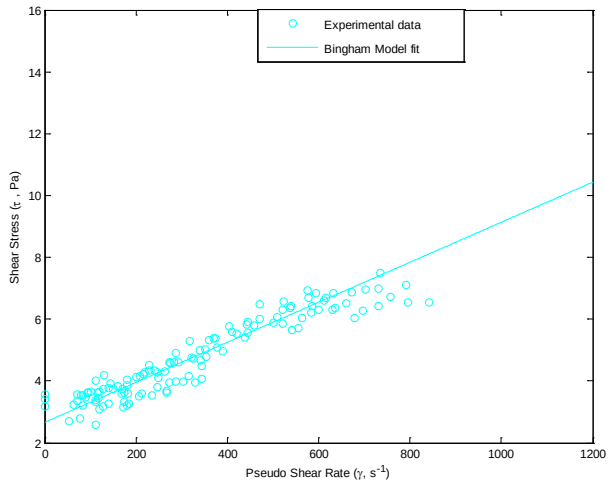

Figure A-7: Bingham Model fit to -75+53microns El Soldado ore rheograms at Cv=60%

Section A 3: Herschel-Bulkley Model fittings to rheogram data for the -75+53microns particle size fractions at different solids concentrations

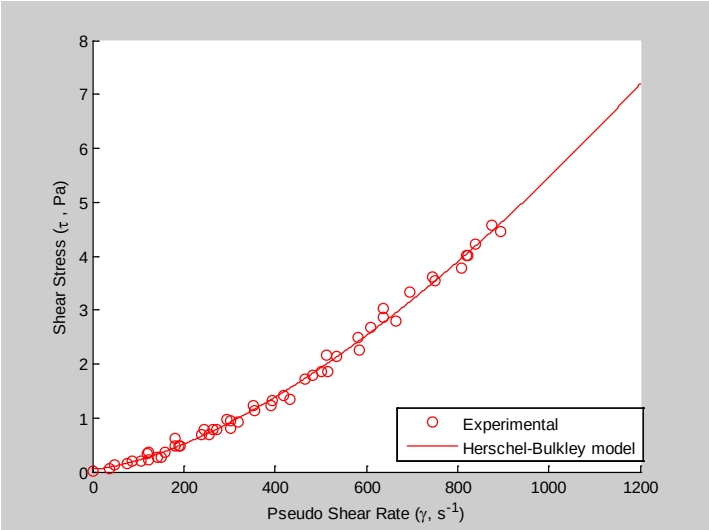

Figure A-8:Herschel-Buckley Model fit to -75+53microns El Soldado ore rheograms at Cv=0%

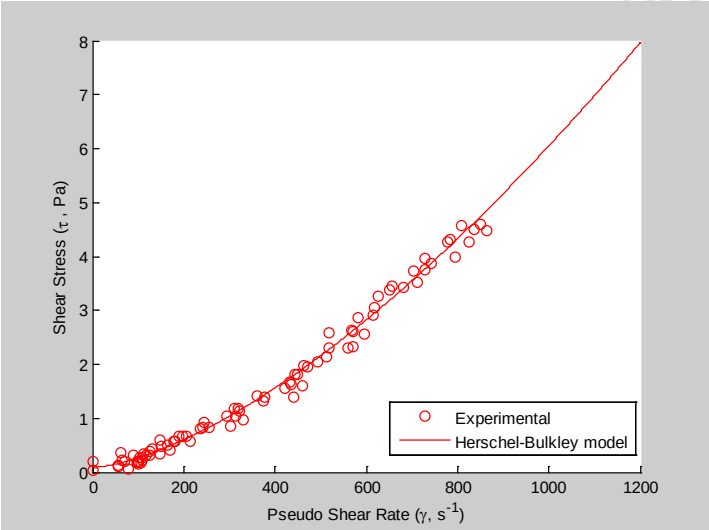

Figure A-9: Herschel-Buckley Model fit to -75+53microns El Soldado ore rheograms at Cv=10%

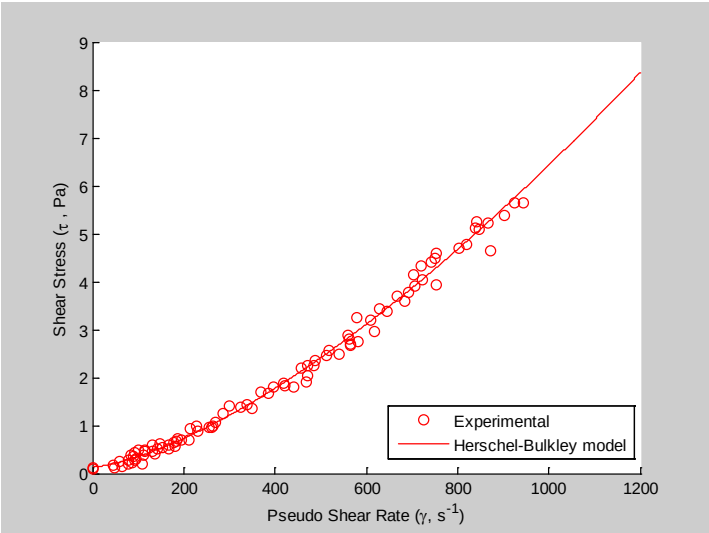

Figure A10: Herschel-Bulkley Model fit to -75+53microns El Soldado ore rheograms at Cv=20%

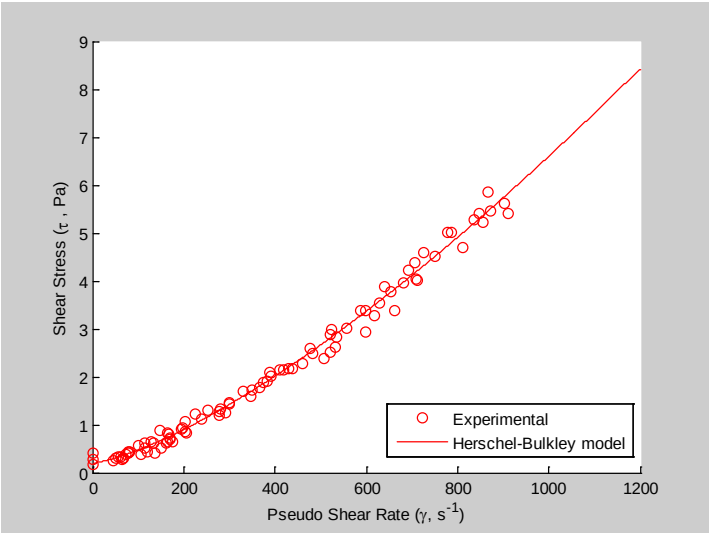

Figure A11: Herschel-Bulkley Model fit to -75+53microns El Soldado ore rheograms at Cv=30%

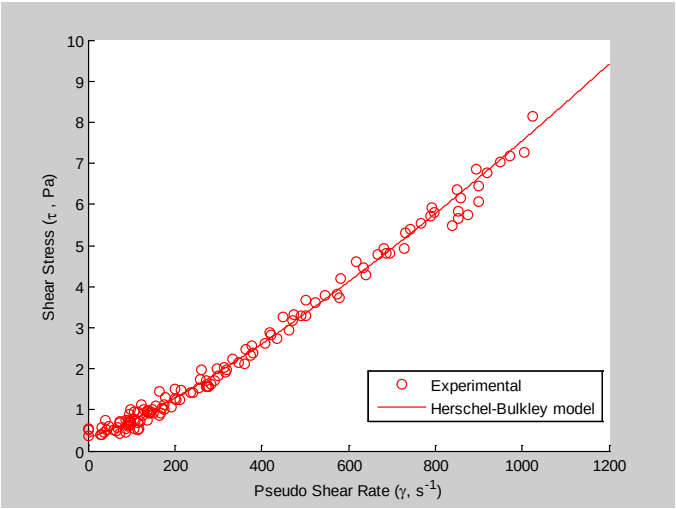

Figure A12: Herschel-Bulkley Model fit to -75+53microns El Soldado ore rheograms at Cv=40%

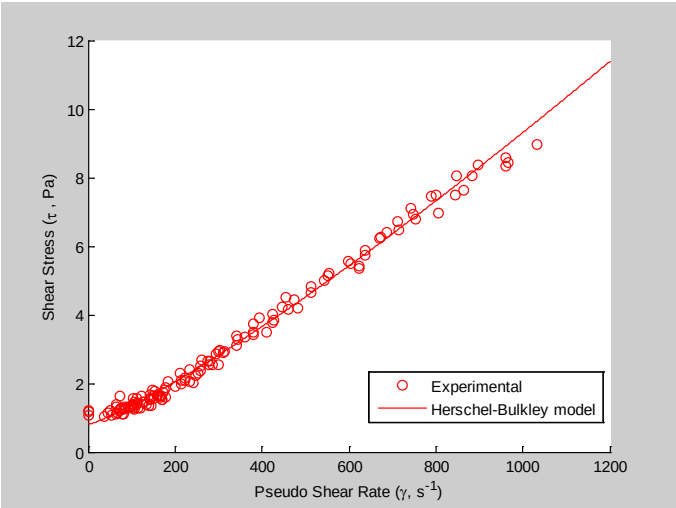

Figure A13: Herschel-Bulkley Model fit to -75+53microns El Soldado ore rheograms at Cv=50%

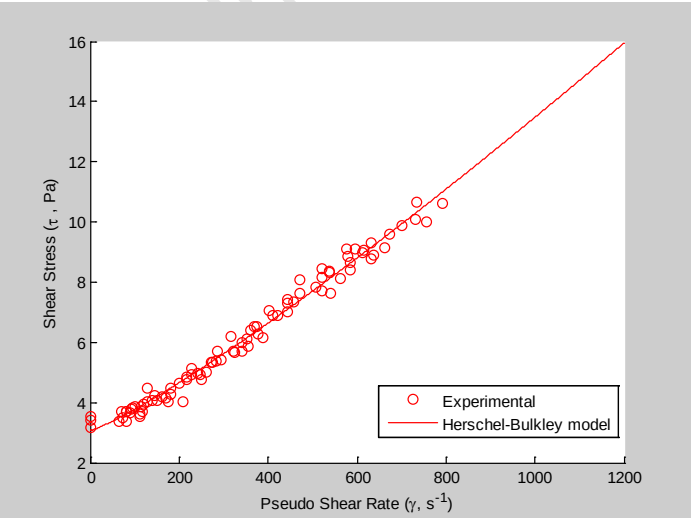

Figure A-14: Herschel-Bulkley Model fit to -75+53microns El Soldado ore rheograms at Cv=60%

Section A4: Casson Model Fittings to El Soldado ore rheogram data for the -75+53microns particle size fractions at different solids concentrations.

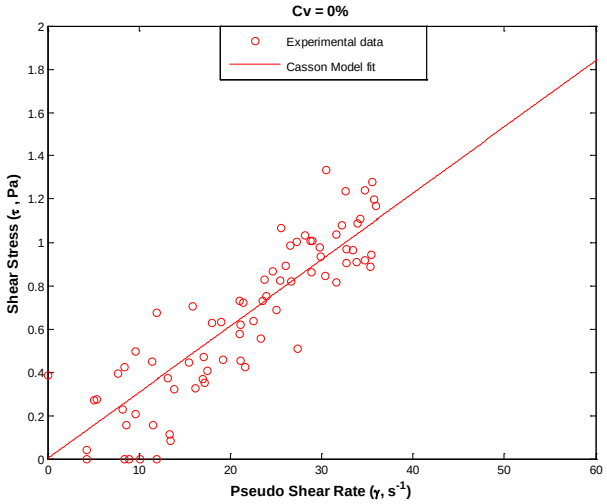

Figure A-15: Casson Model fit to -75+53microns El Soldado ore rheograms at Cv=0%

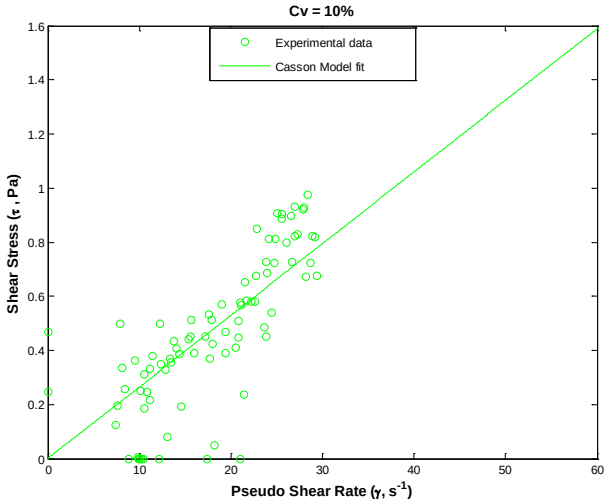

Figure A-16: Casson Model fit to -75+53microns El Soldado ore rheograms at Cv=10%

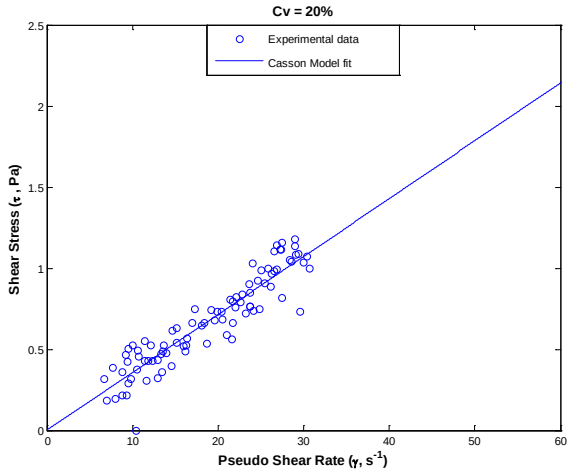

Figure A-17: Casson Model fit to -75+53microns El Soldado ore rheograms at Cv=20%

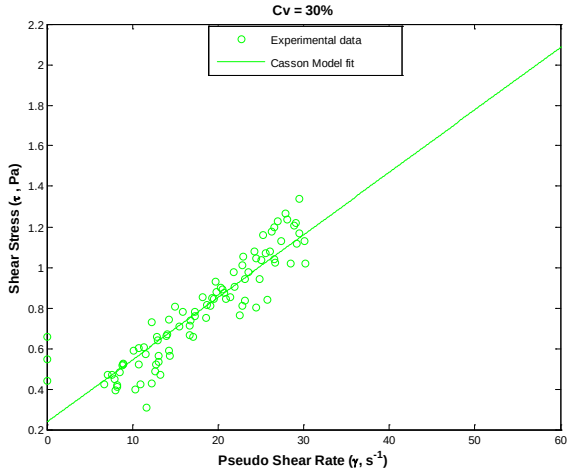

Figure A-18: Casson Model fit to -75+53microns El Soldado ore rheograms at Cv=30%

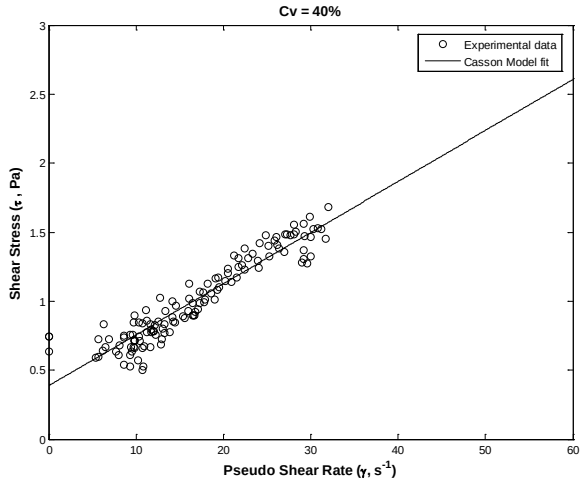

Figure A-19: Casson Model fit to -75+53microns El Soldado ore rheograms at Cv=40%

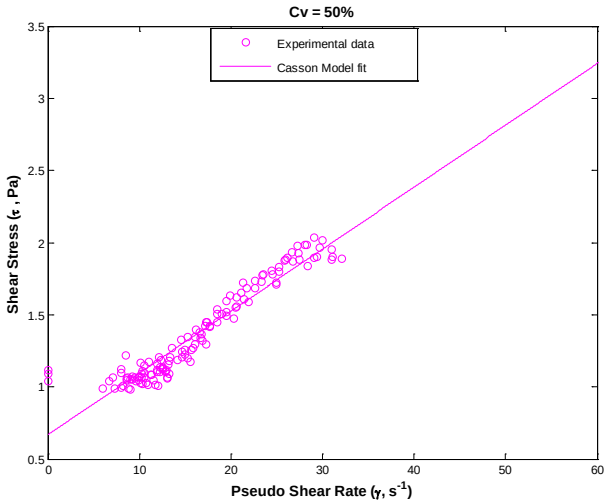

Figure A-20: Casson Model fit to -75+53microns El Soldado ore rheograms at Cv=50%

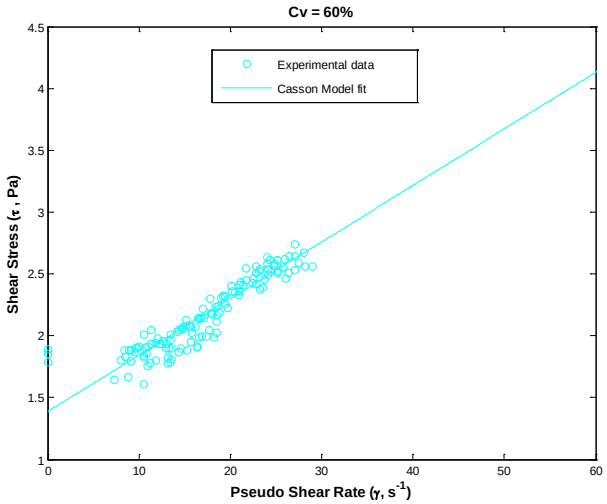

Figure A-21: Casson Model fit to -75+53microns El Soldado ore rheograms at Cv=60%

APPENDIX B: PEPT RESULTS

Section B.1: PEPT occupancy results at a rotational mill speed of 60% critical mill speed

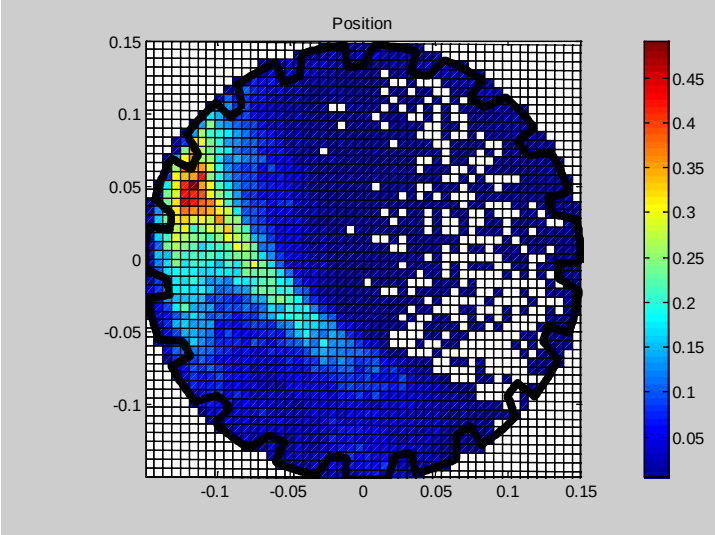

Figure B-1: Occupancy plot of a 1mm bluestone slurry particle at 20%wt solids concentration at 60% critical mill speed

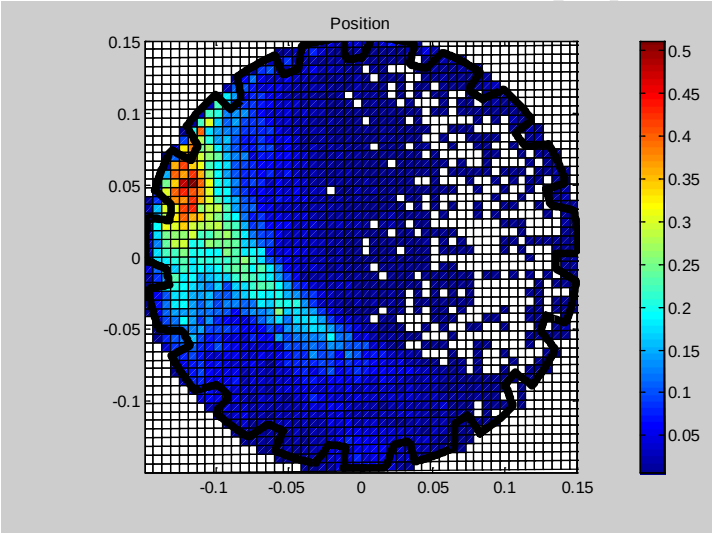

Figure B-2: Occupancy plot of a 1mm bluestone slurry particle at 30%wt solids concentration at 60% critical mill speed

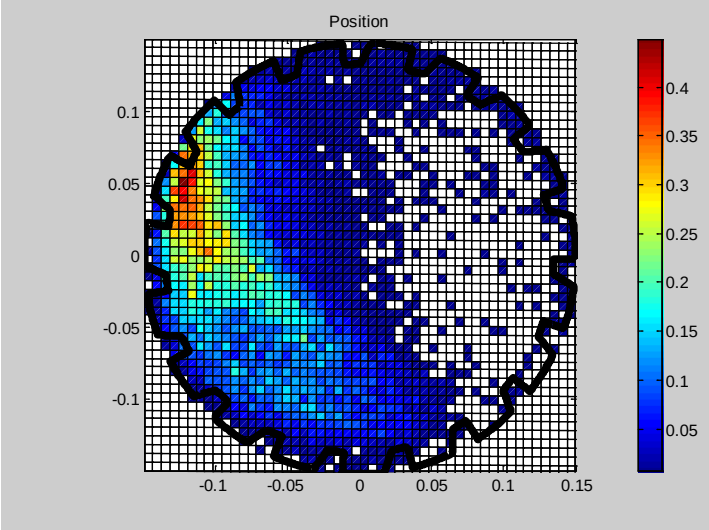

Figure B-3: Occupancy plot of a 1mm bluestone slurry particle at 40%wt solids concentration at 60% critical mill speed

SectionB.1.1: PEPT occupancy results at a rotational mill speed of 75% critical mill speed

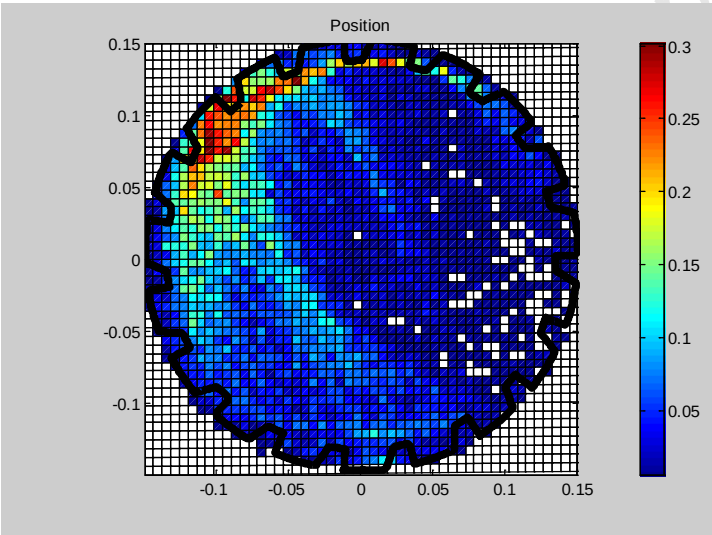

Figure B-4: Occupancy plot of a 1mm bluestone slurry particle at 20%wt solids concentration at 75% critical mill speed

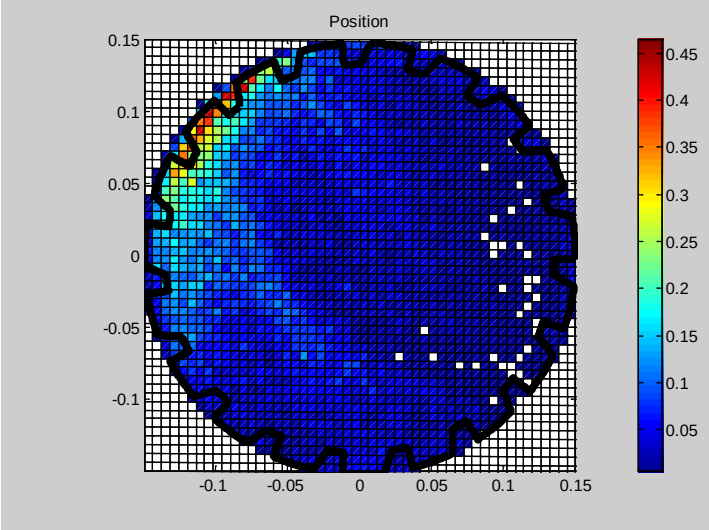

Figure B-5: Occupancy plot of a 1mm bluestone slurry particle at 30%wt solids concentration at 75% critical mill speed

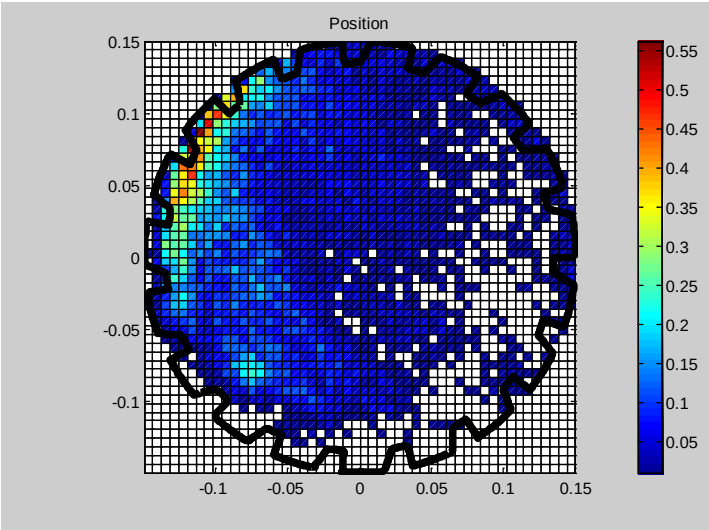

Figure B-6: Occupancy plot of a 1mm bluestone slurry particle at 40%wt solids concentration at 75% critical mill speed

Section B2: Absolute velocity results at a rotational mill speed of 60% critical mill speed.

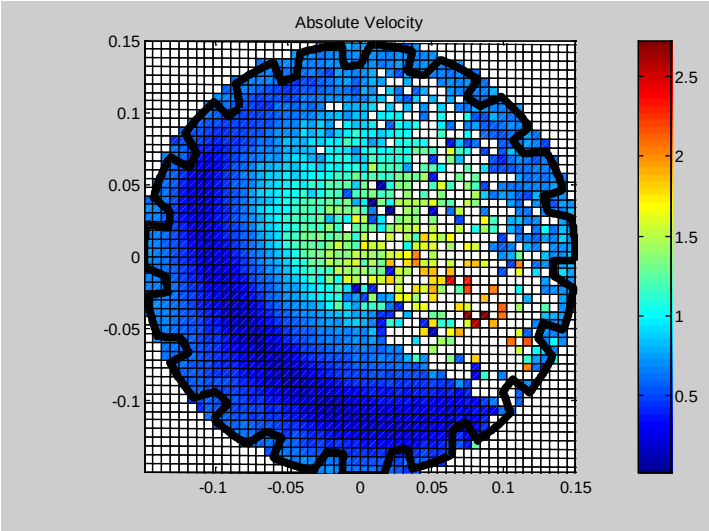

Figure B-7: Magnitude plot of absolute velocity profile for a1mm bluestone slurry particle at 20%wt solids concentration at 60% critical mill speed

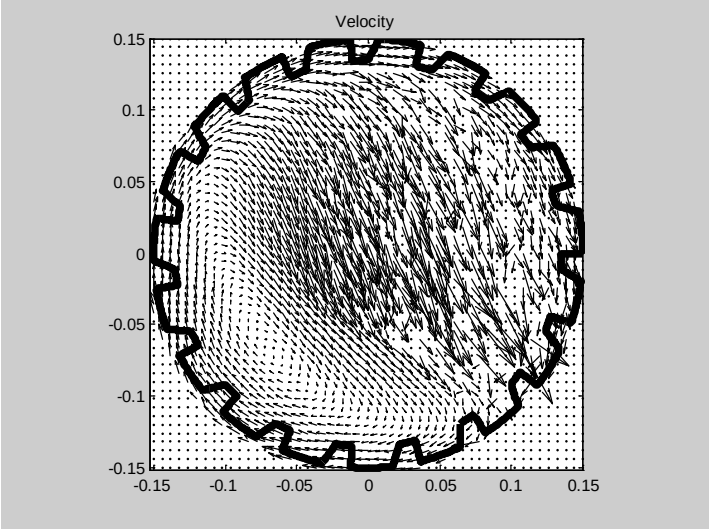

Figure B-7.1: Velocity vector profile for a1mm bluestone slurry particle at 20%wt solids concentration at 60% critical mill speed

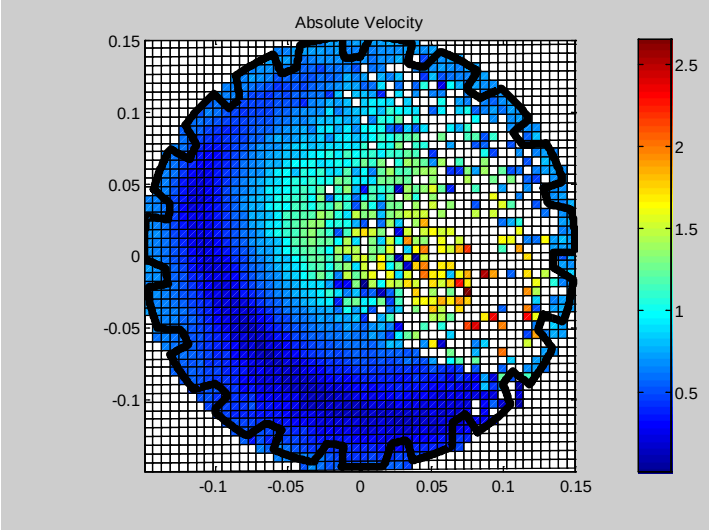

Figure B-8: Magnitude plot of absolute velocity profile for a1mm bluestone slurry particle at 30%wt solids concentration at 60% critical mill speed

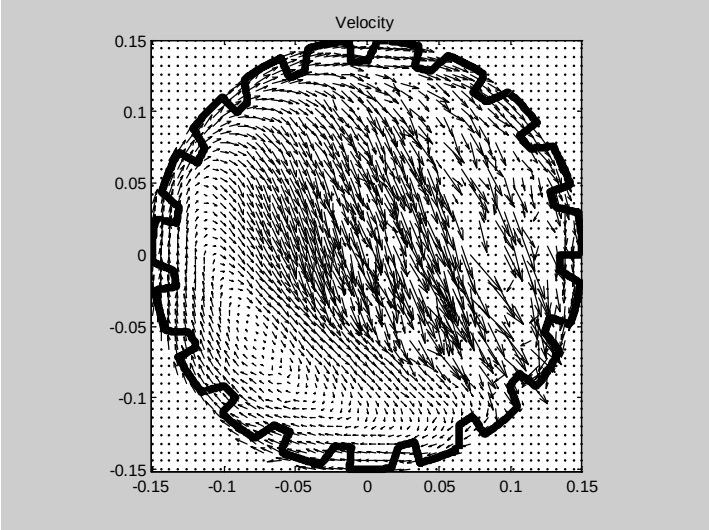

Figure B-8.1: Velocity vector profile for a1mm bluestone slurry particle at 30%wt solids concentration at 60% critical mill speed

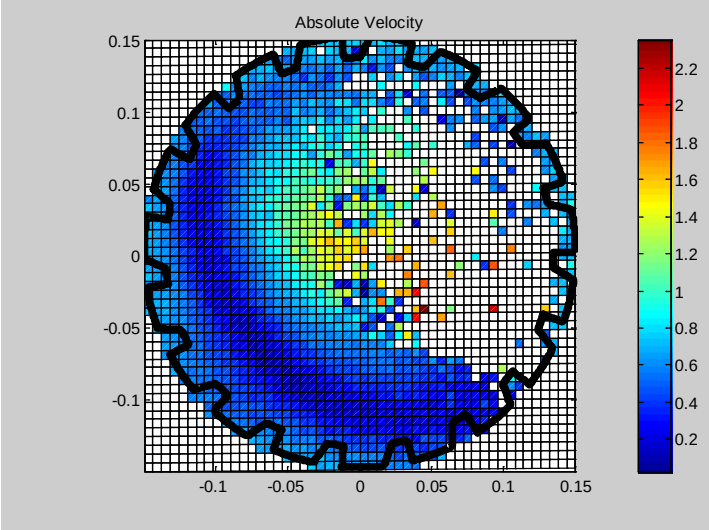

Figure B-9: Magnitude plot of absolute velocity profile for a1mm bluestone slurry particle at 40%wt solids concentration at 60% critical mill speed

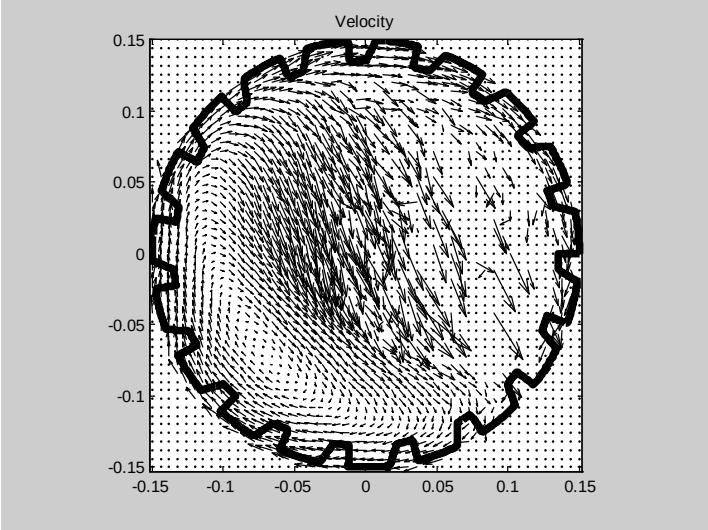

Figure B-9.1:Velocity vector profile for a1mm bluestone slurry particle at 40%wt solids concentration at 60% mill speed

Section B2.1: Absolute velocity results at a rotational mill speed of 75% critical mill speed

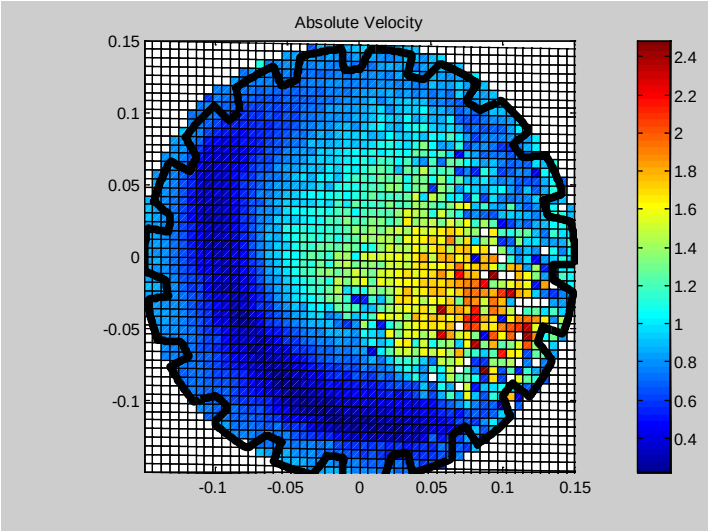

Figure B-10: Magnitude plot of absolute velocity profile for a1mm bluestone slurry particle at 20%wt solids concentration at 75% critical mill speed

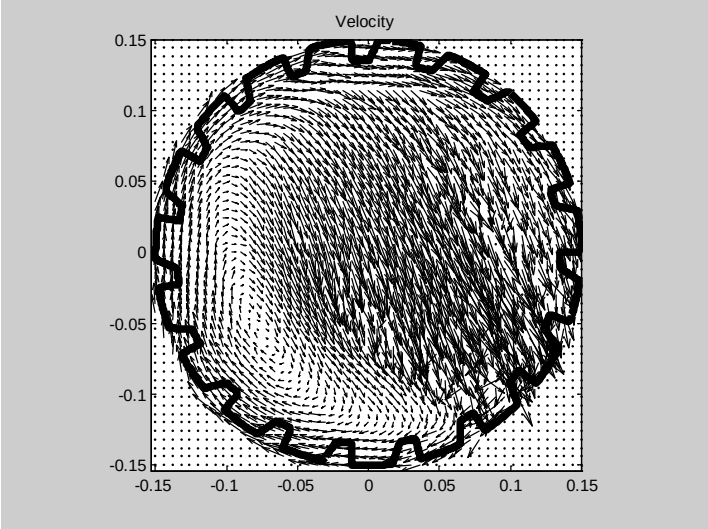

Figure B-10.1: Velocity vector profile for a1mm bluestone slurry particle at 20%wt solids concentration at 75% critical mill speed

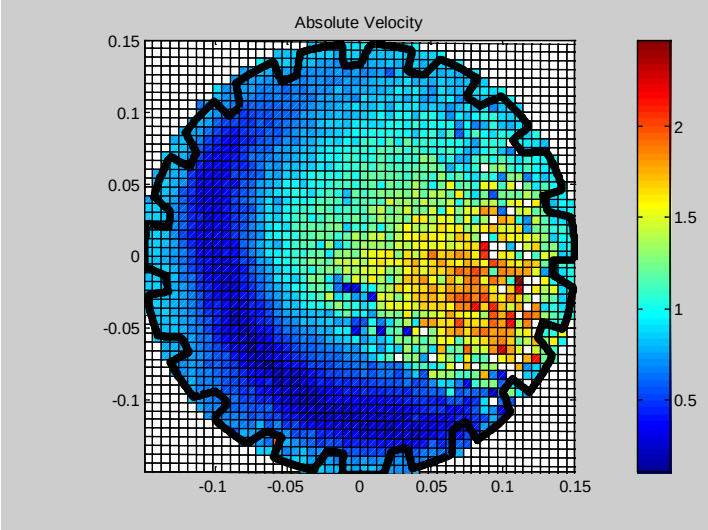

Figure B-11: Magnitude plot of absolute velocity profile for a1mm bluestone slurry particle at 30%wt solids concentration at 75% critical mill speed

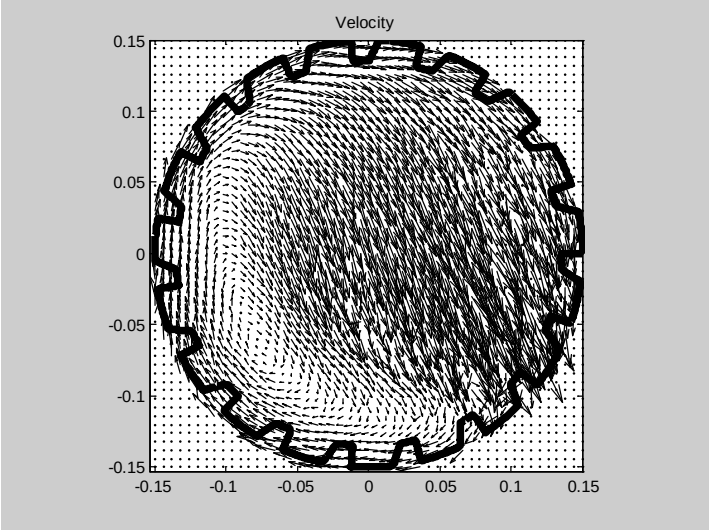

Figure B-11.1: Velocity vector profile for a1mm bluestone slurry particle at 30%wt solids concentration at 75 critical mill speed

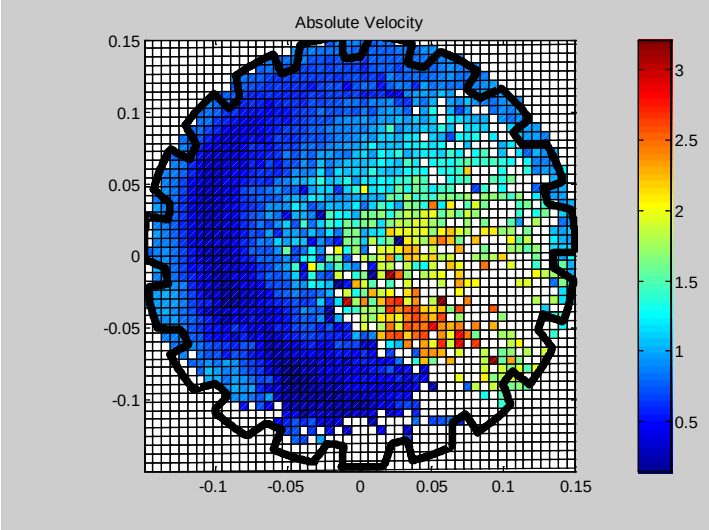

Figure B-12: Magnitude plot of absolute velocity profile for a1mm bluestone slurry particle at 40%wt solids concentration at 75% critical mill speed

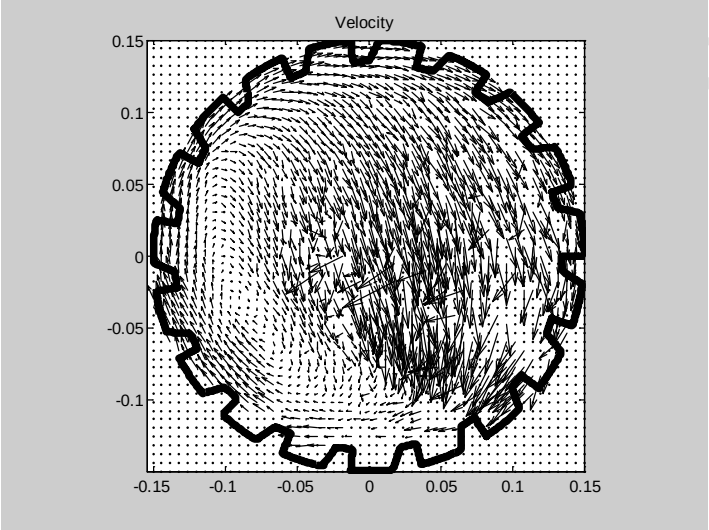

Figure B-12.1: Velocity vector profile for a1mm bluestone slurry particle at 40%wt solids concentration at 75% critical mill speed

Section B.3: Tangential velocity results at a rotational mill speed of 60% critical mill speed

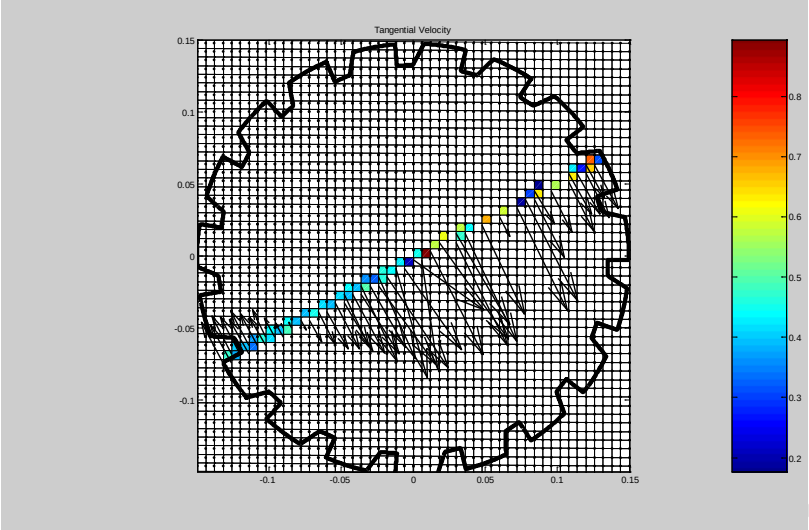

Figure B-13: Tangential velocity magnitude profile along a diametrical line passing through the mean CoC for a1mm bluestone slurry particle at 20%wt solids concentration at 60% critical mill speed

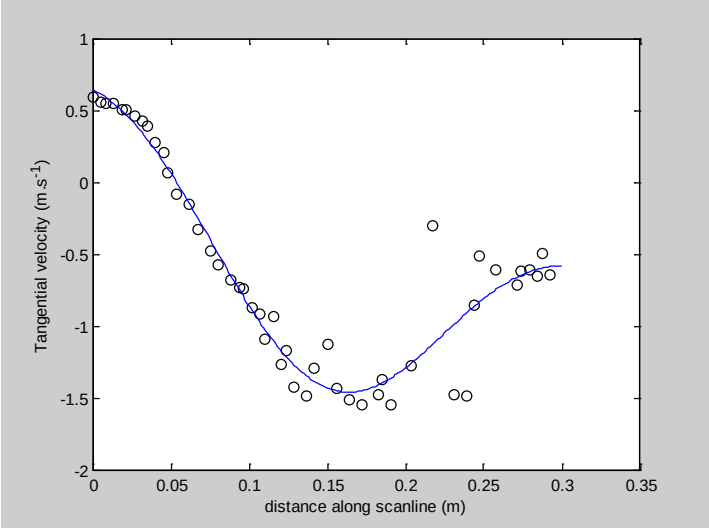

Figure B-13.1: Variation of tangential velocity with radial distance along the diametrical line passing through the mean CoC for a1mm bluestone slurry particle at 20%wt solids concentration at 60% critical mill speed

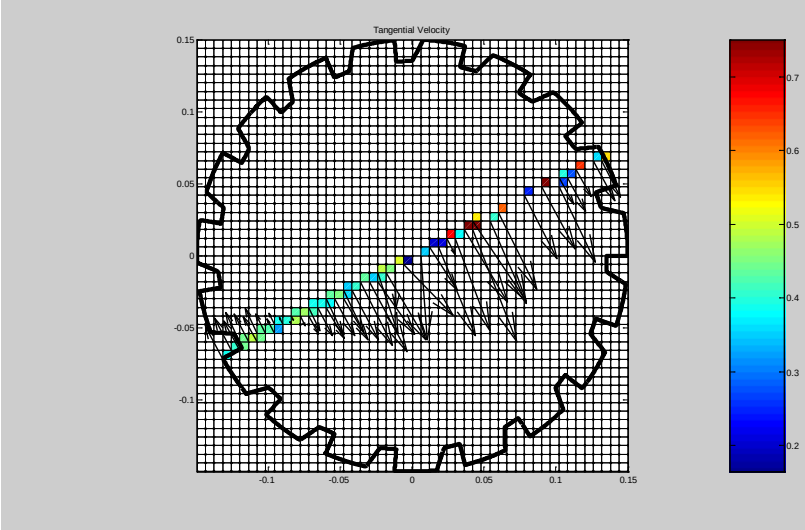

Figure B-14: Tangential velocity magnitude profile along a diametrical line passing through the mean CoC for a1mm bluestone slurry particle at 30%wt solids concentration at 60% critical mill speed

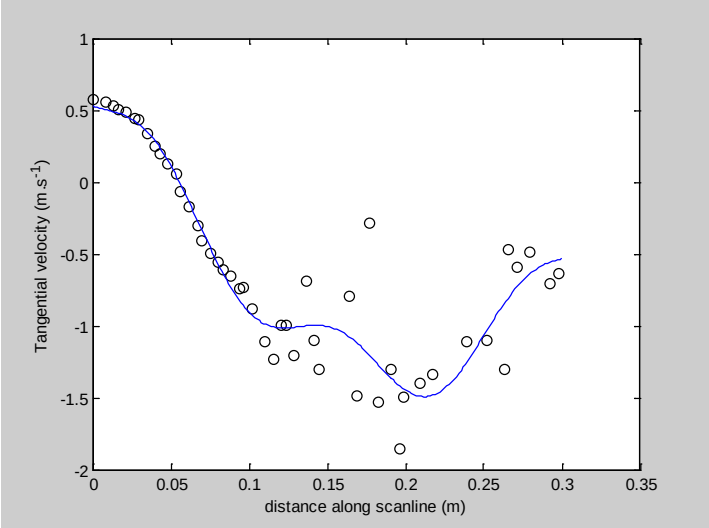

Figure B-14.1: Variation of tangential velocity with radial distance along the diametrical line passing through the mean CoC for a1mm bluestone slurry particle at 30%wt solids concentration at 60% critical mill speed

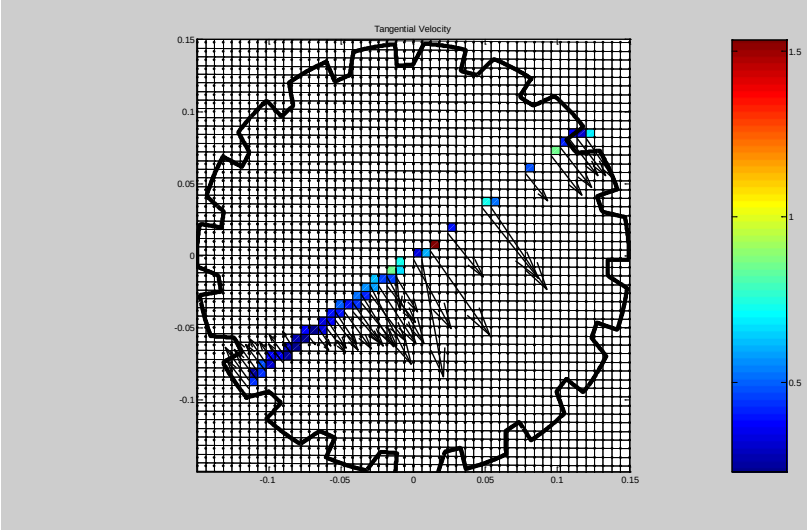

Figure B-15: Tangential velocity magnitude profile along a diametrical line passing through the mean CoC for a1mm bluestone slurry particle at 40%wt solids concentration at 60% critical mill speed

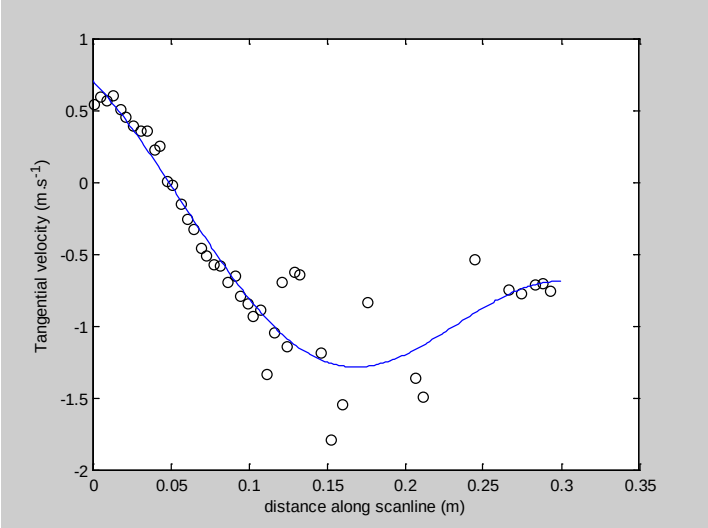

Figure B-15.1: Variation of tangential velocity with radial distance along the diametrical line passing through the mean CoC for a1mm bluestone slurry particle at 40%wt solids concentration at 60% critical mill speed

Section B.3.1: Tangential velocity results at a rotational mill speed of 75% critical mill speed

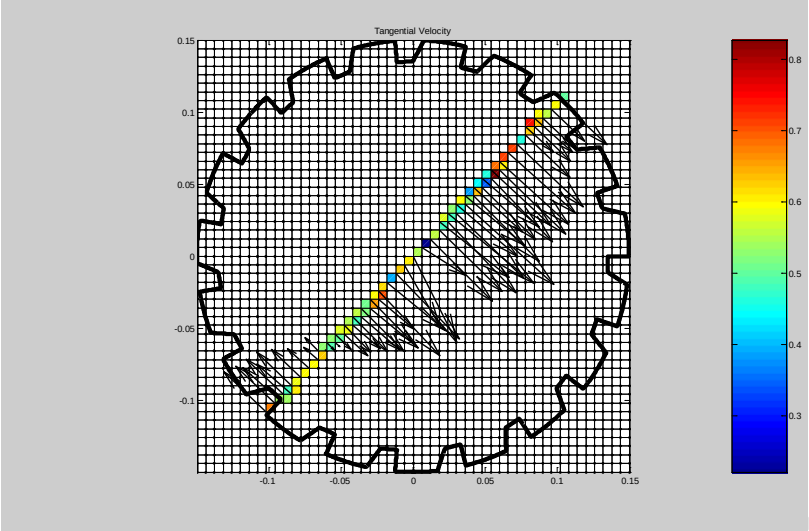

Figure B-16: Tangential velocity magnitude profile along a diametrical line passing through the mean CoC for a1mm bluestone slurry particle at 20%wt solids concentration at 75% critical mill speed

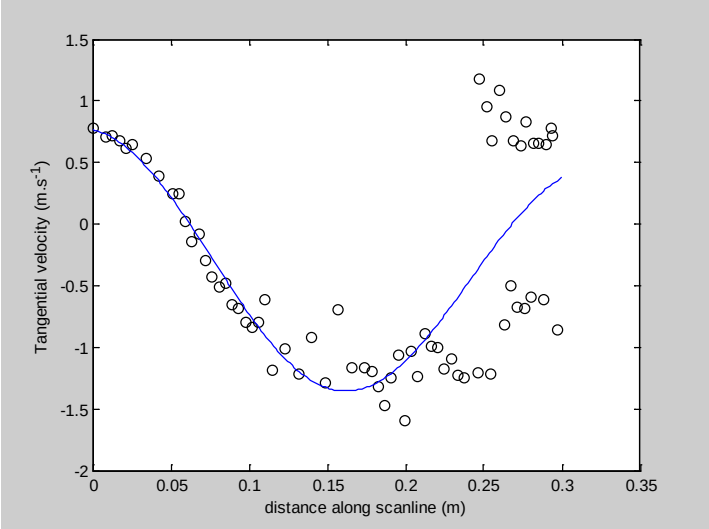

Figure B-16.1: Variation of tangential velocity with radial distance along the diametrical line passing through the mean CoC for a1mm bluestone slurry particle at 20%wt solids concentration at 75% critical mill speed

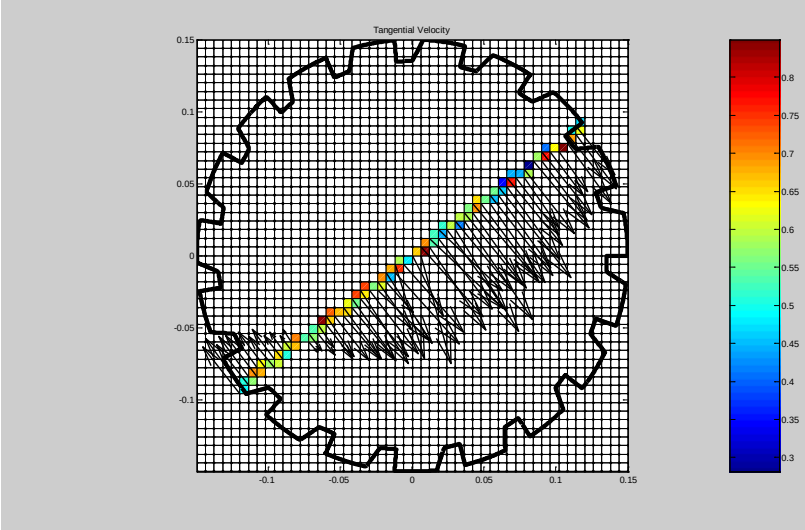

Figure B-17:Tangential velocity magnitude profile along a diametrical line passing through the mean CoC for a1mm bluestone slurry particle at 30%wt solids concentration at 75% critical mill speed

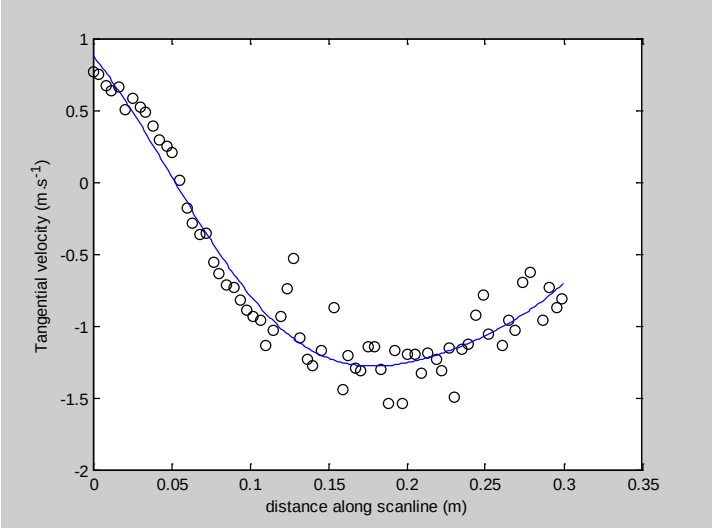

Figure B-17.1:Variation of tangential velocity with radial distance along the diametrical line passing through the mean CoC for a1mm bluestone slurry particle at 30%wt solids concentration at 75% critical mill speed

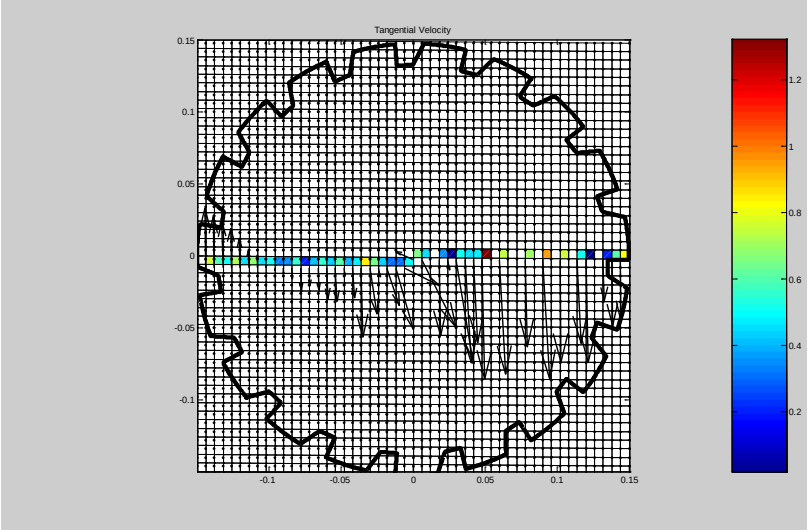

Figure B-18: Tangential velocity magnitude profile along a diametrical line passing through the mean CoC for a1mm bluestone slurry particle at 40%wt solids concentration at 75% critical mill speed

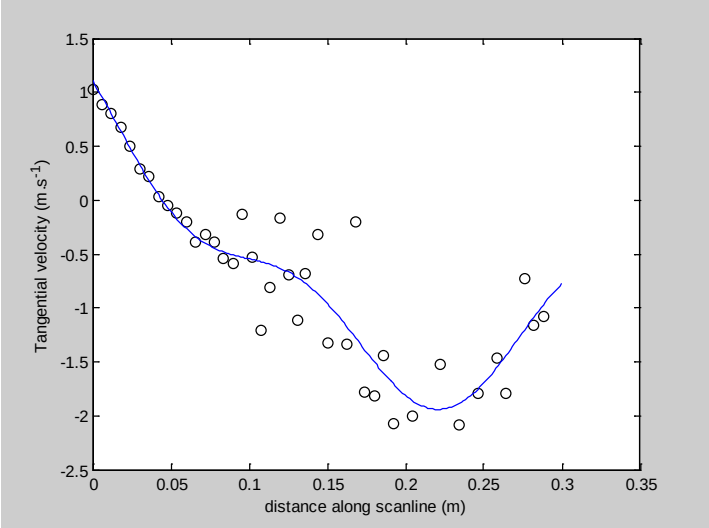

Figure B-18.1: Variation of tangential velocity with radial distance along the diametrical line passing through the mean CoC for a1mm bluestone slurry particle at 40%wt solids concentration at 75% critical mill speed

Section B4: Shear rate results at a rotational mill speed of 60% critical mill speed

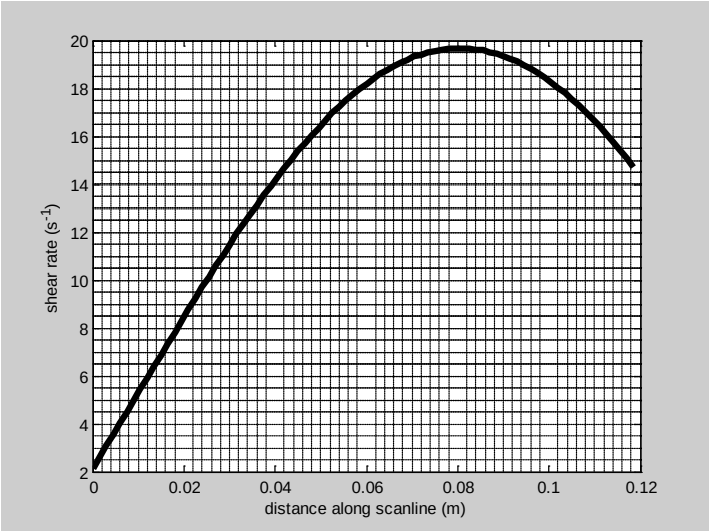

Figure B-19: Shear rate profile along the diametrical line passing through the mean CoC for a1mm bluestone slurry particle at 20%wt solids concentration at 60% critical mill speed

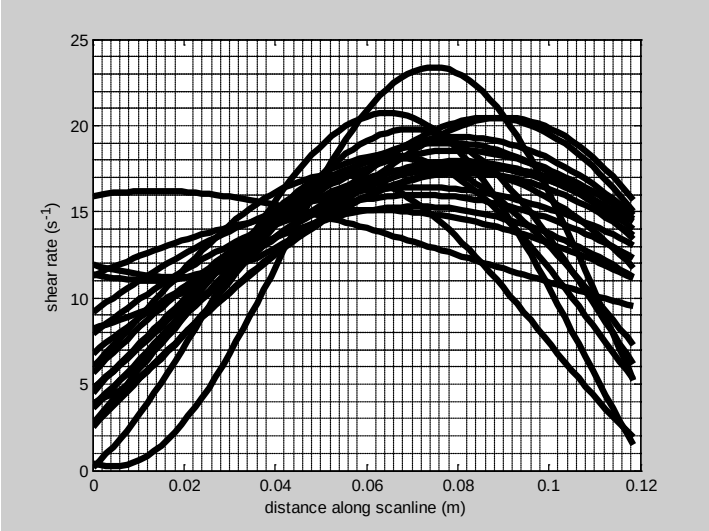

Figure B-19.1: Shear Rate profile for the angular span (θ_{CoC} ± 20°) about the mean CoC position for a 1mm bluestone slurry particle at 20%wt solids concentration at 60% critical mill speed

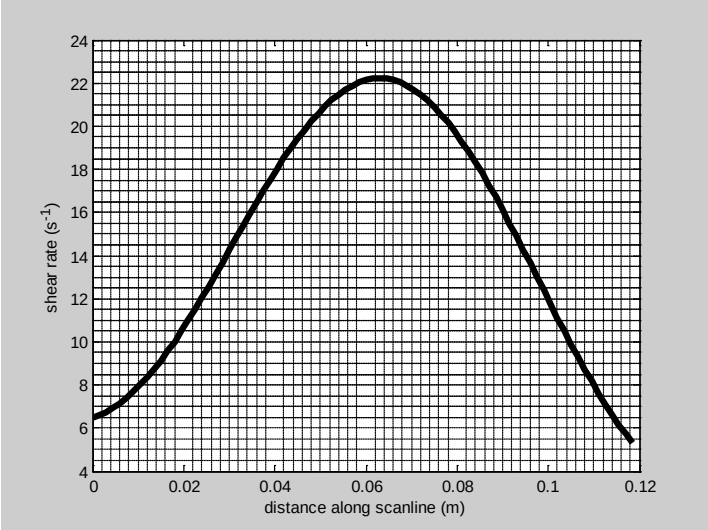

Figure B-20: Shear rate profile along the diametrical line passing through the mean CoC for a1mm bluestone slurry particle at 30%wt solids concentration at 60% critical mill speed

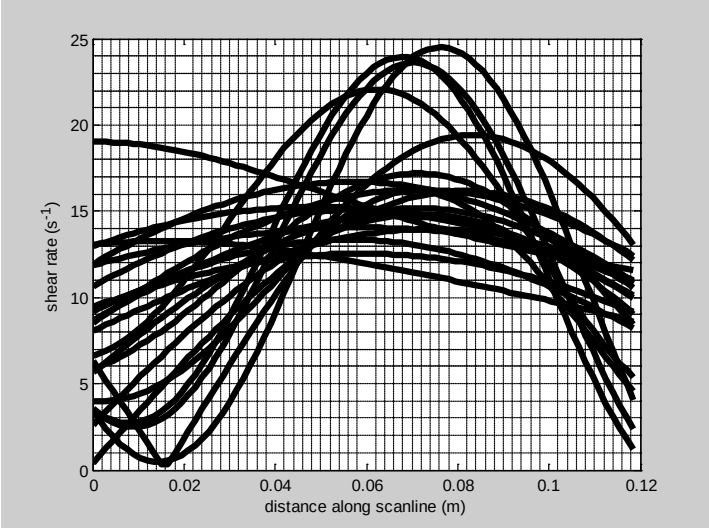

Figure B-20.1: Shear Rate profile for the angular span (θ_{CoC} ± 20°) about the mean CoC position for a 1mm bluestone slurry particle at 30%wt solids concentration at 60% critical mill speed

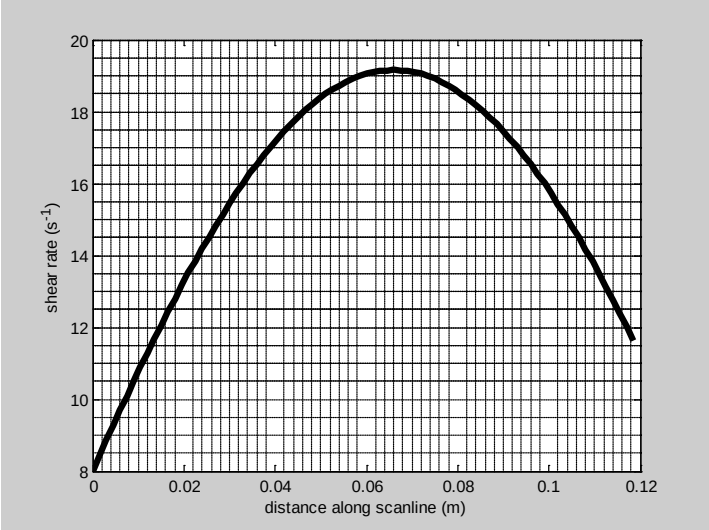

Figure B-21: Shear rate profile along the diametrical line passing through the mean CoC for a1mm bluestone slurry particle at 40%wt solids concentration at 60% critical mill speed

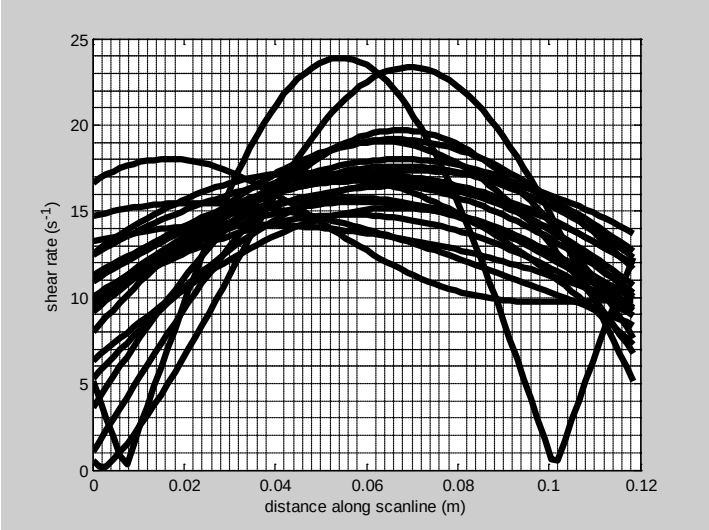

Figure B-21.1: Shear Rate profile for the angular span (θ_{CoC} ± 20°) about the mean CoC position for a 1mm bluestone slurry particle at 40%wt solids concentration at 60% critical mill speed

Section B4.1: Shear rate results at a rotational mill speed of 75% critical mill speed

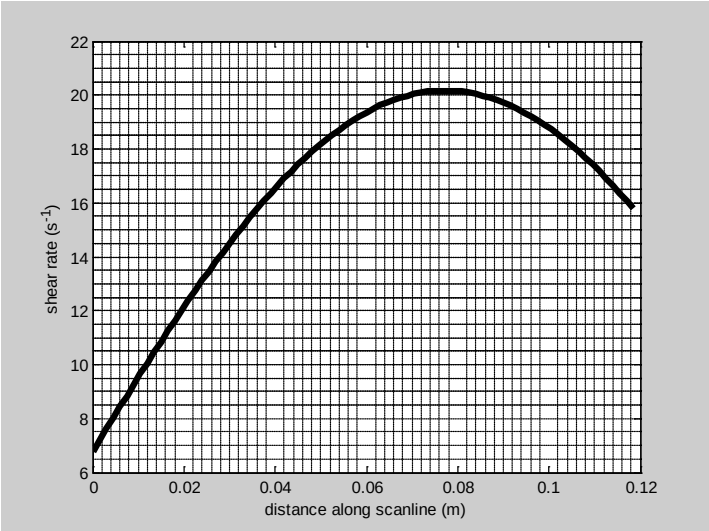

Figure B-22: Shear rate profile along the diametrical line passing through the mean CoC for a1mm bluestone slurry particle at 20%wt solids concentration at 75% critical mill speed

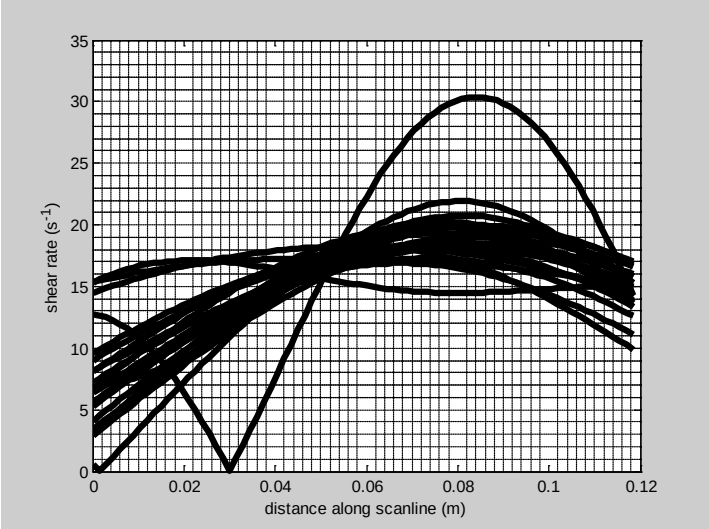

Figure B-22.1: Shear Rate profile for the angular span (θ_{CoC} ± 20°) about the mean CoC position for a 1mm bluestone slurry particle at 20%wt solids concentration at 75% critical mill speed

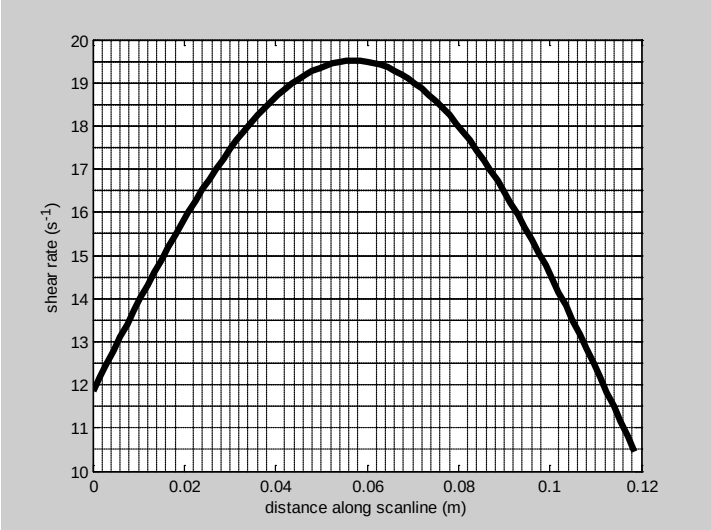

Figure B-23: Shear rate profile along the diametrical line passing through the mean CoC for a1mm bluestone slurry particle at 30%wt solids concentration at 75% critical mill speed

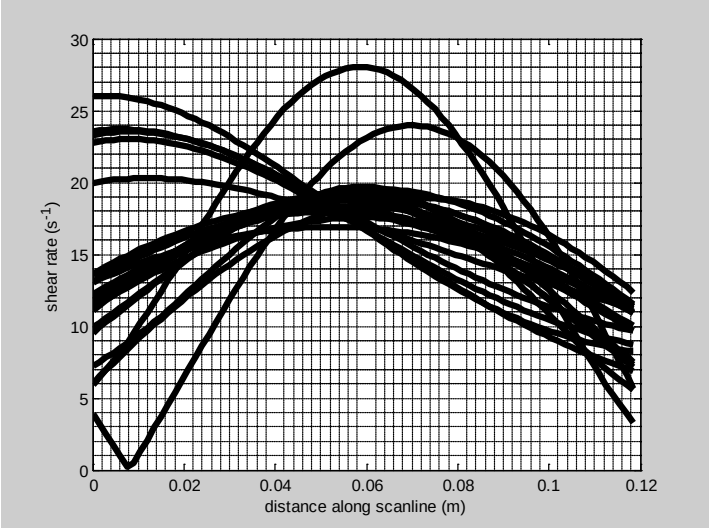

Figure B-23.1: Shear Rate profile for the angular span (θ_{CoC} ± 20°) about the mean CoC position for a 1mm bluestone slurry particle at 30%wt solids concentration at 75% critical mill speed

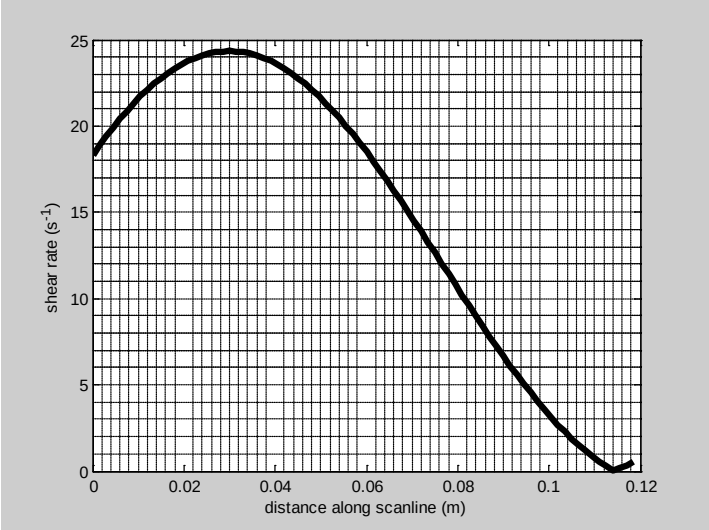

Figure B-24: Shear rate profile along the diametrical line passing through the mean CoC for a1mm bluestone slurry particle at 40%wt solids concentration at 75% critical mill speed

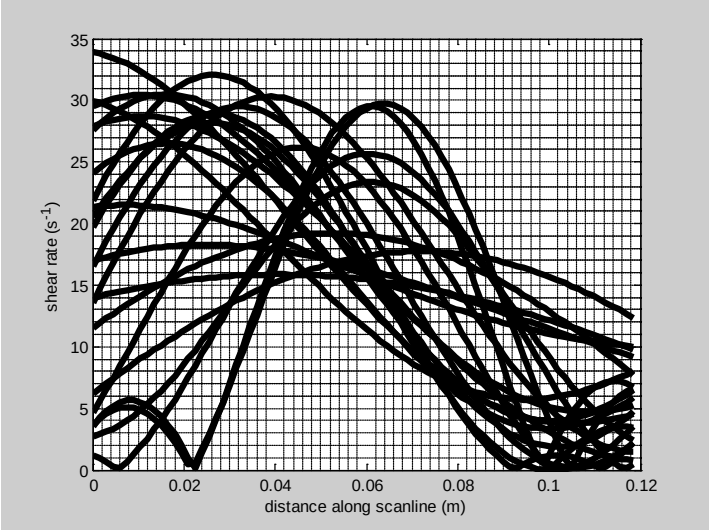

Figure B-24.1: Shear Rate profile for the angular span (θ_{CoC} ± 20°) about the mean CoC position for a 1mm bluestone slurry particle at 40%wt solids concentration at 75% critical mill speed.